IN THE UNITED STATES PATENT AND TRADEMARK OFFICE

In re the Application of:	Group Art Unit: 2828
Deniz K. Armani et al.	Examiner: Tod Thomas Van Roy
Serial No.: 10/678,354	
Filed: October 2, 2003	
For: ULTRA-HIGH Q MICRO-RESONATOR AND METHOD OF FABRICATION	

APPEAL BRIEF

MS Appeal Brief - Patents
Commissioner for Patents
P.O. Box 1450
Alexandria, VA 22313-1450

Dear Sir:

The Notice of Appeal in this case was filed on March 19, 2008. This Appeal Brief was previously filed on August 19, 2008, but was found defective for failure to comply with one or more provisions of 37 CFR 41.37. This Appeal Brief is amended to correct the defects noted by the Examiner in the Notice of Non-Compliant Appeal Brief mailed November 17, 2008.

As this amended Appeal Brief is being re-filed, and all appropriate Appeal Brief fees were previously paid, including extension of time fees, Applicants believe that no additional fees are due with this filing. However, if an additional extension is needed or a fee is due, please consider this a request therefor and charge Deposit Account No. 03-2775, under Order No. 70120-00005-US, from which the undersigned is authorized to draw.

This brief contains items under the following headings as required by 37 C.F.R. § 41.37 and M.P.E.P. § 1205.2:

I.	Real Party In Interest
II	Related Appeals and Interferences
III.	Status of Claims
IV.	Status of Amendments
V.	Summary of Claimed Subject Matter
VI.	Grounds of Rejection to be Reviewed on Appeal
VII.	Argument
Appendix A	Claims
Appendix B	Evidence
Appendix C	Related Proceedings

I. REAL PARTY IN INTEREST

The real party in interest for this appeal is California Institute of Technology, the assignee of record of the entire right, title and interest in the subject patent application.

II. RELATED APPEALS AND INTERFERENCES

Applicants are aware of no related proceedings currently pending before the Board.

III. STATUS OF CLAIMS

A. Total Number of Claims in Application

There are 82 claims that have been filed in the present application.

B. Current Status of Claims

1. Claims canceled: 2, 9, 23-27, 34, 42, 59, 63-66, 68-77, and 80.
2. Claims withdrawn from consideration but not canceled: None.
3. Claims pending: 1, 3-8, 10-22, 28-33, 35-41, 43-58, 60-62, 67, 78, 79, 81, and 82.
4. Claims allowed: None.

5. Claims rejected: 1, 3-8, 10-22, 28-33, 35-41, 43-58, 60-62, 67, 78, 79, 81, and 82.

C. Claims On Appeal

The claims on appeal are claims 1, 3-8, 10-22, 28-33, 35-41, 43-58, 60-62, 67, 78, 79, 81, and 82. Of these, claims 1, 29, 67, 78, and 79 are independent claims. Independent claims 78 and 79, and all dependent claims, stand or fall with the grounds of rejection identified below unless otherwise separately addressed.

IV. STATUS OF AMENDMENTS

Applicant filed an Amendment After Final Rejection pursuant to 37 CFR 41.33(a) on August 19, 2008. That paper amended claims 1, 29, 78, and 79 and canceled claims 2 and 34. The amendment was entered into the record by the Examiner on October 30, 2008, as is confirmed by the Advisory Action mailed on November 5, 2008. (See Exhibit H.) Following that Advisory Action and entry of Applicants' claim amendments, claims 1, 3-8, 10-22, 28-33, 35-41, 43-58, 60-62, 67, 78, 79, 81, and 82 remain pending in the application.

V. SUMMARY OF CLAIMED SUBJECT MATTER

Each of the independent claims is directed toward an ultra-high Q micro-cavity resonator, which includes a micro-cavity supported by a substrate in the form of a pillar. Ultra-high Q values are generally considered Q values in excess of 1.00×10^6. (Spec., p. 2, ll. 10-12.) In each of the claims on appeal, a Q value of at least 1.00×10^8 is recited. The Q value is a measure of the stability of light within the micro-cavity, or in other words, it is an accepted method of describing the relationship between stored optical energy and the rate of dissipation of that energy within the micro-cavity. (Spec., p. 2, ll. 2-4.) The higher the Q value for a micro-cavity, the longer it is capable of storing optical energy without appreciable loss.

A. Claim 1 is directed toward an ultra-high Q planar micro-cavity, having a Q value of at least 1.00×10^8, which is supported by a substrate pillar. In this arrangement, optical energy travels along the inner surface of the micro-cavity. Support for claim 1 in the specification is as follows:

> Ultra-high Q planar micro-cavity having a Q value of at least 1.00×10^8. This element is described in the specification at p. 6, ll. 18-22; p. 8, ll. 3-4; and p. 17, ll. 12-16, and is shown in Fig. 1A-1C as reference numeral 110.
>
> A substrate in the form of a pillar supporting the micro-cavity. This element is described in the specification at p. 6, l. 23 to p. 7, l. 4, and is shown in Figs. 1A & 1B as reference number 120.
>
> Whereby optical energy travels along an inner surface of the ultra-high Q micro-cavity. This limitation is described in the specification at p. 7, ll. 8-13.

B. Claim 29 is directed toward an optical material supported by a substrate. The optical material is meltable so that the periphery adheres to itself and forms an ultra-high Q planar micro-cavity having a Q value of at least 1.00×10^8. In addition, optical energy travels along the inner surface of the micro-cavity. Support for claim 29 in the specification is as follows:

> Optical material. This element is described in the specification at p. 6, ll. 18-22; p. 8, ll. 3-4; and p. 17, ll. 12-16, and is shown in Fig. 1A-1C as reference numeral 110.
>
> A substrate that supports the optical material. This element is described in the specification at p. 6, l. 23 to p. 7, l. 4, and is shown in Figs. 1A & 1B as reference number 120.
>
> The optical material is meltable by heat so that the periphery adheres to itself to form a planar micro-cavity having a Q value of at least 1.00×10^8. This limitation on the optical material is described in the specification at p. 6, ll. 21-22; p. 8, ll. 3-4; p. 8, ll. 18-22; p. 10, l. 12 to p. 11, l. 6; and p. 17, ll. 12-16, and is illustrated in

Fig. 2 as reference number 220 and in Fig. 3 as reference numbers 360, 370, and 380.

Optical energy travels along an inner surface of the ultra-high Q micro-cavity. This limitation is described in the specification at p. 7, ll. 8-10.

C. Claim 67, like claim 1, is directed toward an ultra-high Q planar micro-cavity, having a Q value of at least 1.00 x 10^8, which is supported by a substrate pillar. Claim 67 includes the additional limitations that the ultra-high Q planar micro-cavity is toroid-shaped and formed from silica, and that the substrate is formed from silicon and is isotropically etched to form the pillar. Support for claim 67 in the specification is as listed above for claim 1, with the additional limitations finding support as follows:

Silica toroid-shaped micro-cavity. This element is described in the specification at p. 6, ll. 18-22, and is shown in Fig. 1A-1C as reference numeral 110

Isotropically etched silicon substrate. This element is described in the specification at p. 15, ll. 15-23, and is shown in the Fig. 3 as reference numerals 340 and 350.

D. Claim 78, like claim 1, is directed toward an ultra-high Q planar micro-cavity, having a Q value of at least 1.00 x 10^8, which is supported by a substrate pillar. Claim 78 includes the additional limitation that the ultra-high Q planar micro-cavity includes a biotinylated surface. Support for claim 78 in the specification is as listed above for claim 1, with the additional limitations finding support as follows:

Ultra-high Q planar micro-cavity having a biotinylated surface. This element is described in the specification at p. 19, ll. 2-10.

E. Claim 79, like claim 29, is directed toward an optical material supported by a substrate, wherein the optical material is meltable so that the periphery adheres to itself and forms an ultra-high Q planar micro-cavity having a Q value of at least 1.00 x 10^8. Claim 79 includes the additional limitation that the ultra-high Q planar micro-cavity includes a biotinylated surface. Support for claim 79 in the specification is as listed above for claim 29, with the additional limitations finding support as follows:

Ultra-high Q planar micro-cavity having a biotinylated surface. This element is described in the specification at p. 19, ll. 2-10.

F. Claim 81 depends from claim 1 and introduces the additional limitation that the ultra-high Q micro-cavity resonator has a root mean square roughness of several nanometers. Support for claim 81 in the specification is as listed above for claim 1, with the additional limitations finding support as follows:

Ultra-high Q planar micro-cavity having a root mean square roughness of several nanometers. This element is described in the specification at p. 12, ll. 9-14.

G. Claim 82 depends from claim 29 and introduces the additional limitation that the ultra-high Q micro-cavity resonator has a root mean square roughness of several nanometers. Support for claim 82 in the specification is as listed above for claim 29, with the additional limitations finding support as follows:

Ultra-high Q planar micro-cavity having a root mean square roughness of several nanometers. This element is described in the specification at p. 12, ll. 9-14.

VI. GROUNDS OF REJECTION TO BE REVIEWED ON APPEAL

Whether claims 1, 3-8, 10-18, 22, 28-33, 35-41, 43-47, 49-58, 62, 67, 81, and 82 are unpatentable under 35 U.S.C. § 103(a) over U.S. Patent No. 5,343,490 to McCall (Exhibit A; hereinafter "McCall") in view of U.S. Patent No. 6,259,717 to Stone et al. (Exhibit B; hereinafter "Stone").

VII. ARGUMENT

A. Summary of the Argument

At the center of the claimed micro-cavity resonator is an ultra-high Q planar micro-cavity, which has a Q value of at least 1.00×10^8. The benefits and advantages of such an ultra-high Q micro-cavity have been recognized within the art, both prior and subsequent to the priority date of the present application. However, prior to Applicants' invention of the claimed micro-cavity resonator, no ultra-high Q planar micro-cavities having Q values of at least 1.00×10^8 existed. The cited prior art, while teaching the desirability of ultra-high Q planar micro-cavities, does not teach how to construct such planar micro-cavities to the level at which the skilled artisan would have *any* expectation of success when attempting to do so. In actuality, ultra-high Q planar micro-cavities are not simple to construct—the skilled artisan can't merely apply techniques used for constructing ultra-high Q spherical or other non-planar micro-cavities to construct an ultra-high Q planar micro-cavity. This simple truth is exhibited by the fact that peers have recognized, even more than four years after Applicants' priority date, that the ultra-high Q values achieved by Applicants' planar micro-cavity was still at least two orders of magnitude above any other known planar micro-cavity.

B. Rejection under 35 U.S.C. § 103(a) over McCall in view of Stone

The rejection of the claims at issue asserts that McCall teaches all limitations of the claim with the exception of the Q value being at least 1.00×10^8. The rejection further asserts that Stone teaches planar micro-cavity resonators having Q values exceeding 10^{10}. While the rejection accurately characterizes the teachings of McCall, the characterization of the teachings of Stone are far from accurate. Stone neither teaches planar micro-cavities, nor does it teach that planar micro-cavities are known to have Q values of at least 1.00×10^8. Most importantly, Stone does not impart any expectation of success to the skilled artisan for constructing a planar micro-cavity having a Q value in excess of 1.00×10^8. *In re Vaeck*, 947 F.2d 488, 493 (Fed. Cir. 1991) (for a finding of obviousness, not only must the claimed invention be suggested to the person of ordinary skill in the art, but the prior art must also impart a reasonable expectation of success for making the claimed invention). During examination, Applicants presented independent evidence that a person of ordinary skill in the art could not have had any reasonable expectation of success in view of the teachings of Stone. This evidence was in the form of actual attempts and failure to fabricate un ultra-high Q planar micro-cavity. Since Applicants' evidence was uncontroverted, the obviousness rejection cannot stand.

1. Claims 1, 3-8, 10-18, 22, 28-33, 35-41, 43-47, 49-58, 62, 67, 78, and 79

Each of claims 1, 29, 67, 78, and 79 are independent, and each of the other claims ultimately depends from one of these independent claims. Each of the independent claims recites, in some form, a planar micro-cavity having a Q value of at least 1.00×10^8. This element is not found or taught in the cited prior art.

a. McCall Teaches Planar Micro-Cavities

According to the rejection of these claims, McCall teaches planar micro-cavities supported by a substrate pillar. The rejection acknowledges that McCall does not teach a Q value of at least 1.00×10^8. (See Exhibits E & G). Applicants do not dispute this characterization of the teachings of McCall. However, McCall is actually wholly silent as to the Q value of the disclosed micro-cavities. For this reason, the teaching of a planar micro-cavity having a Q value of at least 1.00×10^8 must be found elsewhere in the prior art for the obviousness rejection to stand. Certainly, the prior art of record does not disclose such planar micro-cavities.

b. Stone Teaches Reducing the Q Value of a Non-Planar Micro-Cavity through Deformation

Stone does not teach planar micro-cavities, let alone ultra-high Q planar micro-cavities. In fact, Stone does not even teach the construction of non-planar ultra-high Q micro-cavities. Rather, Stone starts with the assumption that symmetrical, ultra-high Q micro-cavities, such as cylindrical and spherical micro-cavities, are known in the art. (Stone, Column 1, lines 34-43; and Fig 1.) From these known, symmetrical, non-planar micro-cavities, Stone delves into the benefits of deforming symmetrical micro-cavities to induce directional emissions. (Stone, Column 1, line 66 – Column 2, line 6.) Specifically, Stone discloses how a symmetrical micro-cavity may be deformed to control the location and direction of light output from the micro-cavity. (Stone, Column 2, lines 20-40.) In Figure 5, Stone shows a graph where the Q value versus deformation of a symmetrical micro-cavity is derived from numerical solutions to the wave equation. The Q values listed in this graph are not generated from actual micro-cavity resonators. In Figures Figs 3A and 3B, Stone shows a deformed cylindrical and a prolate spheroidal micro-cavity as examples of asymmetric micro-cavities. A fair reading of Stone leads to the conclusion, through implication, that ultra-high Q micro-cavities were known in the prior art. Most importantly, Stone does not clearly imply that ultra-high Q planar micro-cavities were known in the prior art, nor does it convey how to construct such planar micro-cavities.

c. Extrinsic Evidence Supports a Finding of Non-Obviousness

In response to the obviousness rejection, Applicants submitted the Declaration of Deniz K. Armani and its supporting exhibits (Exhibit C) as evidence that planar micro-cavities having Q values greater than 10^8 were not obvious as of the priority date of the present application.[1] The Armani Declaration provides *uncontroverted* evidence that (1) achieiving Q values in excess of 10^8 in a planar micro-cavity involves a high degree of technical difficulty, and (2) as of the priority date of the present application, and for at least 4 years thereafter, publications by independent authors confirm that attempts had been made to fabricate planar micro-cavities, and those attempts resulted in planar micro-cavities having Q values of no more than 10^4. The two articles attached as exhibits to the Armani Declaration were published in *Optics Letters* (Exhibit 1 to the Armani Declaration, hereinafter referred to as the "*Optics Letters* article") and *IEEE*

---

[1] The Armani Declaration and exhibits thereto were originally informally provided to the Examiner in advance of a telephonic interview Applicants conducted with the Examiner. (*See* Examiner's interview Summary, Exhibit F.) The Declaration and exhibits were later inserted into the record as part of Applicants' interview summary (Exhibit G).

Journal of Selected Topics in Quantum Electronics (Exhibit 2 to the Armani Declaration, hereinafter referred to as the "*IEEEJ* article"), respectively, both publications being well-known and respected within their respective communities. Moreover, *Optics Letters* is a peer reviewed journal, so statements made in it about the general state of the art at the time of publication carry the additional weight of scientific community approval.

In the *Optics Letters* article, which was published in December 2004, the authors discuss planar micro-cavity resonators developed as the basis for the article. The Q value reported for those micro-cavity resonators is on the order of 10^2. The article recognizes that non-planar micro-cavities, i.e., microspheres, were known with Q values approaching 10^{10}. (*See* p. 2861 of the *Optics Letters* article.) As for planar micro-cavities, the *Optics Letters* article recognizes that the highest known Q values were described in a *Nature* article published on February 27, 2003[2] (hereinafter referred to as the "*Nature* article"), which was authored by the inventors of the present application. That *Nature* article, which has substantially the same disclosure as the present application, describes Q values on the order of 10^8. The *Optics Letters* article thus demonstrates that, at the time the present application was filed, creating a planar micro-cavity having a Q value approaching within many orders of magnitude of 10^8 required such a high degree of technical skill that such planar micro-cavities have only previously existed through the processes described in the *Nature* article. Further, the *Optics Letters* article establishes that planar micro-cavities having Q values approaching 10^8 were not known to exist in the prior art even after the priority date of the present application.

The *IEEEJ* article provides further evidence that planar micro-cavities having Q values approaching 10^8 were not known in the prior art to the present application. The *IEEEJ* article was published in March/April 2007 and describes fabrication of a planar microtoroidal cavity formed from silicon and integrated on a substrate with a tunable optical coupler. The unloaded Q value for this microtoroidal cavity was reported to be as high as 10^5, still three orders of magnitude shy of the planar micro-cavity at issue in the claims. The *IEEEJ* article further indicates that the only known planar micro-cavities having Q values higher than 10^5 were described in the *Nature* article. Thus, even more than four years following the priority date of the present application, planar micro-cavities having Q values in excess of 10^5 were known to exist solely based on the description from a single source—the *Nature* article. The prior art of record, namely McCall and Stone, provides no indication that any planar micro-cavities having Q values in excess of 10^2 existed, or were known to have existed, prior to the Applicants invention thereof.

---

[2] D.K. Armani, T. J. Kippenberg, S. M. Spillane, & K. J. Vahala, "Ultra high-Q toroid microcavity on a chip", *Nature*, Vol. 421, No. 6929, pp. 925-929, Feb. 27, 2003.

Where a reasonable expectation of success is required for establishing a *prima facie* case of obviousness, the claims at issue cannot be rendered obvious. *See, In re Dow Chemical Co.*, 837 F.2d 469, 473, 5 U.S.P.Q.2d (BNA) 1529, 1531 (Fed. Cir. 1988) ("Both the suggestion and the expectation of success must be founded in the prior art, not in applicant's disclosure.") At best, the prior art represents an invitation to try and create a planar micro-cavity having a Q value in excess of 10^8, but such an invitation to try is far from teaching how to accomplish such a feat. *See Hybritech Inc. v. Monoclonal Antibodies, Inc.*, 802 F.2d 1367, 1380 (Fed. Cir. 1986). In view of the evidence that others had tried and failed to fabricate ultra-high Q planar micro-cavities after Applicants' invention thereof, and considering the shortcomings in the respective teachings of McCall and Stone, the ordinary skilled artisan would have had no reasonable expectation of successfully creating a planar micro-cavity having a Q value of 10^8 or greater as of the priority date of the present application.

Moreover, the two articles submitted by Applicants' as evidence of non-obviousness have been entirely ignored by the Examiner, who did not so much as address Applicants' evidence in either of the Examiner's Interview Summary (Exhibit F) or the Advisory Action (Exhibit H). This evidence, which was published by wholly uninterested third parties, is a very strong indicator that the prior art of record does not render the claimed subject matter obvious. Without contravention by the Examiner, this evidence should be determinative of the issues presented, such that the obviousness rejection to claims 1, 3-8, 10-18, 22, 28-33, 35-41, 43-47, 49-58, 62, 67, 78, and 79 can not stand.

2. Claims 81 and 82

In addition to the grounds for non-obviousness addressed in independent claims 1 and 29 above, dependent claims 81 and 82 additionally recite that the micro-cavity resonators of claims 1 and 29, respectively, have "a root mean square (rms) roughness of several nanometers." The rejection asserts that McCall teaches that a reduction in the surface roughness is desirable to achieve higher Q values for the micro-cavity. While this characterization of McCall is accurate, the rejection fails to take into account that McCall and all other prior art of record fails to teach how a reduction in surface roughness is to be accomplished. McCall teaches the desirability of reducing the surface roughness, but utterly fails to teach how to accomplish that goal. For this additional reason, the claims 81 and 82 are not obvious over the cited prior art. *Hybritech*, 802 F.2d at 1380 (the prior art must also teach how to practice a claimed invention for a finding of obviousness to be upheld).

C. Conclusion

For the foregoing reasons, Applicants submit that each of claims 1, 3-8, 10-18, 22, 28-33, 35-41, 43-47, 49-58, 62, 67, 78, 79, 81, and 82 are patentable over the combination of McCall and Stone and hereby request reversal of the rejections in this matter.

Respectfully submitted,

CONNOLLY BOVE LODGE & HUTZ LLP

DATE: November 25, 2008

By: ______________________
David M. Morse
Reg. No. 50,505

CONNOLLY BOVE LODGE & HUTZ LLP
1007 North Orange Street
P.O. Box 2207
Wilmington, Delaware 19899
(302) 658-9141
(302) 658-5614 (Fax)

APPENDIX A

Claims Involved in the Appeal of Application Serial No. 10/678,354

1. (Previously Presented) An ultra-high Q micro-cavity resonator, comprising:

an ultra-high Q micro-cavity having a Q value of at least 1.00 x 10^8, the micro-cavity being planar; and

a substrate,

portions of the substrate located below the ultra-high Q micro-cavity being removed to form a pillar, the pillar supporting the ultra-high Q micro-cavity, whereby optical energy travels along an inner surface of the ultra-high Q micro-cavity.

2. (Cancelled)

3. (Original) The resonator of claim 1, the micro-cavity comprising an ultra-high Q silica micro-cavity.

4. (Original) The resonator of claim 1, the micro-cavity being substantially circular and having a diameter of about 10 micrometers to about 500 micrometers.

5. (Original) The resonator of claim 1, the micro-cavity having a toroid shape.

6. (Original) The resonator of claim 5, the toroid-shaped micro-cavity having a thickness of about five to about ten micrometers.

7. (Original) The resonator of claim 1, the micro-cavity having an elliptical shape.

8. (Original) The resonator of claim 1, the micro-cavity being substantially parallel to a top surface of the pillar.

9. (Canceled)

10. (Previously Presented) The resonator of claim 1, the micro-cavity having a Q value of about 10^8 to about 5×10^8.

11. (Previously Presented) The resonator of claim 1, the micro-cavity having a diameter of about 10 micrometers to about 30 micrometers and a Q value of about 500 million.

12. (Original) The resonator of claim 1, the micro-cavity comprising a glass material having a melting point that is lower than a melting point of the substrate.

13. (Original) The resonator of claim 1, a resonant mode within the micro-cavity comprising a whispering-gallery mode (WGM).

14. (Original) The resonator of claim 1, the substrate comprising a silicon substrate.

15. (Previously Presented) The resonator of claim 1, the substrate underneath the micro-cavity being removed by an etchant.

16. (Original) The resonator of claim 15, the etchant comprising a xenon difluoride (XeF_2) gas.

17. (Original) The resonator of claim 16, wherein the XeF_2 gas isotropically etches the substrate beneath a periphery of the micro-cavity to form the pillar.

18. (Original) The resonator of claim 17, the substrate comprising a silicon substrate.

19. (Original) The resonator of claim 1, the pillar having a tapered shape.

20. (Previously Presented) The resonator of claim 1, the micro-cavity including a rare earth dopant.

21. (Original) The resonator of claim 20, the rare Earth dopant being erbium, ytterbium, or neodymium.

22. (Previously Presented) The resonator of claim 1, the micro-cavity including an optically active component.

23. – 27. (Canceled)

28. (Original) The resonator of claim 1, the micro-cavity comprising a silica ultra-high Q micro-cavity, and the substrate comprising a silicon substrate.

29. (Previously Presented) An ultra-high Q micro-cavity resonator, comprising:

an optical material; and

a substrate that supports the optical material, wherein

the optical material is meltable by heat so that a periphery of the optical material adheres to itself to form an ultra-high Q micro-cavity having a Q value of at least 1.00×10^8,

the micro-cavity is planar, and

optical energy travels along an inner surface of the ultra-high Q micro-cavity.

30. (Original) The resonator of claim 29, the optical material comprising silica.

31. (Original) The resonator of claim 29, the optical material comprising a glass material having a melting point that is lower than a melting point of the substrate.

32. (Previously Presented) The resonator of claim 29, the optical material comprising a disk, wherein a diameter of the optical material becomes smaller when heated to form a disk.

33. (Previously Presented) The resonator of claim 32, wherein the diameter decreases until the molten optical material collapses after which the diameter remains substantially constant.

34. (Cancelled)

35. (Original) The resonator of claim 29, the ultra-high Q micro-cavity comprising an ultra-high Q silica micro-cavity.

36. (Original) The resonator of claim 29, the ultra-high Q micro-cavity being substantially circular and having a diameter of about 10 micrometers to about 500 micrometers

37. (Original) The resonator of claim 29, the ultra-high Q micro-cavity having a toroid shape.

38. (Original) The resonator of claim 37, the toroid having a thickness of about five to about ten micrometers.

39. (Original) The resonator of claim 29, the ultra-high Q micro-resonator having an elliptical shape.

40. (Original) The resonator of claim 29, the ultra-high Q micro-cavity being substantially parallel to a top surface of the pillar.

41. (Original) The resonator of claim 29, wherein a size of the ultra-high Q micro-cavity is limited by a size of a top surface of the substrate.

42. (Canceled)

43. (Previously Presented) The resonator of claim 29, the ultra-high Q micro-cavity having a Q value of about 10^8 to about 5×10^8.

44. (Previously Presented) The resonator of claim 29, the ultra-high Q micro-cavity having a diameter of about 10 micrometers to about 30 micrometers and a Q value of about 500 million.

45. (Original) The resonator of claim 29, a resonant mode within the ultra-high Q micro-cavity being a whispering-gallery mode (WGM).

46. (Original) The resonator of claim 29, the substrate comprising a silicon substrate.

47. (Original) The resonator of claim 29, wherein portions of the substrate located below the ultra-high Q micro-cavity are removed to form a pillar, the pillar supporting the ultra-high Q micro-cavity.

48. (Previously Presented) The resonator of claim 47, the pillar having a tapered shape.

49. (Previously Presented) The resonator of claim 29, the substrate underneath the periphery of the ultra-high Q micro-cavity being removed by an etchant.

50. (Original) The resonator of claim 49, the etchant comprising xenon difluoride (XeF_2) gas.

51. (Original) The resonator of claim 50, wherein the XeF_2 gas isotropically etches the substrate beneath the periphery of the micro-cavity.

52. (Original) The resonator of claim 29, the heat source comprising an Excimer laser.

53. (Previously Presented) The resonator of claim 52, wherein the Excimer laser heats and liquefies the optical material.

54. (Original) The resonator of claim 29, the heat source comprising a CO_2 laser.

55. (Original) The resonator of claim 54, wherein the CO_2 laser emits radiation having a wavelength of about 10.6 micrometers.

56. (Original) The resonator of claim 54, wherein the CO_2 laser heats the optical material for about 1 microsecond to about 10 seconds.

57. (Original) The resonator of claim 54, wherein the CO_2 laser heats and liquefies the optical material.

58. (Original) The resonator of claim 29, wherein the optical material comprises silica and the substrate comprises silicon.

59. (Canceled)

60. (Previously Presented) The resonator of claim 29, the ultra-high Q micro-cavity including a dopant.

61. (Original) The resonator of claim 60, the dopant being erbium, ytterbium, or neodymium.

62. (Previously Presented) The resonator of claim 29, the ultra-high Q micro-cavity including an optically active component.

63. – 66. (Canceled)

67. (Previously Presented) A planar micro-cavity resonator, comprising:

an ultra-high Q toroid-shaped planar silica micro-cavity having a Q value of at least 1.00×10^8; and

a silicon substrate;

wherein portions of the silicon substrate located below a periphery of the ultra high-Q toroid-shaped planar silica micro-cavity are isotropically etched to form a silicon pillar, the silicon pillar supporting the ultra-high Q toroid-shaped planar silica micro-cavity, and wherein light energy traverses along an inner surface of the ultra-high Q toroid-shaped planar micro-cavity.

68. – 77. (Canceled)

78. (Previously Presented) A micro-cavity resonator, comprising:

an ultra-high Q micro-cavity having a Q value of at least 1.00 x 10^8 and having a biotinylated surface, the micro-cavity being planar; and

a substrate, portions of the substrate located below the ultra-high micro-cavity being removed to form a pillar that supports the ultra-high Q micro-cavity, whereby optical energy travels along an inner surface of the micro-cavity.

79. (Previously Presented) An ultra-high Q micro-cavity resonator, comprising:

an optical material; and

a substrate that supports the optical material, wherein

the optical material is meltable by a heat source so that a periphery of the optical material adheres to itself to form an ultra-high Q micro-cavity, the ultra-high Q micro-cavity having a Q value of at least 1.00 x 10^8 and having a biotinylated surface,

the micro-cavity is planar, and

optical energy travels along an inner surface of the ultra-high Q micro-cavity.

80. (Canceled)

81. (Previously Presented) The ultra-high Q micro-cavity resonator of claim 1 having a root mean square (rms) roughness of several nanometers.

82. (Previously Presented) The ultra-high Q micro-cavity resonator of claim 29 having a root mean square (rms) roughness of several nanometers.

APPENDIX B

A copy of evidence pursuant to §§ 1.130, 1.131, or 1.132 and/or evidence entered by or relied upon by the Examiner that is relevant to this appeal is attached hereto.

Exhibit	Description	Location in Record
A	U.S. Patent No. 5,343,490 to McCall	Reference cited by Applicants as part of Information Disclosure Statement filed on December 7, 2004
B	U.S. Patent No. 6,259,717 to Stone et al.	Reference cited by Examiner as part of Office Action mailed on April 30, 2007
C	Declaration of Deniz K. Armani and Exhibits thereto	Filed on May 9, 2008 as part of Applicants' Interview Summary, the interview having taken place on February 28, 2008; Entered into record on May 9, 2008 as part of Applicants' Interview Summary (See Exhibit G)
D	Armani et al., "Ultra high-Q toroid microcavity on a chip", *Nature*, Vol. 421, No. 6929, pp. 925-929, Feb. 27, 2003	Reference cited by Applicant in the Information Disclosure Statement filed on December 7, 2004
E	Final Rejection	Entered into record on mailing date

		of October 13, 2007
F	Examiner's Interview Summary	Entered into record on mailing date of March 7, 2008
G	Applicant's Interview Summary	Filed by Applicant and entered into record on May 9, 2008
H	Examiner's Advisory Action	Entered into record on mailing date of November 5, 2008.

APPENDIX C

Applicants are aware of no related proceedings currently pending before the Board.

EXHIBIT A

US005343490A

United States Patent [19]

McCall

[11] **Patent Number: 5,343,490**

[45] **Date of Patent: Aug. 30, 1994**

[54] **WHISPERING MODE MICRO-RESONATOR**

[75] Inventor: **Samuel L. McCall**, Chatham, N.J.

[73] Assignee: **AT&T Bell Laboratories**, Murray Hill, N.J.

[21] Appl. No.: **943,943**

[22] Filed: **Sep. 11, 1992**

Related U.S. Application Data

[63] Continuation-in-part of Ser. No. 761,207, Sep. 17, 1991, abandoned.

[51] **Int. Cl.**^{5} **H01S 3/05**

[52] **U.S. Cl.** **372/94**; 372/43; 372/67; 372/92

[58] **Field of Search** 372/94, 92, 43, 44, 372/45, 50, 66, 67

[56] **References Cited**

U.S. PATENT DOCUMENTS

4,829,537	5/1989	Baer	372/92
5,197,071	3/1993	Yamada	372/94

OTHER PUBLICATIONS

I. Ury et al, "Whispering gallery lasers on semi–insulating GaAs substrates", Appl. Phys. Lett. 36 (8), Apr. 15, 1980, pp. 629–631.

"The Problem of the Whispering Gallery," *Scientific Papers,* v. 5, pp. 617–620, Cambridge University, Cambridge, England (1912). (no month).

T. Krauss, et al, *Electronic Letters,* v. 26, pp. 2095–2097 (Dec. 6, 1990).

Primary Examiner—James W. Davie
Attorney, Agent, or Firm—George S. Indig

[57] **ABSTRACT**

Device for electromagnetic emission depends on total internal reflection-on whispering gallery mode cavitation about the periphery of a disk-shaped element of sub-wavelength thickness. As a laser, operating above threshold, the design is alternative to that of the Surface Emitting Laser for integration in integrated circuitry-either all-optic or electro-optic. Operating below threshold, it may serve as a Light Emitting Diode. The same operational considerations-based on improved efficacy for whispering gallery mode devices as due to relevant dimension/s of sub-wavelength thickness-is of consequence for a category of devices serving other than as simple emitters. Such three port devices may serve as switches, modulators, etc.

27 Claims, 5 Drawing Sheets

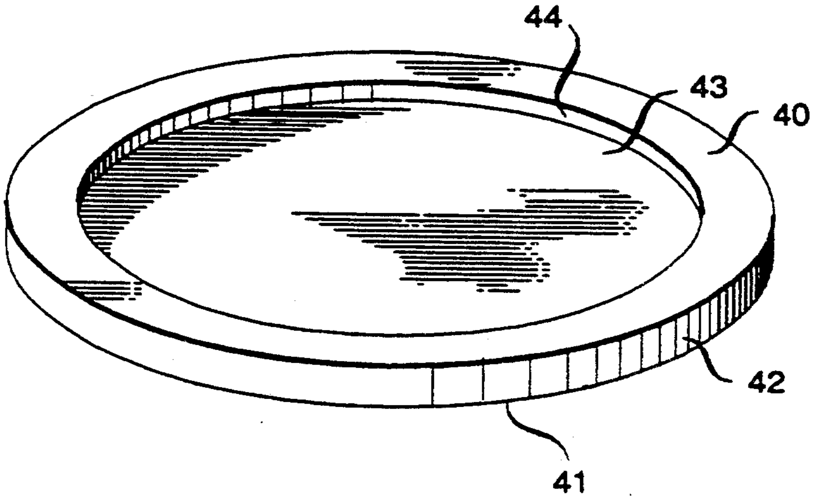

FIG. 1

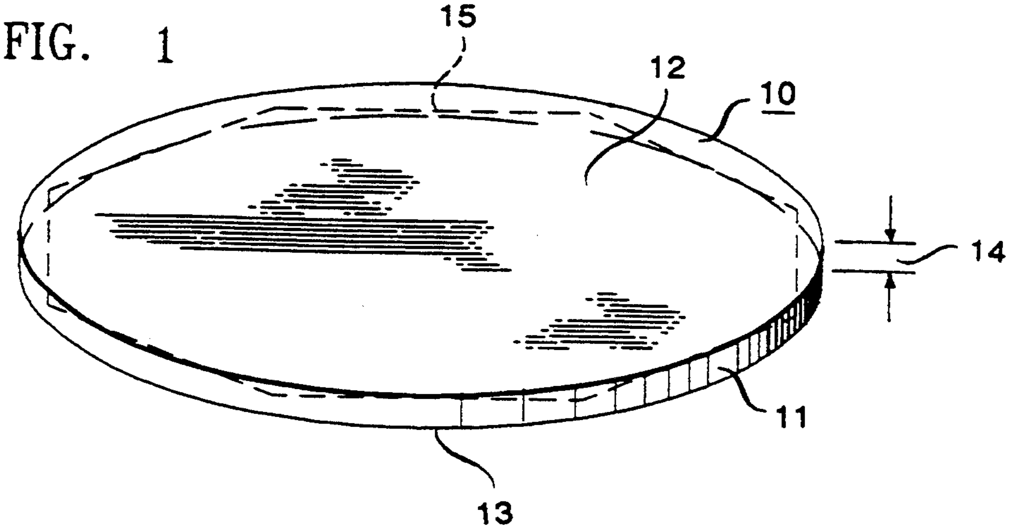

FIG. 2

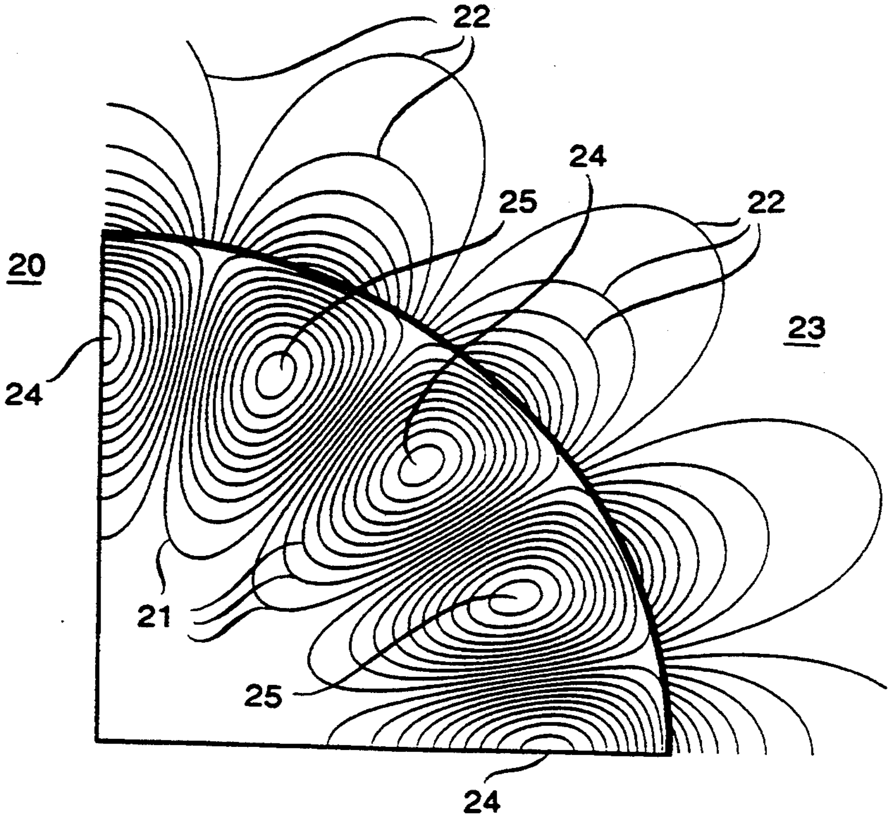

FIG. 3

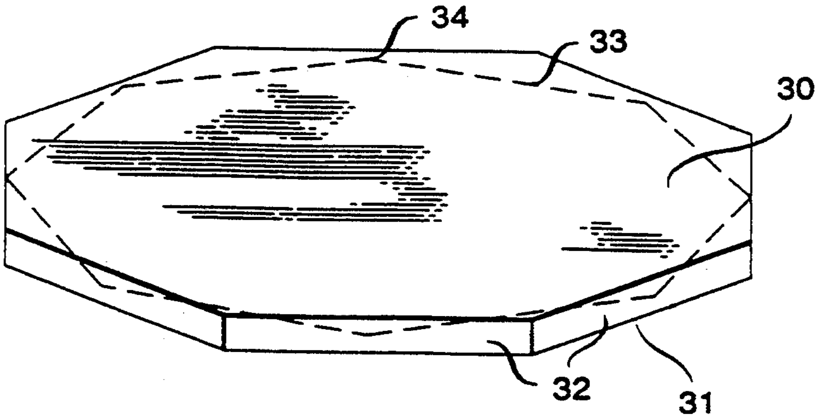

FIG. 4

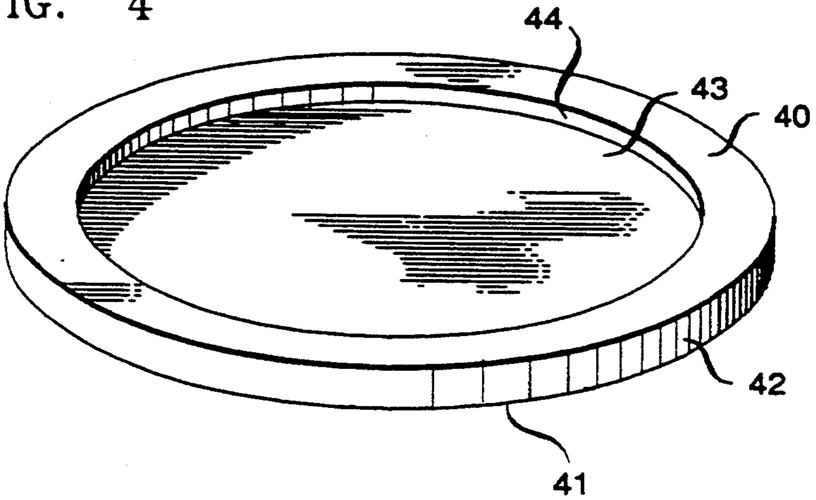

FIG. 5

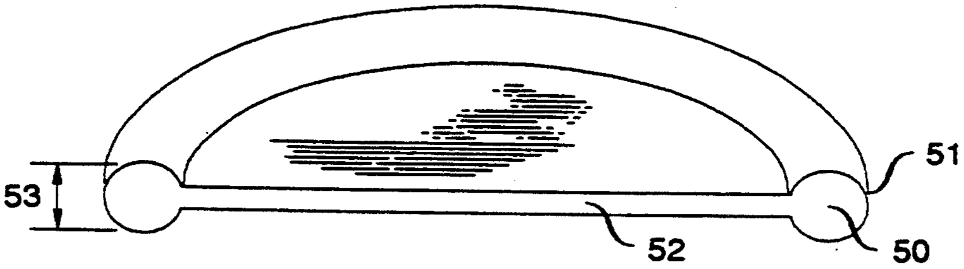

FIG. 6

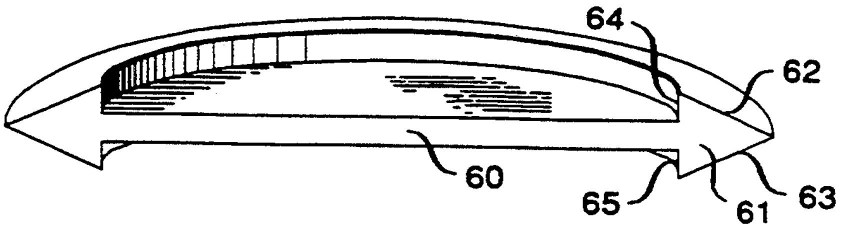

FIG. 7

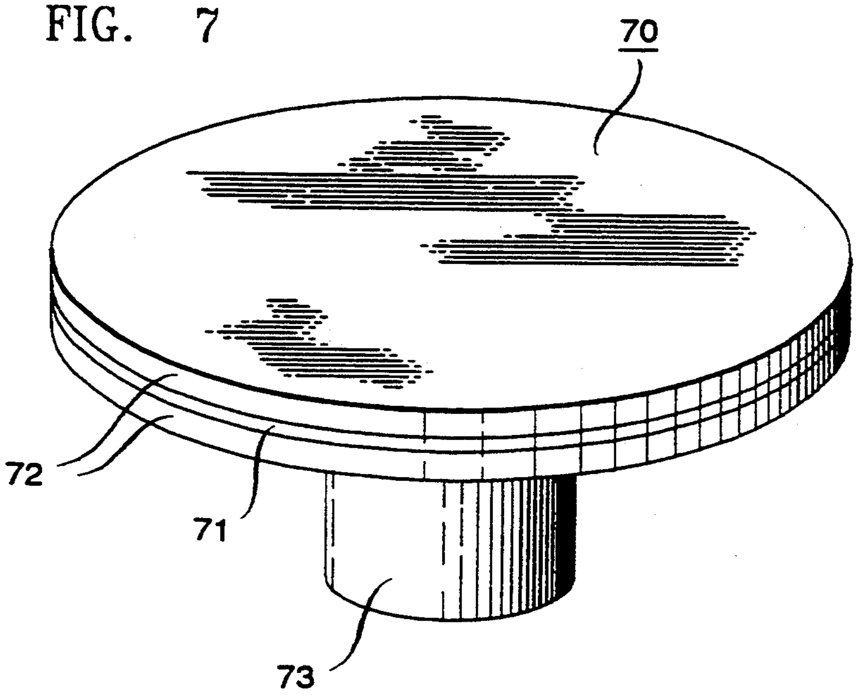

FIG. 8

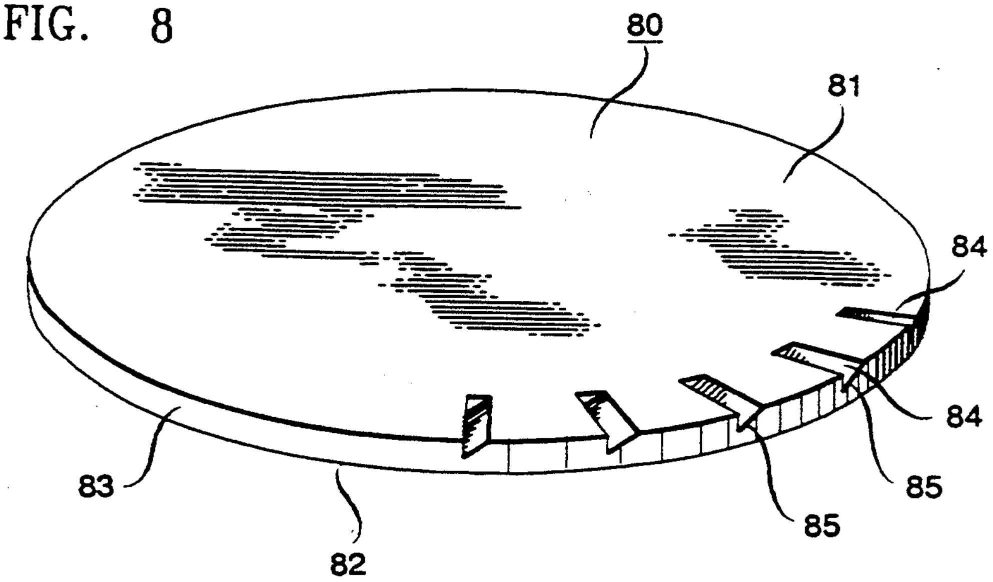

FIG. 9

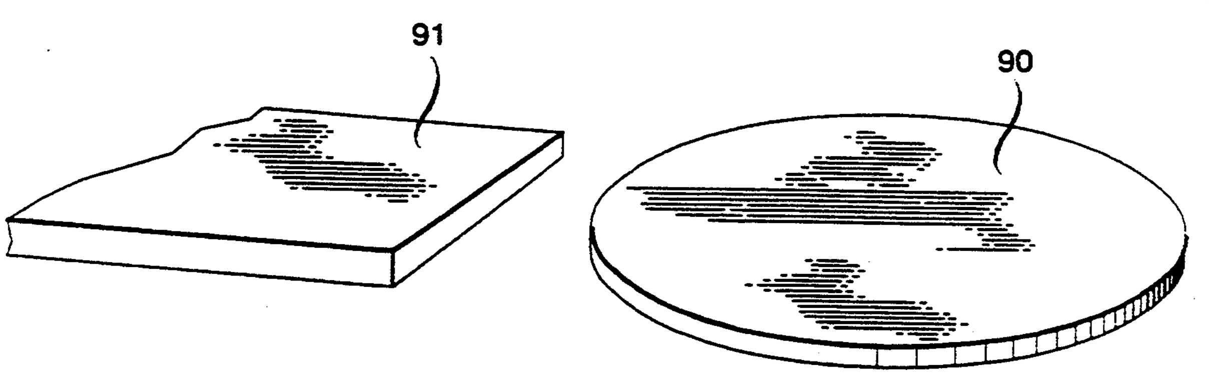

FIG. 10

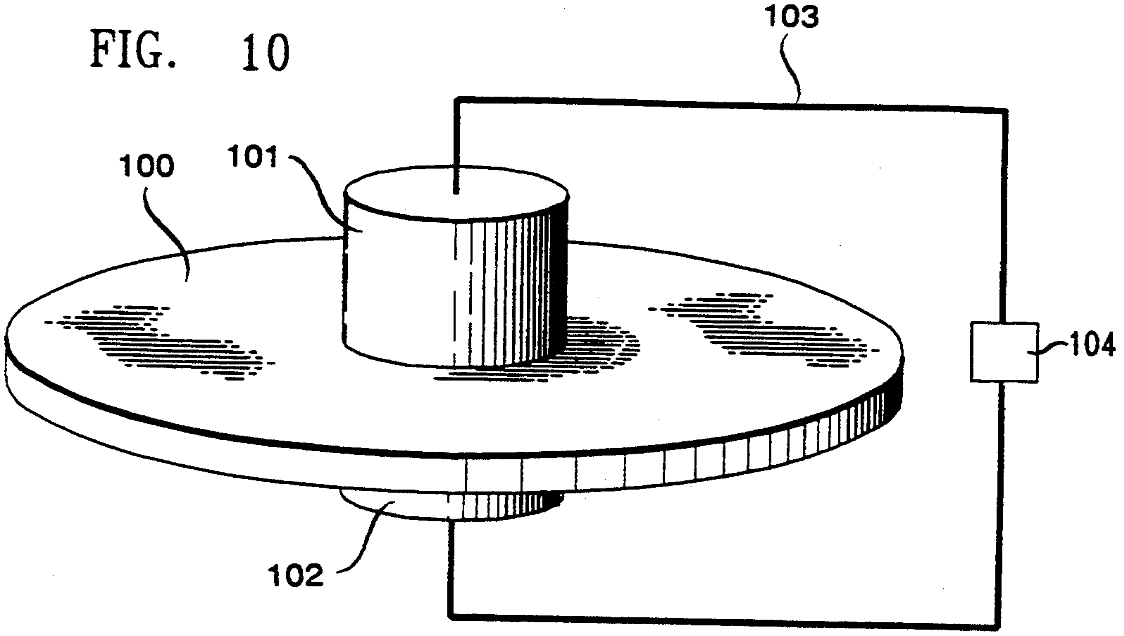

FIG. 11

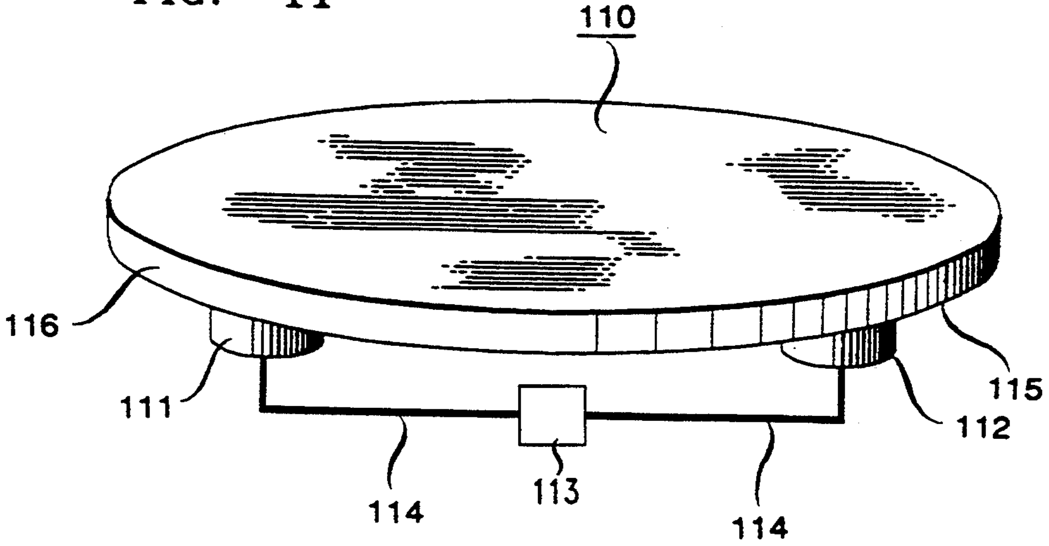

WHISPERING MODE MICRO-RESONATOR

This application is a continuation-in-part of co-pending application, Ser. No. 07/761207, filed Sep. 17, 1991, now abandoned.

BACKGROUND OF THE INVENTION

1. Technical Field

A micro-resonator structure depends upon cavitation of whispering mode energy regardable as defining cavitation about the perimeter of a sub-wavelength thick active region of various configurations. Operating in the lasing mode, it offers an alternative to the Surface Emitting Laser for incorporation in integrated circuitry—either all-optic or electro-optic.

2. Description of the Prior Art

A general category of structures includes optical detectors as well as a variety of two port and three port devices providing for modification either of output or input. Worldwide activity is consistent with the consensus that the SEL offers promise of satisfaction of the longstanding desire for large-scale incorporation of active photonic devices in integrated circuits. Hope is based on the very low lasing threshold values which intrinsically reduce heating, usually I^2R heating losses attendant on pumping considered central to frustration of this desire.

Development of the SEL has entailed a number of design advances. Use of bulk active material has, to significant extent, yielded to quantum well structures—including the ultimate single quantum well structure. Process variations have involved deposition techniques with a view both to compositional uniformity and dimensional regularity. An area of considerable consequence has involved the sandwiching Distributed Bragg Reflector mirrors. Reported operating devices dependably achieve reflectivities of 99+% as yielded by ≈20–40 pair DBRs for 0.8–1.1 μm wavelength emission. This latter consideration—definition of the laser cavity in terms of DBRs—has been of primary consequence in evolution of the SEL. Achievement of excellent reported reflectivities is ascribed to satisfaction of very tight fabrication tolerances.

On the other side of the ledger, achievement of each new SEL design has depended critically on the DBR to, in turn, result in considerable expense as well as some undesirable operational consequence. DBRs, as the name connotes, is distributed-significantly increases modal volume beyond that of the responsible active region. In the instance of a Single Quantum Well structure designed for operation at 1.3 μm, this consideration results in an increase of 20×.

SUMMARY OF THE INVENTION

At the same time, desired population density in the optical or hybrid device gives rise to need for a variety of passive as well as other types of active devices. A design approach alternative to the SEL depends upon cavitation of energy in the form of "whispering gallery modes" as supported within a thin element—an active material element of thickness characteristically of a maximum of a half wavelength (with the wavelength value as measured in bulk material) over some substantial portion of the functioning element. Cavitating energy is generally largely confined to a peripheral portion of the element which latter may be of a variety of configurations, generally of maximum dimension of the order of microns to accommodate integration size desire.

An important category of devices in accordance with the invention, provides for attainment of lasing threshold. The generic concept of the whispering mode micro-resonator is usefully applied as well to structures which designedly, or through operation, do not reach threshold. Resulting Light Emitting Diodes may serve many of the purposes of lasers with advantages in practical terms of e.g. yield, power requirements, etc. One contemplated use is as a switched element, in which functioning depends simply upon presence or absence of output, and not, e.g. on coherence.

Design variations with attention to critical dimensions and other parameters are discussed under "Detailed Description". In general terms, operation depends upon cavitation as involving three or more reflecting positions (as distinguished from usual two-mirror cavities). Requirement for "total internal reflection" in usual contemplated devices—devices of micron/s dimensions—for usually/practically available index contrast generally results in polygonal cavity path of four or more sides.

It is believed that the invention meets a need for replacement of purely electronic IC circuitry. It offers low power consumption for constituent devices in photonic as well as optoelectronic circuits. In-plane as well as out-of-plane, light generation, in devices of micron size dimensions, permits the many inherent advantages of optical circuitry consistent with size and economic requirements.

At the same time, the efficacy of whispering gallery mode operation, as afforded by fractional wavelength, λ, dimension, translates into a variety of optical devices which, together with simple laser and LED emitters, permit design of optical IC's serving the range of functions associated with traditional electronic IC's. Such devices include simple detectors dependent on effective cavitation to improve sensitivity. Other device functions include switching, amplification, wavelength adjustment and variation, etc. Some such devices may introduce control signals via a third port or may use one of the basic input or output ports, e.g. to change cavity Q. The purpose includes amplitude change for a particular wavelength being cavitated, as well as to shift wavelength either regarding detection or output.

BRIEF DESCRIPTION OF THE DRAWING

FIG. **1** is a perspective view of the prototypical disk-shaped structure, usefully employed for tutorial purposes, and also of practical significance.

FIG. **2** is a diagrammatic view of a quadrant of a round disk structure in accordance with FIG. **1** with representation of internal and penetrating field lines for one particular mode of operation.

FIGS. **3** through **6** are representations of some of the structures alternative to a simple planar disk:

FIG. **3** is a perspective view of an octagonal structure,

FIG. **4** is a perspective view of a disk structure in which the peripheral region, within which whispering gallery mode energy is propagated, encloses a relatively thin membrane, a membrane of mechanical or performance consequence,

FIG. **5** is a perspective view, partly in cross-section, of a donut-shaped cavity again including a membrane, of performance characteristics related to those of FIG. **4** and FIG. **6** is a perspective view, partly in cross-section, of a structure alternative to that of FIGS. **4** and **5** in which modal action is within a peripheral path now of triangular section.

FIG. **7** is a perspective view of a representative structure—of a structure used in some of the examples herein—in which the disk-shaped element is supported upon a pedestal, e.g. as shaped by etching of the growth substrate.

FIG. **8** is a perspective view of a structure providing for out-of-plane emission as resulting from grouped notches imposed in the peripheral mode path.

FIG. **9**, again a perspective view, illustrates coupling-extraction of in-plane emission.

FIGS. **10** and **11** are perspective views depicting two device arrangements including electrodes for pumping, for signal input or signal output.

FIG. **10** for electrodes straddling the active element and

FIG. **11** for spaced electrodes on a single element surface.

DETAILED DESCRIPTION

Definition of Terms

While term meaning and context will be familiar to experts in the field, likelihood of study by those of lesser expertise as well as on-going development justify this section.

Disk—this is the active region, or active region-containing portion of the structure responsible for electromagnetic emission, always of some degree of coherence as regards emitting devices—"emitters" as here defined. While for tutorial purposes this term is generally considered as of circular configuration as defined between parallel surfaces of unvarying spacing, the term is intended to have a more generic meaning. In the generic sense, "disk" defines structures in which preponderant cavitating energy is due to total internal reflection largely within such region/s. It is convenient to refer to the disk as defining a symmetrical structure, e.g. a circular structure. As long as the fundamental requirement for total internal reflection is satisfied, the shape of the disk may be asymmetrical—in fact, providing for an oval structure may be advantageous in terms of coupling either input or output. In any event, a dimension (usually the "thickness" dimension) perpendicular to cavitation direction is but a fraction of a wavelength. This fraction, ordinarily $\leqq 0.5\lambda$, and in a category of preferred structures $\approx 0.25\lambda$, is based on wavelength measurement within the structure—taking into account both bulk refractive index and variations introduced by small structural dimensions. The subscript, eff, has reference to effective value so that n_{eff} is a measure of the refractive index taking both factors into account.

Mode—in terms of device design it is not grossly inaccurate to regard preferred structures as being generally of single-mode operation. While this is strictly true only for varying thickness devices—with thickness varying radially—such as in the structure of FIG. **4**, it continues to be approximately true for other contemplated structures. In detailed terms, there is many-mode operation for many structures. Mode multiplication takes the form of radially dependent modes, N, as well as of varying peripheral modes, M or alternatively M_1. As described elsewhere, M_1 defines the number of sides in the polygonal path of cavitating emission energy. The more general mode number, M, defines the number of undulations in the mode path without reference to the number of polygonal path sides. (An undulation is considered as corresponding with a full sinusoidal wave.)

Modal path—this contemplates the description immediately above. Polygonal sides in many circumstances consist of a single full wave (so that $M=M_1$). Operating structures, however, may depend upon modal paths in which $M=M_1$—in which there are multiple full waves, or under certain circumstances, but a half wave per side.

Penetrating field—fields which penetrate from the active region into the surrounding medium. These are the fields which offer both facility for coupling into other elements of the circuit (either through perfect structure or through discontinuity—e.g., the grooved surface of FIG. **8**) but at the same time are susceptible to unintended coupling to result in possible loss.

Whispering gallery mode/whispering mode—this terminology, familiar to those concerned with internally reflecting spherical as well as cylindrical structures, defines the form of cavitation responsible—usually in whole responsible—for operation of devices of the invention. Described in somewhat greater detail further on, the operation depends upon internal reflection as resulting from incidence of cavitating energy on a peripheral structure at an angle $\leqq$ the "critical angle".

Quantum well—it is generally understood this term refers to deviation from the hypothetical sphere defining the effective region of an exciton—within an effectively limitless medium of constant refractive index. For purposes of this description—for purposes meaningful in terms of device design—the critical dimension of a quantum well must be at least 10% shorter than the diameter of such hypothetical sphere.

Emitter—device of the invention in which functioning relies on simple emission, i.e. on presence of optical output.

Three Port Device—a device providing for three or more couplings with the disk—such couplings providing for at least two inputs and one output. Contemplated inputs accommodate pump energy and modulating signal. The output provided for is modulated in accordance with modulating signal/s. While three port devices may include three position-identifiable couplings, a single physical port may designedly be used for both of the inputs. Such a device is here defined as "three port" and is to be distinguished from "two port" devices in accordance with the following definition.

Two Port Device—a device providing for two couplings only—for a single input and a single output. "Two port" devices are, accordingly, intended to be descriptive of an "emitter". It is intended to be generic, as well, in contemplating a "modulated output"—an output providing for some intelligence-bearing variation such as, directional change, phase change, amplitude change, as well as simple presence and absence of output (in which presence, absence, interval of on or off is intelligence bearing), etc. Such a modulated output is as contemplated for a three port device, the difference being that the sole input is an already "modulated" input. The latter form of two port device makes use of the effective cavitation provided for by the invention in the direct cavitation of input. An example of the latter is a cavity enhanced detector.

General

The inventive class of micro-resonator structures present a large index contrast—a large change in refractive index for optical energy of wavelengths of operational consequence—as between a functional, optically thin semiconductor layer (the "active" region) and relatively low index surrounding medium. Structures depend upon mode cavitation similar to whispering gallery modes as described, for example, by Lord Rayleigh, "The Problem of the Whispering Gallery", *Scientific Papers*, Cambridge University, Cambridge, England, vol. 5, pp. 617–620 (1912) and T. Krauss, et al, *Electronics Letters*, vol. 26, p. 2097 (1990). Dependence upon critical angle internal reflection results in high reflectivity without the bulk and increase in modal volume associated with DBR mirrors. Fundamental requirements for "total" internal reflection are well known and are not discussed in detail. In general, the phenomenon as well as the precise angle value are set forth in texts. Basically, the requirement that the wavevector components parallel to the interface must be equal across the boundary of required index contrast results in total internal reflection for incident angles larger than $\sin^{-1}(1/n_{eff})$. Deviation is invariably in the direction of other losses which, while generally of little consequence, dictate lesser angle values to the extent feasible. Generally, it is found that such loss, as critical angle is approached, is characteristically at a value of perhaps 0.1%. A particular configuration providing for an octagonal cavitation path within a smooth circular disk results in loss of approximately one part in 10^6.

Operational advantages which are discussed in terms of emitters—largely lasers—are of the same value for other devices of the invention.

Until now, emphasis has been on emitters of the invention. The same structural approach, in providing for a thickness, or other dimension orthogonal to propagating energy—providing for such a cavity dimension—improves operation for a variety of devices relative to "bulk operation". (This term is here defined as operation in which all cavity dimensions are equal to or larger than one wavelength of the propagating energy—one wavelength as measured within the medium and as influenced by future spacing and other characteristics of the device.)

A contemplated category of three port devices takes the form of microresonators in which output variation—e.g. in direction, in amplitude, in wavelength, or simply in "on-off operation"—is the consequence of a controlling input—of a "signal input". Resulting nonlinear optical response is the consequence of Q change or of resonant frequency. Such operation is conveniently considered as analogous to the traditional electronic triode transistor. Since modulation, in most instances is due simply to change in refractive index for a single cavity to which both input and output are intimately attached, the signal may be introduced at the pump or output position.

For the most part the invention is conveniently discussed in terms of output which is optical, and which is otherwise of the character of the cavitating energy, e.g. of the same wavelength, phase, etc. In a very real sense, such output is, in fact, an extracted portion of the cavitating energy. While all contemplated devices provide for such extraction, there is an important category of devices in which such extracted energy does not, itself, serve as output. Example 4 is such an instance. Structures, for example, as shown in FIGS. **10** and **11** may provide for electrical output. Detectors and other forms of devices may convert such extracted optical (cavitating) energy into electrical form as there discussed. Conversion may take other forms. Optical output may conveniently be of some wavelength other than that of the cavitating energy, e.g. to better interface with subsequent elements, etc. Output, regardless of energy form, may be modulated or unmodulated. While likely optical—of wavelength, phase, and of other characteristics of the cavitating energy—it may take other form, e.g., electronic. The pump, if present, as always, serves to provide gain. Its output may take a variety of energy forms—of suitable optical or electronic form. As indicated, two port devices may provide for modulated output, but no gain. Two port devices may operate on the basis of coherent, as well as of information-bearing input. Such operation, in which no provision is made for gain, may literally take the form of a three port device in which two or more signals influence the output.

The modulating—or controlling—input may cause changes which alter the cavity resonance frequency or its Q value. One form of device using this phenomenon may cancel the unmodulated output, e.g. by means of delicate destructive phase interference. Such cancellation may, in other instances, represent absence of (modulation) input so as to upset the balance to, in turn, result in "on" responsive to presence of such input.

In basic terms the inventive advance depends upon the sensitivity of the internally reflecting cavity as constructed from critically-dimensioned sub-wavelength material. Small energy loss is the consequence of discussed characteristics—e.g. essential elimination of higher modes as well as characteristics associated with whispering gallery mode operation—e.g. essentially lossless reflection (as contrasted with losses associated with DBRs). In general, three port devices, as well as other devices of the invention, may otherwise function in the fashion of prior art devices. For example, a bistable optical device may be switched by means of a light pulse introduced into the cavity through a third port. Similarly, output characteristic—e.g. amplitude—may be controlled by such input. There are many such examples.

The drawing is in general terms as designed to serve as basis for the improved cavity of the invention. It is not designed to explicitly serve as discussion of any of the many possible device functions—two port or three port. Any of the structures described in the figures may serve many such functions.

Microstructures of the invention, while usefully employed as discrete devices, are of primary interest for their value in integrated circuitry. In particular, operating as lasers, permitted low power operation satisfies desire for low threshold consistent with small heat loss. Contribution to this operating desire is advanced by permitted effective matching between small gain volume and single optical mode—generally the first TE mode. Optical gain for disk modes is provided by one or more optically pumped quantum wells in the plane of the disk. Generally, active region thickness—for single quantum well structures, disk thickness—is less than $\lambda/2n_{eff} \approx 2{,}000$ Å for $\lambda = 1.5\ \mu m$ and $n_{eff} = 3.5$. Structures are desirably characterized by high index contrast as between the disk and the surrounding medium, in particular, as concerns the disk region of greatest modal energy concentration. This contrast is generally defined as between active material—in accordance with usual structures defined as including active layer/s together with encompassing spacer/barrier layers. Surrounding media for structures described may be space—e.g., vacuum or air—or some, likely passive, low index medium such as amorphous silica, SiO_2. The illustrative values set forth translate into an index contrast (or index ratio) n_{eff}/n_o where n_o equals index of the surrounding medium. Index contrast of this order of magnitude or greater is attainable for likely operating wavelengths which are less than 1.5 μm. Other considerations having to do e.g., with ease of fabrication, may dictate lesser contrast values. While the teachings of the invention may be implemented by appropriate variation in such design considerations as disk radius, other considerations such as desire for small size for convenient integration, as well as fabrication ease, all suggest values of contrast of a minimum of 1.3 or preferably greater, e.g., greater than 1.5. This high index contrast coupled with sub-λ thickness dimension effectively confines the active optical mode/s and is a key feature in assuring effective overlap with the gain layer (i.e., with the active region—generally the quantum well active region).

FIG. 7 depicts one form of structure designed with a view to the above considerations. It provides for a disk **70** consisting of active region **71** sandwiched between spacer layers **72** and supported upon cylindrical pedestal **73** as fabricated from material initially serving as an epitaxial growth substrate, for example, in accordance with a procedure outlined below.

Fabrication

The device of FIG. 7, as used in Example 1, was fashioned from epitaxially-grown InP/InGaAsP layered material. One such device consisted of a 100 Å thick quantum well layer **71** of InGaAs sandwiched between 200 Å thick barrier layers **72** of InGaAsP to result in a total disk **70** thickness of 500 Å. In other work, use was made of a 1500 Å disk consisting of 6 such 100 Å active layers as separated by barrier material. Initial growth was on an InP substrate part of which was retained upon etching to result in pedestal **73**. Photolithographic techniques were used to pattern disks with diameters of 3 μm, 5 μm and 10 μm. An HCl solution was used to selectively etch substrate material while leaving the functional InGaAs/InGaAsP disk unetched.

In a working example the InP pedestal **73** retains a rhombus shape cross section as due to the anisotropic nature of the HCl etchant. One such pedestal was approximately 1 μm in diameter and 2 μm in height, so leaving a peripheral region of radial dimension ≃1 μm within which index contrast is defined as between disk **70** and ambient—in the instance of Example 1, of ambient air. In another working example, such a structure was encapsulated in 0.5 μm of SiO_2 deposited by Chemical Vapor Deposition.

EXAMPLE 1

A microdisk as described above, of diameter 5 μm, is optically pumped with a HeNe laser operating at $\lambda=0.63$ while cooling with liquid nitrogen. The spectrum for the single quantum well structure lases at a center wavelength of 1.3 μm with a spectral linewidth of <1 Å. The 1.3 μm laser spike rises above the broad photoluminescent background by a factor approaching 10×.

The threshold value for the structure of Example 1 is below 200 μW. Since the disk **70** has a volume of the order of 10^{-12} cm^{-3}, the pump power of the order of 1 milliwatt is equivalent to a power density in the disk which approaches 10^9 watts cm^{-3}. Heat sinking for the structure depicted in FIG. 7 is sufficient to prevent destructive temperature rise.

EXAMPLE 2

The procedure of Example 1 is carried out for a 5 μm diameter disk of thickness of 1500 Å containing 6 quantum wells. Measured output laser power approaches 1 μw for a pump power slightly below 500 μW. The spike intensity as coupled out vertically is more than 100× greater than the background photoluminescence.

Micro-cavity design, depends, inter alia, on active region film thickness approximating one-quarter wavelength, λ_b (as measured in bulk material)—which may be increased to greater, still sub-λ thickness to increase figure of merit accounting for imperfections defining departure from the hypothetical device. High reflectivity and sub-λ thickness results in good matching efficiency between small gain volume and single optical mode to result in low power requirement, e.g., in low laser threshold. High index contrast reduces loss associated with penetrating field, and enhances mode selectivity. Designation of operating modes is yielded by solution of Maxwell's equations (see, for example, J. D. Jackson, "Classical Electrodynamics", John Wiley & Sons, New York (1975)). Importantly, functional layers less than $\lambda/2\ n_{eff}$, in which n_{eff} is the effective refractive index for electromagnetic wave energy at the device operational wavelength, λ as measured in vacuum, support only the lowest order TE and TM guided waves. For thickness value of approximately $\lambda/4\ n_{eff}$, coupling to the TE mode dominates to such extent that interactions with TM waves as well as all unguided waves may be disregarded.

EXAMPLE 3

A six quantum well structure similar to that of Example 2, of the form shown in FIG. **11**—5 μm diameter, 1500 Å thick—is operated as an electrically pumped laser. Coupling of output is by means of a light guide of shape and spacing as diagrammatically shown in FIG. **9**. The guide is of 800 μm in length and 4 μm in width—the same guide used for coupling input energy to be detected in Example 4. Drive energy as applied across the spaced electrodes, consists of 1 milliampere pulses of 200 psec duration and 10 μsec spacing to result in a repetition rate of 10^5/sec. Laser emission, as coupled into the light guide, is of 1.5 μm vacuum wavelength.

EXAMPLE 4

A structure as used in Example 3—six quantum well, 5 μm diameter, 1500 Å thickness—arranged in the configuration of FIG. **11** is operated as a two-port detector—as a cavity-enhanced detector. For purposes of the Example, element **113** is a simple current meter. Input optical energy is coupled in by means of a light guide of the configuration of element **91** of FIG. **9**. The dielectric light guide is 800 μm in length and 4 μm in width. Pulses of nominal wavelength 1.5 μm (always as measured in vacuum) of approximately 200 psec as delivered from the laser operated in accordance with Example 3, serve as signal to be detected. Output signal consists of current pulses approximately 0.4 microampere of duration of 175 psec.

EXAMPLE 5

A disk of the dimensions and otherwise of the character described in Example 4 is operated as a three-port, all-optical device. Provision is made for a first optical input by coupling with a dielectric light guide as described in Example 4. Light output is by means of a second guide of the same dimensions and character. Provision is made for a second optical input by means of a laser beam made incident on the broad upper face of the disk. Operation—device function—may take any of several forms. In one form, light entering by means of the first optical input is only seen at the output when the disk is pumped by laser light entering by means of the second input. In a second form of operation, the disk structure is brought just shy of lasing threshold by means of light entering by means of the second input. Light is seen at the output only upon light introduction by means of the first input. In this form of operation the device may be considered as a gated amplifier.

A disk of the dimensions and otherwise of the character described in Example 4 is operated as a three-port, all-optical device. Provision is made for a first optical input by coupling with a dielectric light guide as described in Example 4. Light output is by means of a second guide of the same dimensions and character. Provision is made for a second optical input by means of a laser beam made incident on the broad upper face of the disk. Operation—device function—may take any of several forms. In one form, light entering by means of the first optical input is seen at the output when the disk is pumped by laser light entering by means of the second input. In a second form of operation, the disk structure is brought just shy of lasing threshold by means of light entering by means of the second input. Lasing threshold is attained upon light introduction by means of the first input. In this form of operation the device may be considered as a gated amplifier.

Active Region—Configuration, Dimensions

Reference is made to FIGS. **1** through **6** in this section.

A cautionary note—it is convenient to discuss devices in terms of ray optics (in terms of particles rather than of more complex but accurate wave energy). "Critical angles" for "total internal reflection", as well as cavitation paths defined in terms of bounce points are usefully employed. Inaccuracies so introduced are of particular consequence for the involved dimensions—of the order of whole and fractional wavelengths.

The polygonal path, simplistically representing the mode path, is generally discussed here in terms of M_1, the "mode number" corresponding with the number of sides of the polygon. The more general mode number, M, corresponds with the number of undulations or oscillations in the mode path without reference to number of "bounces". (So, for example, a four-sided polygon—$M_1=4$—may correspond with a path of a total of 8 undulations or one wave per side.)

FIGS. **1** through **6** are generally illustrative of a larger variety of configurations.

FIG. **1** depicts a disk **10**, having a smooth continuous curved edge **11**, in this instance defining a circle. The figure is intended as representative of a subset of configurations defined by parallel planar surfaces e.g., surfaces **12** and **13**, at least over some relevant region of the device, with such planar surfaces being separated by the critical sub-wavelength dimension **14**, e.g. the usually preferred $\approx\frac{1}{4}$ wavelength discussed. This subset is of lateral configuration which may be circular as well as elliptical or irregular shape. Dimensions and operating conditions are such as to result in cavitation defining octagonal path **15** ($M_1=8$).

FIG. **2** is a contour map including a quadrant of disk **20**, representing positions of constant electromagnetic field lines **21**, for such values within disk **20** and lines **22** for such values relating to penetrating field within region **23** external to the disk. As depicted, maximum positive field values are positioned at hillocks or peaks **24** and maximum negative field values are positioned at depressions **25**. Accordingly, FIG. **2** is representative of two undulations per quadrant, or eight undulations for the entire disk, so corresponding with an octagonal modal path such as path **15** of FIG. **1** in which each side of the path is made up of one full wave. Field portions represented by contour lines **22**, in representing field penetrating to external region **23**, are potential coupling areas but represent potential loss as well, e.g. as due to surface roughness-scattering as well as unintended coupling.

FIG. **3** is representative of a subset of configurations again defined by parallel planar surfaces **30**, **31** of critical spacing as discussed, e.g. with regard to appropriate mode selection but, in this instance, defined by a perimeter constituted of equal length flat faces **32**. As in other figures, the configuration shown is intended as representative of a larger class—e.g., as constituted by polygons, irregular as well as regular, of lesser or greater number of sides Modal path **33**, shown as a broken line, is depicted as octagonal and, to first approximation, is equivalent to modal path **15** defined within a circular version of disk **10** of FIG. **1**. Operationally, such a path **33** as defined within a disk connecting positions **34** is equivalent to modal path **12** but for second order variations, e.g. with regard to loss or other implication of variation in magnitude of penetrating field as related to the lateral thickness of material encompassing path **33** particularly in proximity at positions **34**. Representation is meant to include irregular as well as regular shapes so that, in this instance, sides **32** may be unequal in lateral dimension always providing for a predominant polygonal modal path, which while possibly of differing numbers of undulations for different path lines, is so designed as to maximize desired coupling and to minimize undesired coupling. An irregular polygonal shape may, for example, serve to accommodate an arrangement such as that of FIG. **11**—to provide for an irregular path of more nearly constant coupling independence of the pedestal supports/electrodes shown.

FIG. **4** depicts a cavity configuration physically differing but functionally similar to that of FIG. **1**. Critical spacing to accommodate the whispering modes, common to all embodiments of the invention, is that between surfaces **40** and **41**, in this instance defining a smooth curved edge surface **42**. Likely of little device-function significance, although possibly involved in pumping—e.g. electrical or optical, membrane **43** may serve for physical stabilization of the structure. Edge **44**, together with a possible mating edge on the underside of membrane **43**, will be elemental in mode selection—will be of influence in selection of a modal path of sufficient M_1 as to lessen energetically unfavored field penetration. This figure is intended as representative of flat-sided (polygonal) as well as curve-sided structures, both of regular or irregular configuration.

FIG. **5** is representative of a class of embodiments similar to that of FIG. **4** but depending upon modal path selection/containment within a perimeter region of varying thickness. The specific example shown depends upon a functional region **50** of generally circular cross-section as defined by surface **51**. Again, structural rigidity is afforded by membrane **52** forming a continuum within the enclosed portion of region **50**. Dimension **53** is relevant, e.g. from the standpoint of confinement, consistent with the inventive thrust—for a preferred embodiment is $\approx\lambda/4n_{eff}$. Again, as in FIG. **4**, the lateral dimension of region **50** is determinative of mode selection and, if of sub-wavelength dimension as discussed, may additionally offer useful confinement as well.

FIG. **6** depicts a configuration alternative to FIG. **5**. It depends upon a membrane **60** for stabilization of a modal path region **61** of cross section defined by surfaces **62–65**. As with other configurations depicted, the category represented may be of regular or irregular shape, may be defined by curved or faceted surfaces. The particular triangular cross-section shown is usefully employed for more specific mode selection for given dimensions.

While a significant advantage of the inventive approach as compared with that of the SEL involves in-plane emission to facilitate coupling with other elements of an IC, it is useful to provide for out-of-plane emission as well. FIG. **8** depicts a disk **80** defined by planar surfaces **81** and **82** within circular perimeter **83**. Grooves **84** are designed to couple a part of cavitating energy, not shown out-of-plane. In this version, whispering mode structures of the invention may serve in the manner of the familiar SEL, for example, in chip-to-chip communication. For cavitating energy in a clockwise direction, out-of-plane direction is determined by the angle of groove sides **85** as coupled with index contrast. In an alternative approach, counter clockwise cavitation may result in out-of-plane emission by virtue of simple reflectivity of groove surfaces **85**—perhaps as effected by use of mirror layer/s, not shown.

FIG. **9** depicts a disk structure **90** in proximity with path member **91**, so positioned and of such interspacing as to provide for in-plane coupling. Experimental work including that reported in Examples 1 and 2 has involved light pumping. A number of considerations including ease of fabrication dictate this approach, and it is likely that it will continue to define an area of consequence. On the other hand, the inventive principle, in being generically based, upon whispering mode operation in critically thin structures, is not so limited. Principle of operation is applicable to the various pump arrangements that have been found or may be found functional. For many purposes, direct electrical pumping continues to be desirable—may justify fabrication complications which are aggravated at the small dimensions contemplated.

FIGS. **10** and **11** depict electrically pumped lasers otherwise in accordance with the foregoing. In FIG. **10** the disk structure **100**, which may take any of the forms described, may be regarded as electrically pumped by means of straddling electrodes **101** and **102** shown as biased via circuit **103** as powered by power source **104**. Alternatively, element **104** may be an element permitting operation as a detector. Simplistically, this element **104** may be a current meter responsive to the emf developed across straddling electrodes **101** and **102** by virtue of cavitating energy responsive to pumping—e.g. responsive to light pumping. In this use detection may take the form of that described in Example 4 which makes use of the alternate structure of FIG. **11**. This structural approach may find favor in that the electrodes may serve as physical support for one or both sides of disk **100**. Either or both of the embracing electrodes **101** and **102** may be formed by selective etching from a growth substrate as discussed in fabrication of pedestal **73** of the structure of FIG. 7. Addition of dopant, e.g., to the InP—likely into the entirety before etch-definition—may be desirable to lessen series resistance. Since now forming a junction—likely a pn junction—conductivity-imparting dopant will be significant dopant, in one instance, n-type; in the other, p-type. Specific design parameters with a view to electrical pumping are not properly within the province of this description and are well known.

FIG. **11**, operating as an electrically pumped disk structure **110** is alternative to that of FIG. **10**. In this arrangement, positive and negative electrodes **111** and **112**, respectively, powered by dc current source **113**, via leads **114**, are affixed to a common plane **115** of disk **110**. Spacing and, more generally, positioning of electrodes **111** and **112** are such as to provide for a peripheral cavitation path of desirable independence of the electrodes and, if surface is of roughness to result in performance-significant, unwanted scattering, of peripheral surface **116**. Regardless of configuration—whether smooth or faceted-design optimization may result in a disk **110** of a greater major dimension in the direction defined by the electrodes. The resulting oval or irregular polygonal configuration may better provide for lessening of unwanted coupling between cavitating energy and the electrodes. Alternatively, such electrode/s may serve as well for coupling of emitting energy.

Operating as a detector, element **113** is a current meter or other device sensitive to voltage developed across electrodes **111** and **112**. Examples 4 and 5 concern use as a detector—as a two-port, simple cavity-enhanced detector, and as a three-port light pumped amplifying detector, respectively.

Other Considerations

The invention has been described in terms sufficient to those of requisite skill in the art. Experimentally observed design/material implications have been set forth where relevant to matters under discussion. Additional observations are briefly noted.

It has not been considered appropriate to exhaustively describe presently available suitable active materials. In general, material choice is with regard to the same considerations as applied to earlier laser structures. Choice is accordingly on the basis of desired wavelength of operation with a view to a variety of other matters, most importantly with regard to fabrication.

Selected pump power may serve to favor a particular desired mode. In certain experiments, for example, it was found that decreasing pump power in a device operating above lasing threshold often resulted in mode switching—in the instance of 5 μm diameter disks, in switching by 0.06 μm. This observation, usable for optical laser use, is consistent with a whispering mode having a modal number $M \approx 38$. The lowest loss modes for this structure appear to have a radial mode number $N \approx 4$. The mode so defined has a maximum energy modal path which is sufficiently separated from the outer edge to lessen loss due to surface scattering. In addition separation from the pedestal is sufficient to prevent significant unwanted coupling. In this connection, it has been observed, as expected, that coupling, and therefore surface emission, emanates from the two points of the rhombus-shaped pedestal most distant from the center of the disk.

I claim:

1. Apparatus comprising at least one element providing for cavitation of electromagnetic energy with cavitation being primarily dependent upon whispering gallery modes in accordance with which modal path is defined within a body of high refractive index for such energy relative to refractive index of surrounding ambient at an interface between such body and ambient, such path being polygonal and of at least three sides with retention being primarily due to incidence of cavitating wave energy at or below the critical angle defined at such interface

Characterized in that the said element, at least over a region corresponding with a substantial portion of such cavitation path, has a dimension of a maximum of $\lambda/2n_{eff}$ as measured in a direction normal to the plane of the path, in which λ is the wavelength of cavitating energy as measured in a vacuum and n_{eff} is the actual refractive index for such cavitating energy, such value accounting both for variation in bulk index for the medium of the body and for such variation on such bulk index as is introduced due to constraining surfaces, and in which such interface is of refractive index contrast for cavitating energy which is numerically equal to at least 1.5, such value yielded by the fraction n_{eff}/n_S in which n_{eff} is the effective refractive index for cavitating energy within the said body and n_S is the refractive index for such energy outside the defining interface of such body.

2. Apparatus of claim **1** in which said at least one element provides for electromagnetic emission of the wavelength and phase character of cavitation energy

3. Apparatus of claim **2** in which the said normal dimension approximates the value $\lambda/4n_{eff}$.

4. Apparatus of claim **2** in which a substantial portion of such cavitation path is within a region in the said body defined by plane parallel flat interfaces.

5. Apparatus of claim **2** in which such cavitation path is within a peripheral region of the said body and in which such peripheral region encloses an inner region which is substantially thinner than the said normal dimension.

6. Apparatus of claim **2** in which the said element is of maximum dimension of the order of microns.

7. Apparatus of claim **2** in which such element designedly attains lasing threshold in operation.

8. Apparatus of any of claims **1–7** in which the said cavitational path defines a polygon of at least four sides.

9. Apparatus of claim **2** together with means for coupling emitted energy.

10. Apparatus of claim **9** in which such means provide for in-plane coupling.

11. Apparatus of claim **10** in which coupling includes a gap intermediate said element and the defined emission path.

12. Apparatus of claim **9** in which such means provides for out-of-plane coupling.

13. Apparatus of claim **12** in which such means entails at least one physical groove on a lateral surface of said body.

14. Apparatus of claim **13** in which such means entails a plurality of such grooves.

15. Apparatus of claim **2** comprising an integrated circuit.

16. Apparatus of claim **15** in which said integrated circuit includes a plurality of said elements.

17. Apparatus of claim **16** in which said integrated circuit is optoelectric.

18. Apparatus of claim **17** in which said integrated circuit includes means for pumping said elements.

19. Apparatus of claim **18** in which said means is optical and is provided by a laser pump.

20. Apparatus of claim **1** in which said at least one element constitutes a three port device, the first port providing for input pump energy, the second port providing for exiting output energy, and the third port providing for variation in some property of the output energy.

21. Apparatus of claim **20** in which such property is time-dependent elimination of output energy so resulting in intervals between output energy pulses.

22. Apparatus of claim **20** in which such property is exiting direction.

23. Apparatus of claim **20** in which such property is variation in amplitude.

24. Apparatus of claim **20** in which such property is variation in phase.

25. Apparatus of claim **1** in which said at least one element provides for electromagnetic input, a substantial part of which is of frequency and polarization to satisfy cavitation requirements.

26. Apparatus of claim **25** in which said at least one element is a detector.

27. Apparatus of claim **26** in which said at least one element provides for electrical output.

* * * * *

EXHIBIT B

US006259717B1

(12) **United States Patent**
Stone et al.

(10) **Patent No.:** **US 6,259,717 B1**
(45) **Date of Patent:** ***Jul. 10, 2001**

(54) ASYMMETRIC RESONANT OPTICAL CAVITY APPARATUS

(75) Inventors: **Alfred Douglas Stone**, North Haven; **Richard Kounai Chang**, Hamden, both of CT (US); **Jens Uwe Noeckel**, Dresden (DE)

(73) Assignee: **Yale University**, New Haven, CT (US)

(*) Notice: Subject to any disclaimer, the term of this patent is extended or adjusted under 35 U.S.C. 154(b) by 0 days.

This patent is subject to a terminal disclaimer.

(21) Appl. No.: **09/056,525**

(22) Filed: **Apr. 7, 1998**

Related U.S. Application Data

(63) Continuation of application No. 08/725,127, filed on Oct. 2, 1996, now Pat. No. 5,742,633.

(51) **Int. Cl.**^{7} **H01S 3/08**

(52) **U.S. Cl.** **372/92**; 372/108; 385/146

(58) **Field of Search** 372/92, 108; 385/146

(56) **References Cited**

U.S. PATENT DOCUMENTS

5,742,633 * 4/1998 Stone 372/92

* cited by examiner

Primary Examiner—Teresa M. Arroyo
Assistant Examiner—Gioacchino Inzirillo
(74) *Attorney, Agent, or Firm*—Ohlandt, Greeley, Ruggiero & Perle, LLP

(57) **ABSTRACT**

An asymmetric resonant optical cavity is constructed of an optically transmissive dielectric material having an index of refraction n. The cavity is configured as an oval cross-section of area A, having major and minor axes. An optical input couples an optical signal of wavelength λ into the cavity. An output coupler is positioned in a near-field region of a surface point of the cavity thereby enabling coupling thereinto of optical energy of wavelength λ. The surface point on the cavity is determined by a minimum value of an expression which relates the Sin of the angle of incidence, at an angle ø, to the curvature of the outer surface of the cavity. Further, the index of refraction n of the cavity's dielectric is chosen so as to avoid emission of physically separated beams at the point of exit of a beam

5 Claims, 6 Drawing Sheets

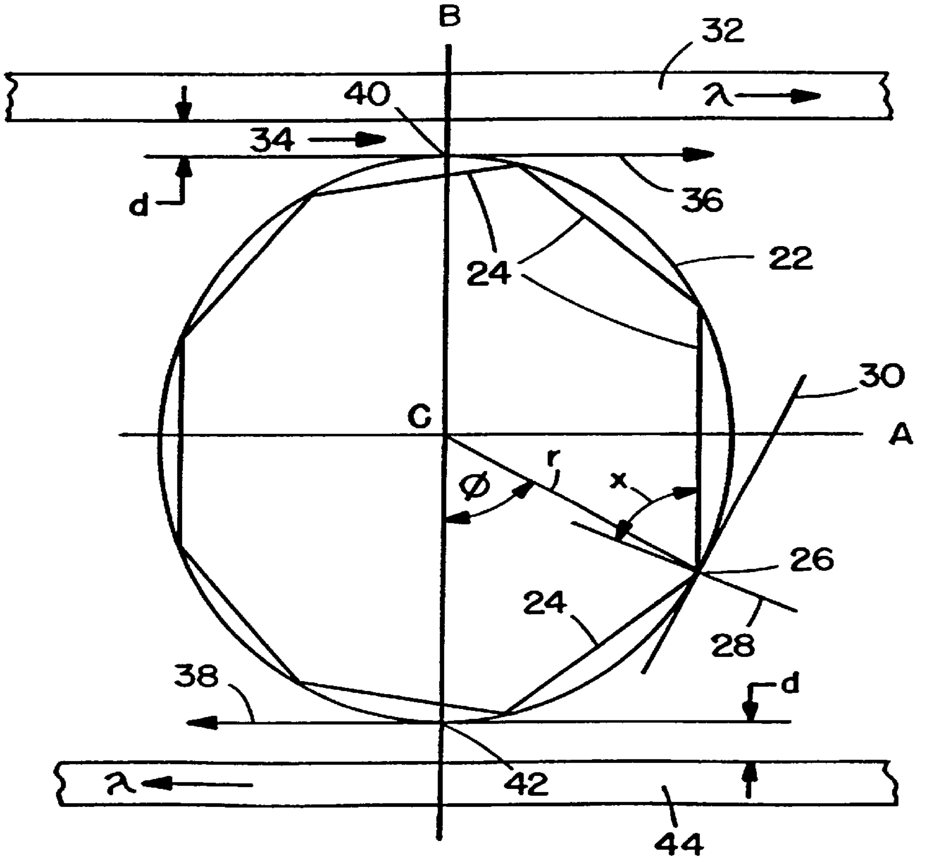

FIG. 1.
(PRIOR ART)

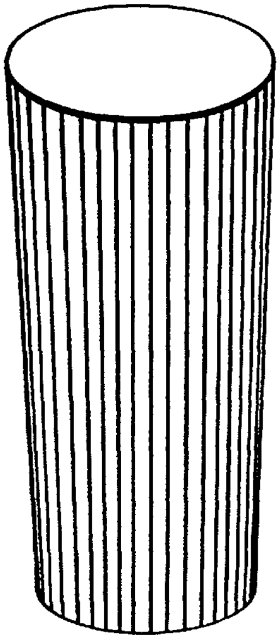

FIG. 2A.
(PRIOR ART)

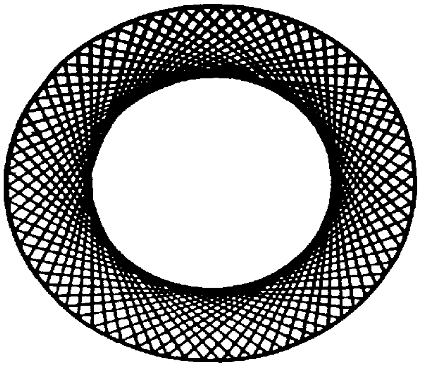

FIG. 2B.
(PRIOR ART)

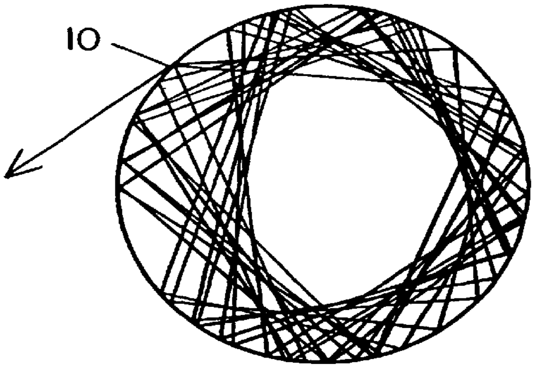

FIG. 2C.
(PRIOR ART)

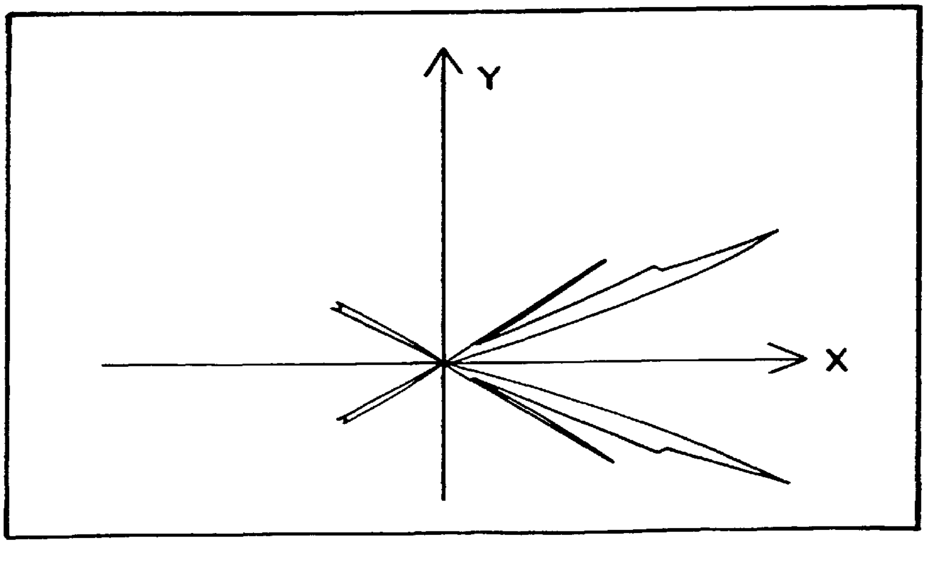

FIG. 3A.

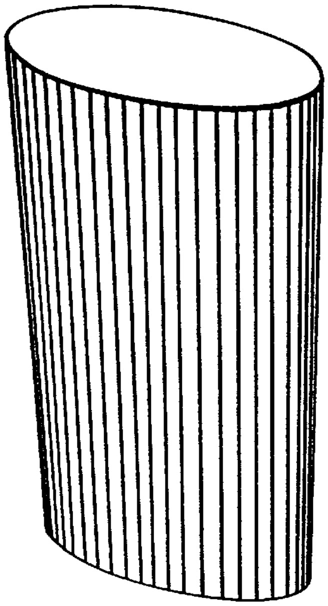

FIG. 3B.

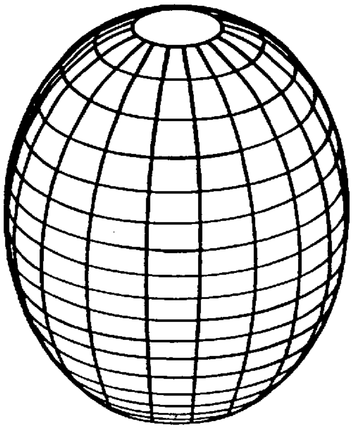

FIG. 4.

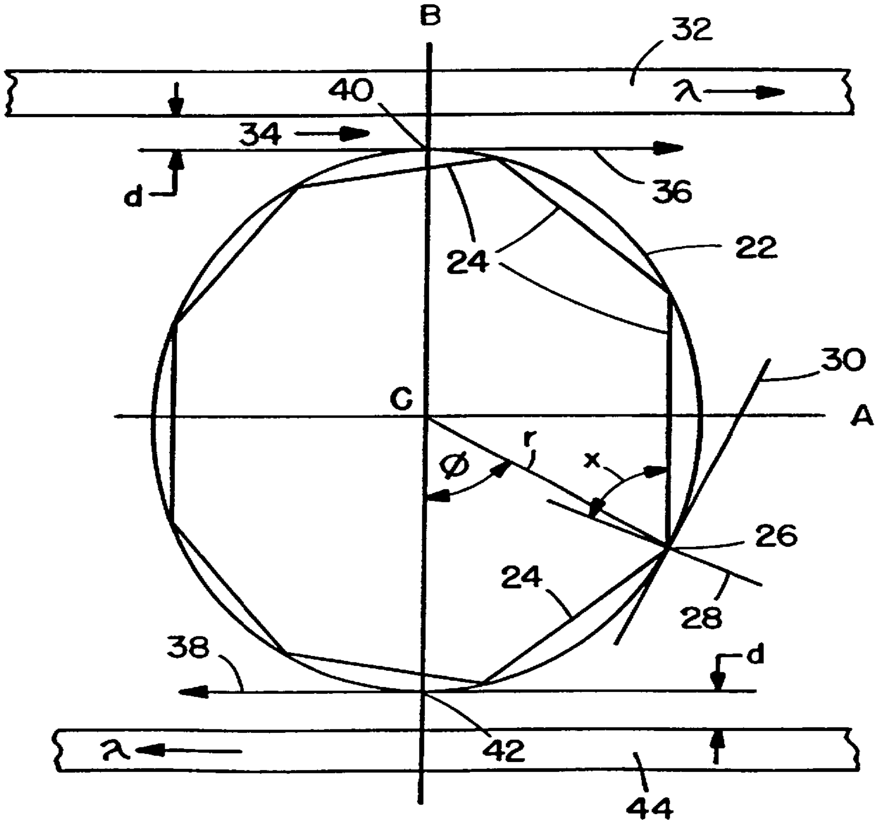

FIG. 5.

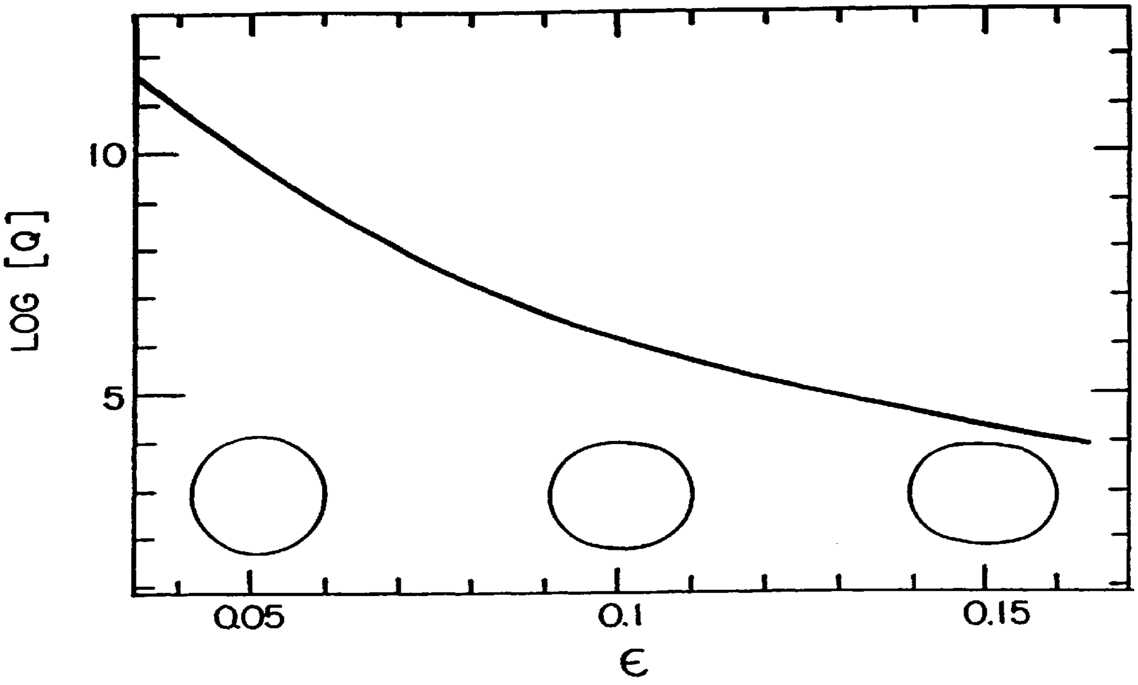
10
5
LOG [Q]
0.05
0.1
0.15
ε

FIG. 6.

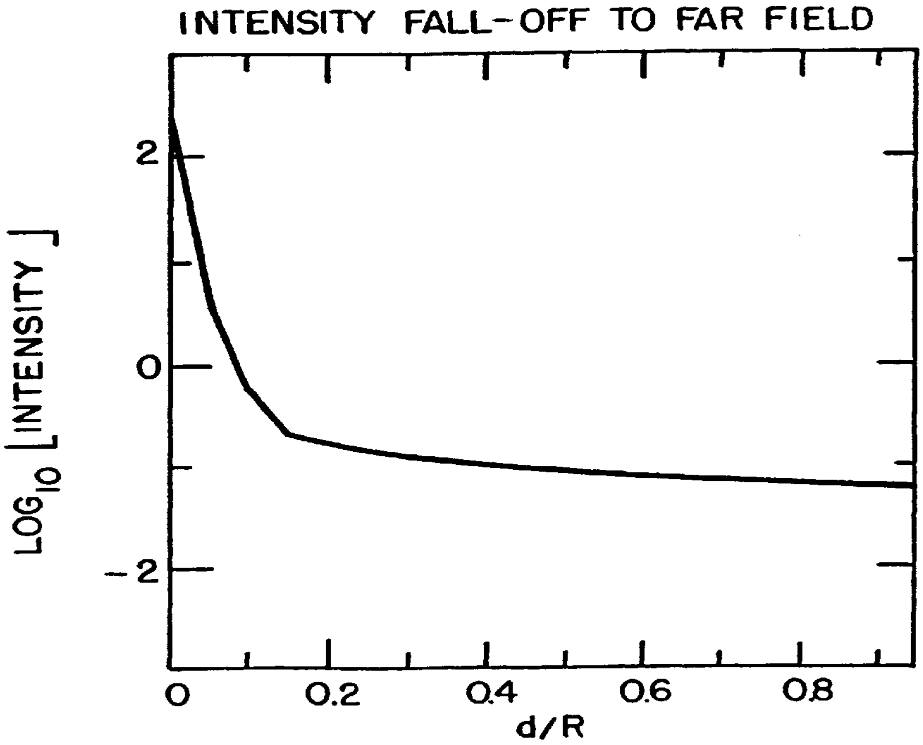
INTENSITY FALL-OFF TO FAR FIELD
2
0
-2
LOG10 [INTENSITY]
0
0.2
0.4
0.6
0.8
d/R

FIG. 7.

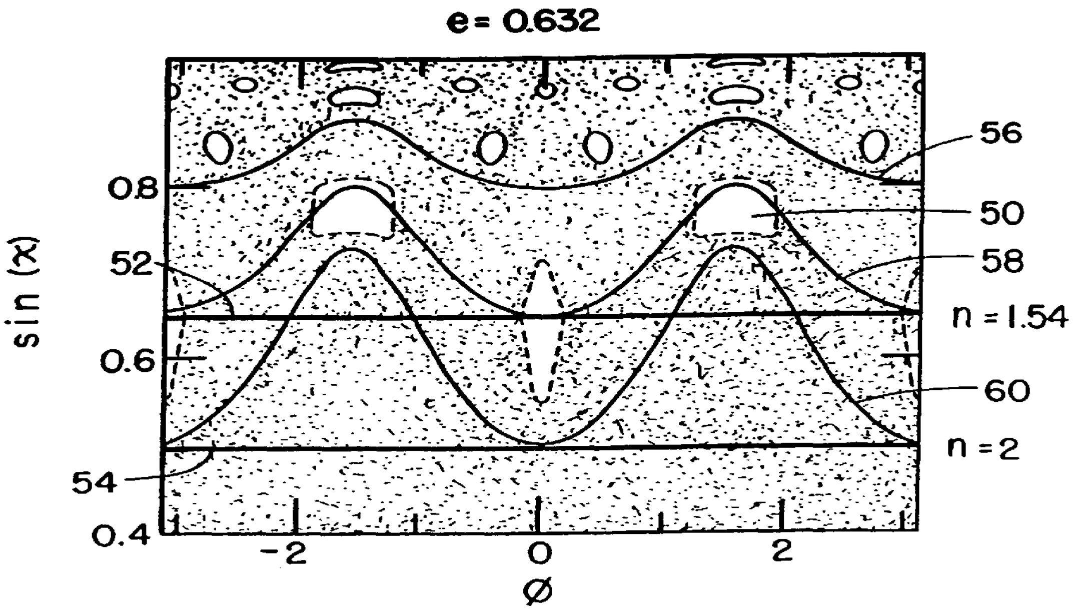
e= 0.632
0.8
0.6
0.4
sin (χ)
-2
0
2
Ø
56
50
58
n = 1.54
60
n = 2
52
54

FIG. 8.

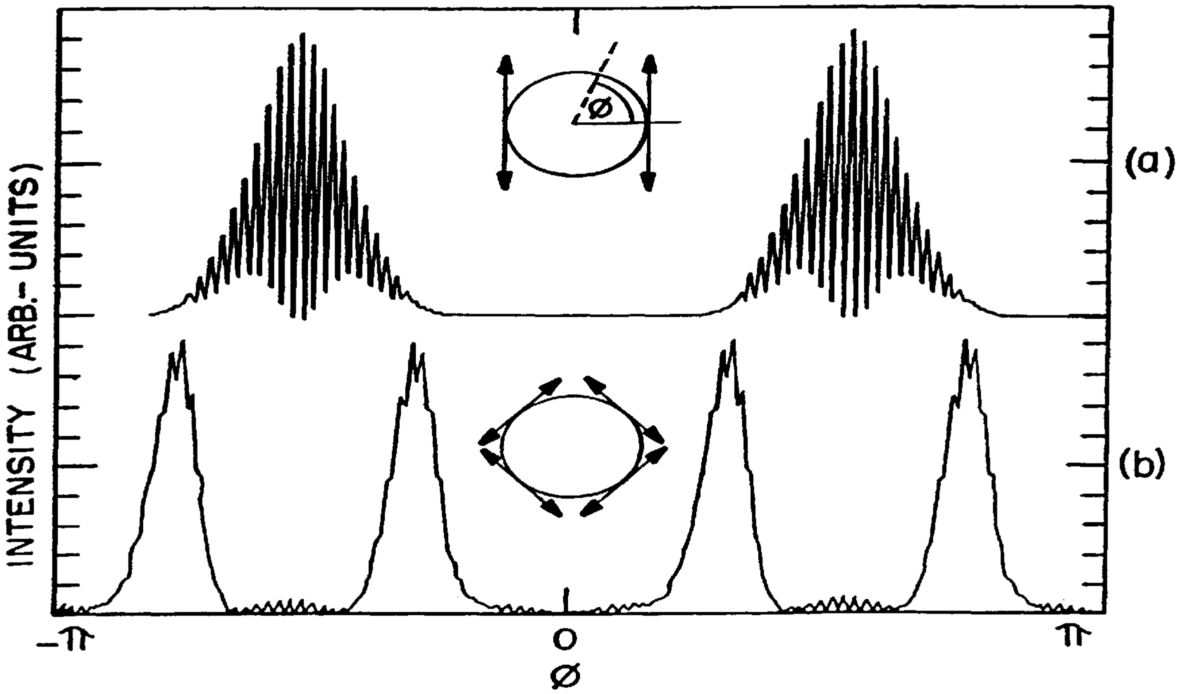
INTENSITY (ARB.- UNITS)
Ø
(a)
(b)
-π
0
π
Ø

FIG. 9A.

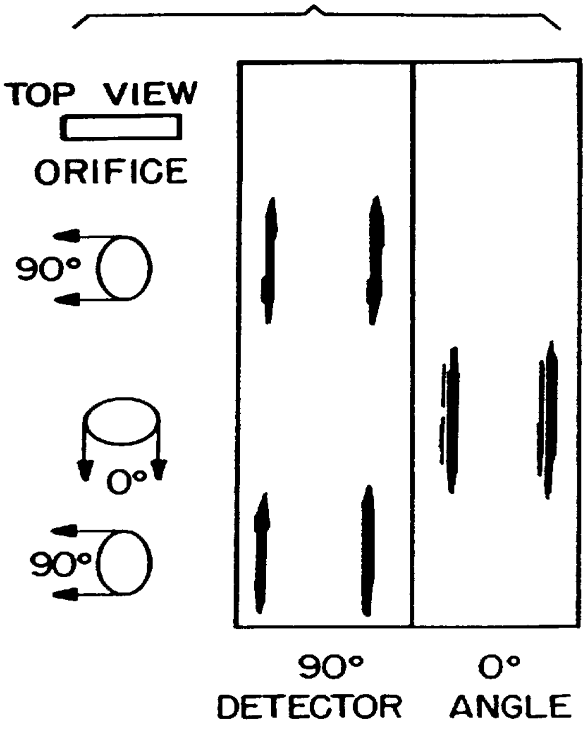

FIG. 9B.

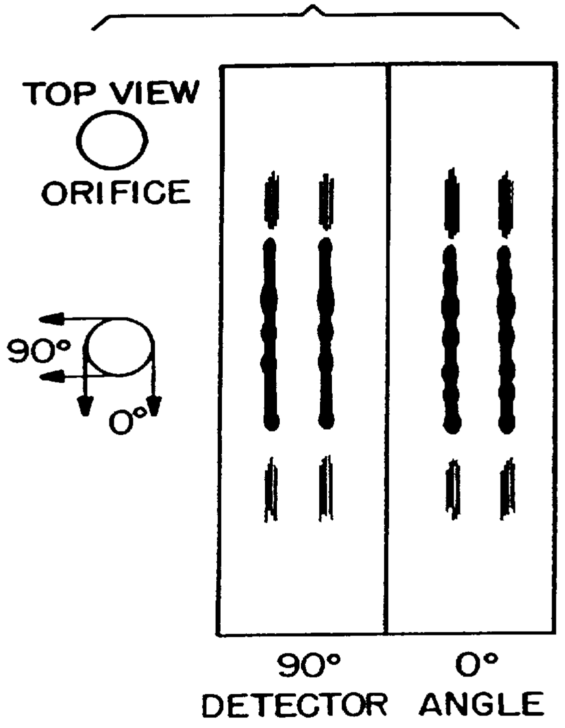

FIG. 10.

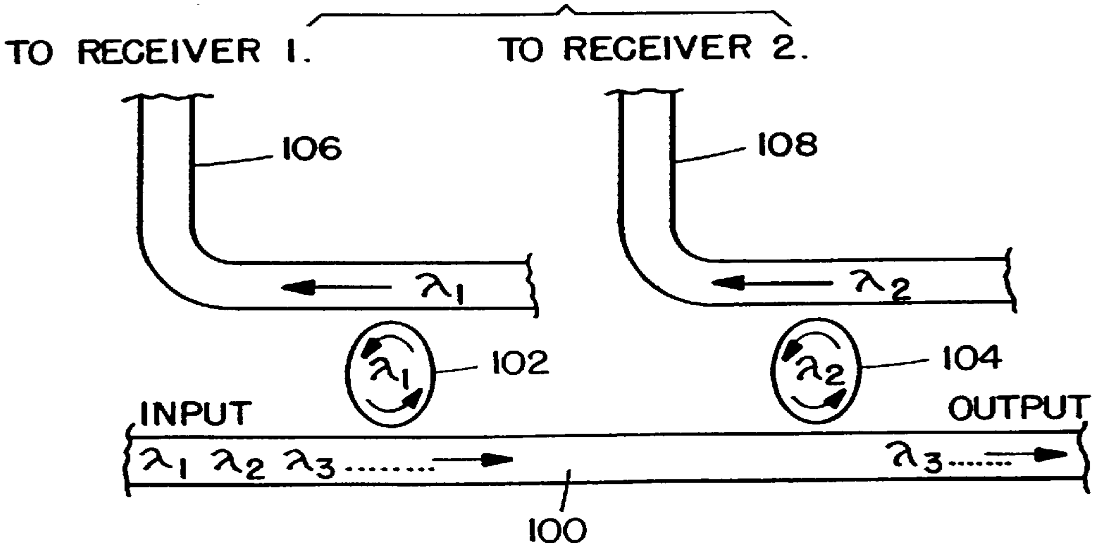

FIG. 11.

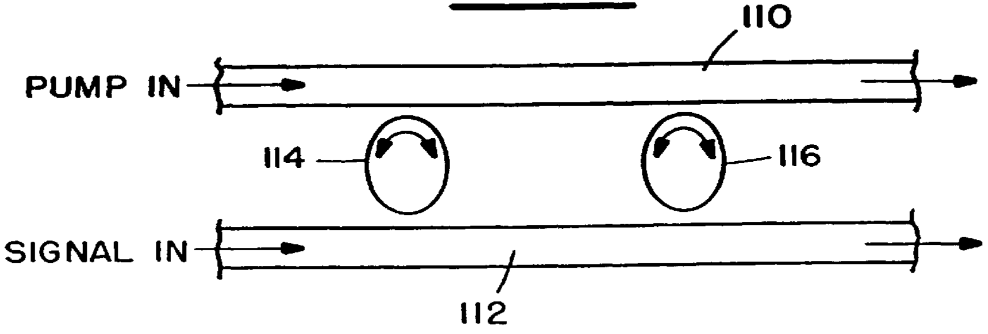

FIG. 12.

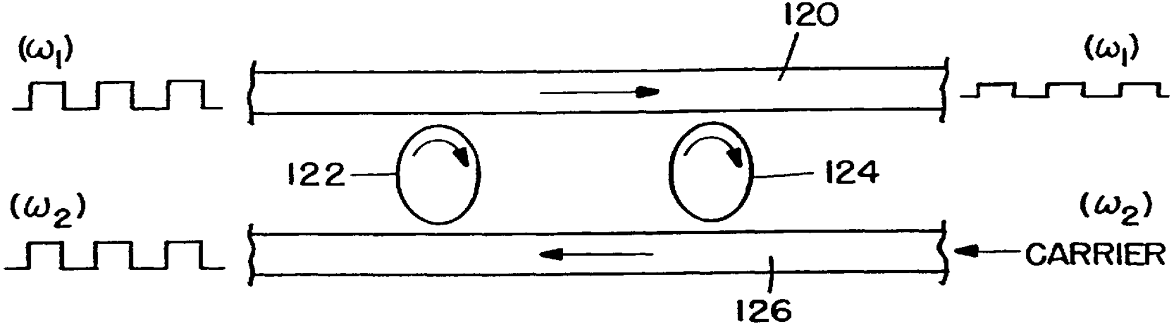

FIG. 13.

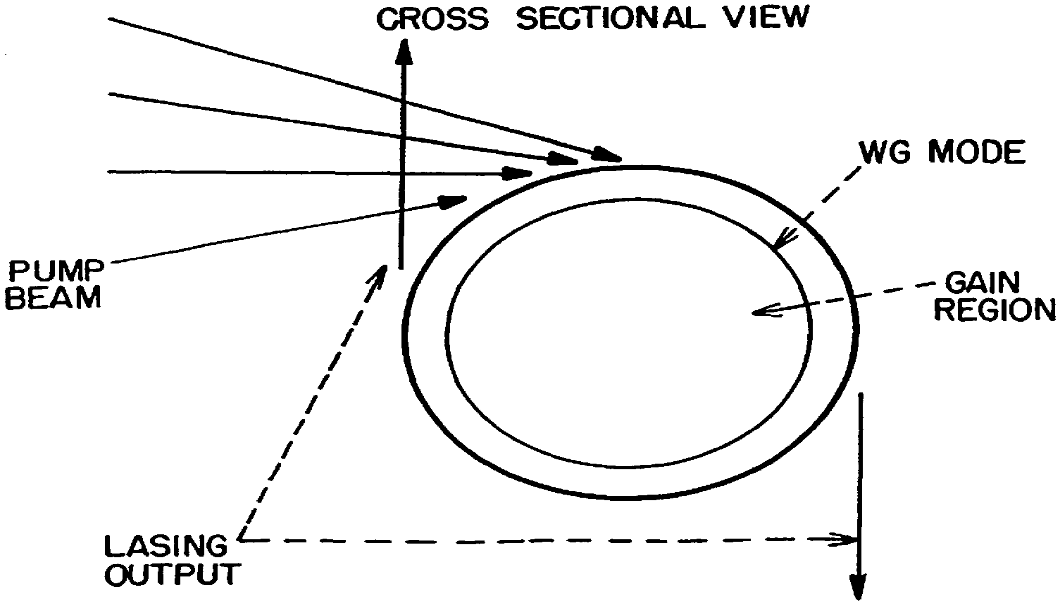

ASYMMETRIC RESONANT OPTICAL CAVITY APPARATUS

This Application is a continuation of U.S. patent application Ser. No. 08/725,127, filed Oct. 2, 1996, now U.S. Pat. No. 5,742,633.

The U.S. Government has license rights to this invention as a result of partial support of its development under U. S. Army Research Office Grant DAAH 04-94-G 0031 and NSF grant DMR 9215065.

FIELD OF THE INVENTION

This invention relates to resonant optical cavities and, more particularly, to asymmetric optical cavities which provide directional light emission at a wavelength dependent upon the structure of the optical cavity.

BACKGROUND OF THE INVENTION

A new class of optical resonators is comprised of convex dielectric bodies which are substantially deformed from cylindrical or spherical symmetry. See: J. U. Nöckel, A. D. Stone and R. K. Chang, Optics Letters 19, 1693 (1994); A. Mekis, J. U. Nöckel, G. Chen, A. D. Stone and R. K. Chang, Phys. Rev. Lett. 75, 2682 (1995); J. U. Nöckel and A. D. Stone, in *Optical Processes in Microcavities,* editted by R. K. Chang and A. J. Campillo (World Scientific Publishers, 1996). Such asymmetric resonant cavities (henceforth ARCs) exhibit high-Q (quality factor) whispering gallery (WG) modes (Q>1000) at distortions as large as 50% of the undeformed radius, R, of the corresponding circular (symmetric) resonant cavity. The emission pattern from these modes is highly directional, in contrast to the isotropic emission from symmetric cavities.

WG modes of symmetric cavities (dielectric spheres and cylinders) have high Q (long lifetime) because the light trapped in such a mode (when described by ray optics) always impinges on the boundary at the same (conserved) angle of incidence, χ, where $\sin \chi >= 1/n$ (n is the index of refraction of the dielectric); hence the light is almost totally internally reflected. Due to the curvature of the surface, there is an exponentially small correction to the law of total internal reflection which allows light to escape after very long times (this is called “evanescent leakage”). In ARCs on the other hand, the dominant mechanism for emission of light is not evanescent leakage but direct refractive escape via Snell's law because the angle of incidence $\sin \chi$ is not conserved. In the ray-optics language these ARC resonances correspond to ray trajectories which initially are in WG orbits with $\sin \chi > 1/n$, but after a large number of reflections with the boundary eventually impinge on it with $\sin \chi < 1/n$ and are then directly emitted according to Snell's law of refraction. The high-intensity regions in the near-field correspond to the regions on the boundary of the ARC where most of the refractive escape occurs; the far-field directionality can be determined by following the refracted rays.

In FIG. **1**, a prior art cylindrical resonator of radius R is shown. The motion of a light ray in a WG mode circulating around its cross-section is shown in FIG. **2***a*. The motion forms a regular pattern with the angle of incidence the same at each reflection. As noted above, since this angle is initially above the angle required for refractive escape and remains so indefinitely, escape of optical energy occurs isotropically (equally in all directions) by the exponentially slow process of evanescent leakage (this escape is not shown in the figure).

Nöckel, Stone and Chang, in the paper entitled “Q spoiling and directionality in deformed ring cavities”, introduced the idea that a deformation of the cross-section might induce directional emission due to refractive escape. The deformation they considered, shown in FIG. **2***b*, causes irregular (chaotic) ray motion and leads to refractive escape at a point **10** (FIG. **2***b*) with the far-field high emission directions shown in FIG. **2***c*. Note that the high emission directions are not parallel and hence intersect in the near-field leading to interference effects not describable by ray-optics. Moreover there are secondary (split) peaks at angles near those of the largest peaks. The near-field behavior of ARCs was not known at that time due to the limitations of the ray model used.

The occurrence of multiple and non-parallel emitted beams make the prior art deformed resonator unsuitable for optical devices employing ARCs. Moreover the lack of information about the near-field radiation pattern of ARCs made it impossible to design input and output couplers for this resonator.

SUMMARY OF THE INVENTION

We have now determined that the high emission intensity points typically correspond to the regions of highest curvature on the ARC surface and that an ARC based on the deformation of FIG. **2***b* would produce non-parallel beams because the regions of highest curvature on the boundary are not 180° opposite one another. This defect is avoided in ARCs with two-fold reflection symmetry, as discussed below. It is also shown how to avoid the occurrence of multiple intersecting beams.

Accordingly, it is an object of this invention to provide an ARC wherein the light is emitted at a predetermined location and in a predetermined direction.

It is another object of this invention to provide an improved ARC wherein the emitted light comprises a single beam or parallel (non-intersecting) beams.

It is still another object of this invention to provide an ARC with predetermined Q-value and directional emission pattern so as to maximize the input-output coupling to a range of optical devices.

An asymmetric resonant optical cavity is constructed of an optically transmissive dielectric material having an index of refraction n. The cavity may be in the form of a cylinder with a cross-section deformed from circularity or a spheroid with an oblate or prolate deformation. These deformations should be larger than 1% of the undeformed radius R but it is crucial that they maintain convexity, i.e. at no point should the curvature of the relevant cross-section change its sign. In the cylindrical case the resulting cross-section should be oval in shape and we will use this descriptive term henceforth. The oval cross-section will have a major (long) axis and a minor (short) axis and the ARC should have mirror symmetry with respect to both axes. The shape and index of refraction of the ARC is chosen so as to avoid multiple beams. For signal processing in optical communications, an ARC will be coupled in the near-field region to an input optical signal at a wavelength λ which is in resonance with one of the whispering gallery resonances of the ARC. Typically this signal will be transmitted (possibly in modified form) through the ARC to an output coupler also positioned in the near field. The couplers must be oriented parallel to the tangent line at the point(s) of high emission intensity, which are determined (see below) to be approximately the points of highest curvature of the boundary. ARCs may also be used in signal generation, for example as resonators in microlasers or LEDs. In signal generation ARCs will produce highly directional beams of light along directions tangent to the points of highest curvature.

BRIEF DESCRIPTION OF THE DRAWINGS

FIG. **1** is a schematic view of a symmetric optical cavity resonator of cylindrical shape, having a radius R.

FIG. **2***a* is a ray tracing diagram of resonant ray paths within the optical resonator of FIG. **1**.

FIG. **2***b* is a ray tracing diagram of resonant ray paths when a deformation is introduced of the type discussed in Nöckel et al., Optics Letters 19, 1693 (1994). Points where refractive escape occurs are indicated.

FIG. **2***c* is a polar plot of the far-field emission intensity for the deformation shown in FIG. **2***b* showing the multiple and intersecting beams which are avoided in the invention.

FIG. **3***a* is a schematic of a deformed cylindrical ARC with appropriate shape to avoid multiple intersecting beams.

FIG. **3***b* is a schematic of a prolate spheroidal ARC.

FIG. **4** is a schematic diagram of the cross-section of an asymmetric resonant cavity which defines certain of the dimensions and quantities used in the analysis of ray paths within the cavity.

FIG. **5** is a plot of the logarithm of the Q value of a typical ARC whispering gallery resonance as a function of deformation ϵ for an ARC with a quadrupolar deformation. Three schematic pictures of the cross-section are shown for different values of ϵ.

FIG. **6** is a plot of the electric field intensity of an ARC resonance as a function of distance from the surface of an ARC with a 12% distortion, a mean radius of R=7.5 μm, a refractive index n=2 and a resonant wavelength of 1.5 μm

FIG. **7** is a "surface of section" for a cylindrical ARC which represents many possible ray trajectories within the ARC. Each point on the plot represents one collision of a ray trajectory which occurs at that particular value of the sine of the angle of incidence $\sin\chi$, and ϕ, the azimuthal angle (see definitions of FIG. **4**).

FIGS. **8**(*a*)–**8**(*b*) are plots of the intensity of light emitted from a quadrupole-deformed ARC versus angle ϕ for n=2 when there are two parallel beams and n=1.54 where there are four non-parallel beams emitted.

FIGS. **9**(*a*)–**9**(*b*) illustrates the experimental results confirming the directional emission from a cylindrical ARC as described in the text.

FIG. **10** is a schematic of a channel-dropping filter which makes use of ARCs incorporating the invention hereof.

FIG. **11** is a schematic of an optical amplifier which makes use of ARCs incorporating the invention hereof.

FIG. **12** is a schematic of wavelength converter which makes use of ARCs incorporating the invention hereof.

FIG. **13** is a schematic of a laser which makes use of an ARC incorporating the invention hereof.

DETAILED DESCRIPTION OF THE INVENTION

FIG. **3** gives perspective drawings of cylindrical and spheroidal ARCs; FIG. **4** illustrates a cross-section **20** of the cylindrical ARC with the required reflection symmetry about the minor axis A and the major axis B. To describe the properties of the ARC **20** we must discuss the motion of a light ray within the ARC; we will use certain parameters to do so. A point on the outer surface **22** of the ARC is specified by a radius, r, and an angle ϕ which can be measured from either of the axes A,B. A light ray 24 circulates in a WG mode within ARC **20** with an angle of incidence χ defined at each reflection from the boundary as the angle between ray 24 and the normal direction **28** which is drawn perpendicular to a tangent 30 at point of incidence **26**.

It is to be understood that the index of refraction n and the shape of the cross-section **20** determine the wavelengths of light which are resonantly enhanced along the ray path. The Q of the resonance determines how sharp is the resonance, i.e. how close to the prescribed wavelength the input signal must be to be resonantly enhanced or transmitted. Since the Q of the resonance is inversely proportional to its lifetime, there is a trade-off between greater frequency selectivity (higher Q) and faster switching capability (lower Q). By increasing the deformation of the ARC, the intrinsic Q of the resonances can be decreased from a very high value to any prescribed value which optimizes this trade-off. For lightwave communications at a switching rate of 5 Gigabits per second at the 1.53 micrometers communications wavelength, assuming a reasonable wavelength selectivity (bandwidth) of 0.05 nanometers requires a Q of order 10^4. The simplest useful cylindrical ARC has a cross-section given by the formula:

$$r(\phi) = \frac{R}{\sqrt{1+\epsilon^2/2}}(1+\epsilon\cos 2\phi). \tag{1}$$

Here the parameter e measures the degree of deformation, the aspect ratio (ratio of minor to major axes) being $(1-\epsilon)/(1+\epsilon)\approx 1-2\epsilon$. $\epsilon=0$ corresponds to the case of a circular (symmetric) resonator. The shapes of the cross-section for three values of epsilon are shown in FIG. **5**, where we also plot Q versus deformation for this ARC (obtained by numerical solution of the wave equation). Note that at roughly 10% deformation the Q value is in the range 10^4 which we estimated above was optimal for lightwave communications; whereas for symmetric resonators the intrinsic Q is much too large.

Returning to FIG. **4**, we now discuss directional coupling into and out of the ARC. Optical energy may be coupled into the ARC **20** by a variety of means, for example from a tangentially incident laser beam, perhaps combined with a prism coupler, or by an optical fiber **32** which is parallel to the tangent at the points of highest curvature and positioned within the nearfield of the outer surface **22**. In FIG. **6** we show a plot of the numerically calculated light intensity from a WG resonance as a function of distance from the surface moving perpendicular to the points **40, 42** (FIG. **4**). It is found that the near-field fall-off extends for a distance, d, where d is of order 10% of the radius R of the ARC. In order to have good coupling the fiber **32** must be positioned within this distance; if it is, then an optical signal at a resonant wavelength λ will be coupled from the input waveguide **32** into the ARC **20** at the point **40**, inducing a clock-wise propagating beam **24**. This beam will then transmit the signal to the output fiber **44** in the form of beam **38** which exits the ARC at the point 42 diametrically opposite the point of injection **40**. The output signal **38** propagates parallel to the input signal, but in the opposite direction; some of the input signal is reinjected into the fiber at **40** as well. This configuration will be efficient only if: 1) The ARC has an appropriate shape and index of refraction. 2) The points **40, 42** are correctly chosen. 3) The coupling fibers are placed within the distance d. We now indicate how this is achieved.

As discussed briefly above, a light ray initially trapped in an ARC resonance can ultimately escape by refraction, whereas this cannot occur for a symmetric cavity. In order to design an ARC with predictable and controllable emission, which is also highly directional, it is then necessary to understand at what points on the boundary of the ARC this refractive escape occurs, and how to confine-this escape to a narrow region resulting in a highly directional beam. The motion of the light rays within an ARC is partially chaotic. That means that for a large fraction of initial conditions nearby ray trajectories diverge exponentially rapidly. Therefore the necessary concepts come from the theory of non-linear dynamics and chaos. We now present a brief summary of the most relevant concepts.

In order to understand the high emission directions from ARCs, it is essential to analyze the ray dynamics in phase space, which in this context means analyzing not only where the trajectories of interest collide with the boundary, but also at what angle χ they collide. The standard technique used in non-linear dynamics to obtain an understanding of such system is the Poincare surface of section (SOS). It is obtained by plotting, for successive reflections of a ray, the angular position ϕ along the boundary surface **22** where the reflection occurs, and the value of sin χ at this collision. Recording on the SOS a relatively small number of ray trajectories (~10–20) for about 500 reflections yields a detailed picture of the possible ray trajectories. Such a plot representing ray trajectories in the cylindrical ARC described by Eq. (1) is shown in FIG. **7**. It exhibits three types of regions. First one sees regions of "random" disconnected points which are caused by chaotic trajectories. Second there are closed curves **50** which are known as islands or island chains. The centers of these islands represent stable periodic trajectories. A trajectory is periodic if it repeats itself after a finite number of collisions with the boundary and stable if a slight change in direction yields a trajectory which remains near the original one. These islands then represent possible regular (non-chaotic) ray trajectories. Other types of non-chaotic trajectories can exist as well but are not relevant to this discussion. The thick solid lines **52,54** represent the value of sin $\chi=1/n$ at which refractive escape is possible. Any trajectory which hits the boundary below those lines will escape with high probability, hence the points below the line are only for illustrative purposes and do not represent trajectories in a real ARC (but rather a hypothetical ARC with no refractive escape). The SOS shown in FIG. **7** is typical of cylindrical ARCs with two reflection symmetry axes, so it represents a case of practical interest. An ARC with precisely elliptical cross-section is unique as it has no chaotic trajectories and will behave differently from the generic case; hence this is not a preferred embodiment of the invention.

There are two crucial ideas for predicting the direction of light emission from such an ARC. First, a trajectory which starts anywhere in a chaotic region will eventually explore the whole chaotic region; however it will never cross over into the island regions. Second, as such a chaotic ray "explores" the chaotic region it does not actually move randomly within it, but rather for hundreds of collisions follows "adiabatic curves" given by the equation

$$\sin\chi(\phi)=\sqrt{1-(1-S^2)\kappa(\phi)^{2/3}}, \qquad (2)$$

where $\kappa(\phi)$ is the curvature of the interface and S is a constant parametrizing the curves; S is roughly equal to the average value of sin χ on the curve and varies between 1 and 0. Three examples of the adiabatic curves **56,58,60** for different values of S are drawn in FIG. **7**, including two examples which are tangent to the bold lines delineating the angle at which refractive escape occurs. (The tendency of chaotic trajectories to follow these curves is not directly visible in the Figure, but is well-established by computer simulations).

We have determined that rays with initial conditions in the chaotic region and with an initial sin $\chi>1/n$ will have the highest probability of escape exactly at the points at which the adiabatic curve is tangent to the escape line, unless an island in the surface of section excludes those points from the chaotic region. The first points of tangency will be given by the minima of the function sin $\chi(\phi)$ in Equation (2). It follows from the form of Equation (2) that these are the two points of highest curvature on the boundary. Hence the points of highest emission intensity can be found simply from Equation (2) or equivalently from a knowledge of the curvature of the ARC surface. FIG. **7** shows both the case where there is no blocking island which occurs for refractive index n=2; and the case with a blocking island, for refractive index, n=1.54. In the case n=1.54 (blocking island), light escapes equally on both sides of the island. Thus the case n=2 leads to two parallel beams, as illustrated in FIG. **4**; whereas the latter case, n=1.54 leads to four intersecting beams. This difference is also seen in the far-field intensity patterns calculated in FIG. **8**. For n=2 there are two peaks corresponding to the two parallel beams and for n=1.54 there are four peaks. Thus for an ARC of this shape a material with n≈2 would be necessary to generate a single beam. In general, by using these concepts and Equation (2) we can design ARCs for which the points of high emission intensity are known and which do not generate multiple, non-parallel beams.

Experimental evidence demonstrating the correctness of these concepts has been recently obtained from a measurement of the lasing emission produced by liquid dye columns. Ethanol containing Rhodamine B dye was forced through circular and rectangular orifices. The dye column produced by the circular orifice (of radius 75 μm) is cylindrical, whereas that produced by the rectangular orifice (of dimension 1000 μm×25 μm) has an oval cross-section with an eccentricity which decays (because of viscous damping) until it is nearly circular at 2 cm from the orifice. The cross-sectional distortion which experiences the smallest damping is quadrupolar, so that we expect the dominant deformation to be roughly given by Eq. (1). Hence the dye column at the appropriate height provides a realization of a cylindrical quadrupolar ARC. The surface tension causes the major axis of the quadrupole to oscillate in orientation with respect to the long axis of the orifice. The index of refraction for ethanol is n≈1.3 and there are no blocking islands at the high curvature points. Thus we expect to see high emission intensity in the direction perpendicular to the long axis of the deformed cross section which will be rotated by 90° with each half-cycle of the quadrupolar oscillation. The dye column was pumped with a 537 nm pulsed dye laser with pulse duration≈5 ns. The pump laser is oriented perpendicular to the long-axis of the rectangular orifice. Two collection lenses set to f/22 were placed at 0° and 90° relative to the pump laser beam. By using mirrors and a beam splitter, lasing images produced by the two lenses were combined side by side on a single CCD detector and were recorded simultaneously with appropriate calibration to preserve spatial correspondence anywhere along the column. As predicted by the theory, we observe (FIG. **9***a*) a striking oscillatory rotation of the high emission intensity between the 90° and 0° images, commensurate with the oscillation of the deformation of the cross section. No such oscillatory behavior is observed in the lasing emission from the circular control column (FIG. **9**(*b*)). This experiment demonstrates that the basic concepts for achieving useful directional emission from ARCs are sound and can be used in the design of optical devices. We now list four device designs which make use of the ARC invention.

Channel-dropping Filter

The current state-of-the-art fiber-optic communications networks use wavelength-division-multiplexing to maximize data transmission rates. These systems send different signals simultaneously at many different wavelength and require channel-dropping filters to receive selectively each wavelength channel. FIG. **10** illustrates a channel-dropping filter employing the ARC resonator. The input fiber **100** is carrying signals on wavelengths λ_1, λ_2, λ_3, . . . The ARCs **102**, **104** are constructed so as to have resonances at the wavelengths λ_1 and λ_2 respectively. As a result λ_1 is coupled into output fiber **106** and into receiver **1**, whereas λ_2 is coupled into output fiber **108** and into receiver **2**. Thus such an ARC array may function as a selective filter for wavelength division multiplexed (WDM) signals. The directional emission property of the ARC will improve the efficiency of filtering compared to symmetric resonators by at least one order of magnitude and the optimization of the Q-value may increase it even further.

Optical Amplifier

Fiber-optic communication networks also require optical amplifiers to regenerate signals on long-haul fibers. Rare-earth (erbium) doped glass is currently used for all-optical amplification at the wavelength 1.5 μm however there is a need for all-optical amplifiers outside the gain region of conventional erbium amplifiers. It has been proposed that microcavity amplifiers would shift the gain spectrum appropriately. FIG. **11** illustrates an optical amplifier employing an array of ARC microcavities. The pump which provides the energy for amplification is applied to the signal fiber **112** via rare-earth doped ARCs **114** and **116** which amplify the outgoing signal.

Wavelength Converter

Fiber-optic communication networks also require converting signals from one wavelength to another, preferably in an all-optical manner. A method for doing this is cavity-enhanced four-wave mixing which can be combined with the ARC invention as illustrated in FIG. **12**. The input signal at ω_1 to be converted is fiber **120** and is resonantly transmitted to the ARCs 122 and 124. At the same time a continuous wave (CW) carrier signal at frequency ω_2 is also transmitted from fiber **126** into the ARCs. These ARCs are fabricated of a material with a high non-linear mixing optical coefficient $\chi^{(3)}$ and hence generate a copy of the first signal at the new frequency ω_2 which is then transmitted as output on waveguide **126**.

Microlasers

Finally ARCs can employed as resonators for microlasers (or LEDs). In FIG. **13** we show a schematic of such a device. A pump signal (electrical or optical) is applied to an ARC doped with a gain material in the spatial region where WG resonances exist. The ARC generates a lasing signal at resonant wavelengths which are amplified by the gain profile of the gain material. Such a design would generate directional emission automatically, without the need for gratings or auxiliary waveguides which have been used in micro-disk and micro-ring lasers.

It should be understood that the foregoing description is only illustrative of the invention. Various alternative applications and modifications can be devised by those skilled in the art without departing from the invention. Accordingly, the present invention is intended to embrace all such alternatives, modifications and variances which fall within the scope of the appended claims.

What is claimed is:

1. A resonant optical apparatus, comprising:

a resonant cavity (ARC) of non-circular cross-section and having a dielectric constant n, an outer surface and an oval cross-section of area A defining a plane, having a long dimension arrayed along a major axis of said plane and a shorter dimension arrayed along a minor axis of said plane, said major axis and minor axis intersecting at a center of said ARC, said oval cross-section exhibiting mirror symmetry about both said major axis and said minor axis, said oval cross-section deformed from a circular resonator of cross-section of area A; and

input means for inducing an optical signal of wavelength λ into said ARC to cause a circulation of induced optical energy of wavelength λ in said plane and emission of said optical energy of wavelength λ from said ARC in said plane.

2. The resonant optical apparatus as recited in claim **1**, wherein said surface point is determined from the following expression for Sin $\chi(\emptyset)$

$$\mathrm{Sin}X(\phi) = \sqrt{1-(1-S^2)\kappa(\phi)^{2/3}} = 1/n$$

for a minima of Sin$\chi(\emptyset)$,

where: S is a constant which parameterizes the outer surface,

$\chi(\emptyset)$ is the angle of incidence at angle $(\emptyset)$,

$\theta(\emptyset)$ is a local curvature of the outer surface.

3. The resonant optical apparatus as recited in claim **1**, wherein n and S are adjusted so that light is emitted at and about said surface point with a single peak intensity.

4. The resonant optical apparatus, as recited in claim **1**, wherein said resonant cavity exhibits a deformed cylindrical shape.

5. The resonant optical apparatus, as recited in claim **1**, wherein said resonant cavity exhibits a deformed oblate or prolate spheroid shape.

* * * * *

EXHIBIT C

Patent Docket:
70120-00005

IN THE UNITED STATES PATENT AND TRADEMARK OFFICE

In re the Application of:	Group Art Unit: 2828
Deniz K. Armani et al.	Examiner: Tod Thomas Van Roy
Serial No.: 10/678,354	
Filed: October 2, 2003	
For: ULTRA-HIGH Q MICRO-RESONATOR AND METHOD OF FABRICATION	

DECLARATION OF DENIZ K. ARMANI SUBMITTED IN SUPPORT OF NON-OBVIOUSNESS

I, Deniz K Armani, one of the named inventors in the above-encaptioned patent application, hereby declare as follows:

1. I am familiar with the timeline associated with the development of the technology disclosed in the present application and the subsequent publication reporting on the technological developments. The present application claims priority to U.S. Provisional Application Serial No. 60/415,412, filed October 2, 2002 (hereinafter the "Priority Application"). The technological developments disclosed in the present application were publicly reported in an article published as D. K. Armani et al., "Ultra high-Q toroid microcavity on a chip," *Nature*, Vol. 421, pp. 925–929, Feb. 2003 (hereinafter the "*Nature* Article").

2. I have reviewed the article entitled "Ultrahigh-quality-factor silicon-on-insulator microring resonator", as published by Jan Niehusmann et al. in *Optics Letters*, Vol. 29, No. 24, December 15, 2004, a true and correct copy of which is attached as Exhibit 1.

Niehusmann et al. describe the development of Silicon-on-insulator (SOI) microring resonators.

3. Niehusmann et al. state that SOI integrated technology is anticipated to be highly beneficial for the convergence of microelectronics and photonics because due to cost savings that can be realized by integrating photonic and electronic functions on the same substrate. These same benefits were understood, but not fully realized, in October 2002 when the Priority Application was filed. This article also describes possible applications for microring resonators having a “high Q factor” or a “very high Q factor”, such as for telecommunication applications in providing wavelength selective filtering, add-drop multiplexing, compact dispersion compensation, and frequency-selective coupling, or for chemical or biomolecule sensor applications, or even to enhance evanescent-field fluorescence sensing.

4. The Q factor reported for the SOI microring resonators developed by Niehusmann et al. were 139.000 ± 6.000. These SOI microring resonators were fabricated directly on a substrate, and Niehusmann et al. reported that the Q factor was “much higher than [any Q factor values that] have been reported up to now” for integrated microring resonators. Niehusmann et al. recognized a single exception to their statement based upon SOI microring resonators fabricated by utilizing surface tension in the materials generated by a melting process. In recognizing this exception, Niehusmann et al. cited to the *Nature* Article. Moreover, Niehusmann et al. stated in the abstract of the paper that:

> “These [(the Q factor reported)] are *believed to be the highest values reported* for a curved SOI waveguide device and for any directly structured semiconductor microring fabricated without additional melting-induced surface smoothing.”

(Emphasis added.)

5. I have reviewed the article entitled "Silicon Microtoroidal Resonators With Integrated MEMS Tunable Coupler", as published by Jin Yao et al. in *IEEE Journal Of Selected Topics In Quantum Electronics*, Vol. 13, No. 2, March/April 2007, a true and correct copy of which is attached as Exhibit 2. Yao et al. describe an silicon microtoroidal resonator integrated on a substrate with a tunable optical coupler.

6. In this 2007 paper, Yao et al. report a process for fabricating a microtoroidal resonator integral to a substrate that also includes a MEMS-actuated tunable optical coupler. The process used to fabricate the microtoroidal resonator is a hydrogen annealing process, which enables creation of the microtoroidal structure and preserves the desired optical qualities of the microtoroidal resonator. The unloaded Q factor achieved by this fabrication process is reported to be as high as 1.0×10^5. Yao et al. indicate that very high Q factors have been demonstrated in SiO^2, but that because of the thermal reflow process used to create such microtoroidal resonators, such processes cannot be applied to integrated SOI photonics devices. The thermal reflow process referred to by Yao et al. is the one described in the *Nature* Article authored by the named inventors of the present application, which produces microtoroidal resonators having Q factors as high as 5×10^8.

7. Through my work in developing the technology disclosed in the present application, I am now and was, at the time the Priority Application was filed, familiar with the state of the art for microring and microdisk resonators. When the Priority Application was filed, I was aware of microdisk resonators having Q factors as high as 17,000. Those microdisk resonators were constructed from GaAs formed into disks upon a pedestal formed from a substrate AlGaAs. The article reporting and describing these microdisk resonators was included as part of the Information Disclosure Statement filed on March 1, 2004 as cite No. 7 in the Non-Patent Literature Documents section of form PTO/SB/08B. I was also aware of microring resonators having Q factors as high as 13,000. Those microring resonators were constructed from polymers forming a

microring on a silicon substrate (but not on a pedestal). The article reporting and describing these microdisk resonators was included as part of the Information Disclosure Statement filed on March 1, 2004 as cite No. 12 in the Non-Patent Literature Documents section of form PTO/SB/08B. At the time the Priority Application was filed, I was not aware, nor am I currently aware, of any other microring or microdisk resonators achieving Q factors approaching within three orders of magnitude of 10^7, other than those fabricated using the techniques developed by myself and my co-inventors.

8. I have reviewed U.S. Patent No. 6,259,717 to Stone et al., which is part of the prosecution record for the present patent application. Stone et al. do not disclose any of microring resonators, microtoroidal resonators, or any other type of substantially planar microresonator. Rather, Stone et al. disclose deformed cylindrical resonators and prolate spheroidal resonators as shown in Figs. 3a & 3b, respectively. Moreover, Fig. 5, which is a plot obtained by numerical solutions to the wave equation, illustrates *anticipated* Q factors for a cylindrical asymmetric resonant cavity only. As such, the stated theoretical values for such a cylindrical resonator are inapplicable to Q factors achievable for microring resonators.

9. I further declare under penalty of perjury that all statements made herein of my own knowledge are true and that all statements made on information and belief are believed to be true; and further that these statements are made with the knowledge that willful false statements and the like so made are punishable by fine or imprisonment, or both, under Title 18, United States Code § 1001, and that such willful false statements may jeopardize the validity of the application or any patent issuing thereon.

DATE: 2/12/2008

By: Deniz K. Armani

EXHIBIT 1

Ultrahigh-quality-factor silicon-on-insulator microring resonator

Jan Niehusmann, Andreas Vörckel, and Peter Haring Bolivar

Institut für Halbleitertechnik, Rheinisch-Westfälische Technische Hochschule Aachen, Sommerfeldstrasse 24, 52056 Aachen, Germany

Thorsten Wahlbrink and Wolfgang Henschel

Advanced Micro-electronic Center Aachen (AMICA), AMO GmbH, Huyskensweg 25, 52074 Aachen, Germany

Heinrich Kurz

Institut für Halbleitertechnik, Rheinisch-Westfälische Technische
Hochschule Aachen, Sommerfeldstrasse 24, 52056 Aachen, Germany, and
Advanced Micro-electronic Center Aachen (AMICA), AMO GmbH, Huyskensweg 25, 52074 Aachen, Germany

Received May 27, 2004

The development of ultrahigh-quality-factor (Q) silicon-on-insulator (SOI) microring resonators based on silicon wire waveguides is presented. An analytical description is derived, illustrating that in addition to low propagation losses the critical coupling condition is essential for optimizing device characteristics. Propagation losses as low as 1.9 ± 0.1 dB/cm in a curved waveguide with a bending radius of 20 μm and a Q factor as high as 139.000 ± 6.000 are demonstrated. These are believed to be the highest values reported for a curved SOI waveguide device and for any directly structured semiconductor microring fabricated without additional melting-induced surface smoothing. © 2004 Optical Society of America

OCIS codes: 130.3120, 230.5750.

Silicon-on-insulator (SOI) technology is a promising platform for the convergence of microelectronics and photonics. It has a large potential given the high photonic integration capabilities that are made possible by the high refractive-index contrast between silicon and typical cladding materials, the natural vertical confinement of optical waves given by the buried oxide layer, and the potential cost-efficient integration of photonic and electronic functions on the same substrate given by silicon technology.[1,2] However, at the same time, these beneficial characteristics lead to stringent manufacturing tolerances and a high sensitivity to surface roughness, as the higher refractive index of silicon in comparison with silica implies smaller silicon wire waveguide dimensions.[3] It is therefore critical to optimize manufacturing tolerance and to minimize surface roughness to facilitate useful low-loss SOI photonic solutions.[4]

In this Letter we present the development of high-quality SOI microring resonators based on silicon wire waveguides. These microrings can find direct application in the areas of telecommunication, sensors, quantum electrodynamics, and nonlinear optics.[5] For telecommunication, microrings have a multitude of applications, allowing wavelength-selective filtering, add–drop multiplexing, compact dispersion compensation, and frequency-selective coupling in optical networks.[6–8] Additionally, microrings are excellent model systems for deriving fundamental properties of curved waveguides as a crucial building block of photonic integrated circuits. Here we demonstrate a microring resonator with maximized quality factor Q to illustrate and quantify the low loss that can be achieved by use of an improved SOI process technology. Although the high Q factor demonstrated here surpasses typical needs of actual telecommunication data channels, the associated low loss is an indicator of the large degree of freedom in the future design of more complex and very large scale integrated telecommunication components that can be achieved with advanced SOI waveguide technology.

Microrings with a very high Q factor can also be used directly for sensor applications, where the dielectric loading and concomitant frequency shift of a resonator are used to monitor chemicals or biomolecules[9,10] or the higher field in the resonator is used to enhance evanescent-field fluorescence sensing.[11] In this type of application higher Q factors allow smaller resonance shifts to be detected. The internal field enhancement also increases sensitivity. Ultrahigh-Q optical microcavities with Q factors of up to 8×10^9 were recently demonstrated by use of microspheres.[12] However, these and similarly attractive microtoroids demonstrated in silicon[13] make use of the formation of ultraflat surfaces on the spheres and (or) microtoroids by using the surface tension during a melting process. This makes integration into photonic circuits and the dimensional control of the device during manufacture problematic. Here we present directly structured SOI-based microring resonators with Q factors that are much higher than have been reported up to now.

For proper design and optimization of a high-quality resonator, several aspects have to be considered. Most obviously, a sharp resonance, i.e., a high Q, is desired to observe small resonance wavelength shifts, which is necessary for sensing or switching applications. The

0146-9592/04/242861-03$15.00/0 © 2004 Optical Society of America

Q factor of a microring resonator coupled to a single waveguide is given by

$$Q = \frac{2\pi n_{\mathrm{eff}}}{\lambda_0} \frac{L}{2 \arccos\{[1 - 4t/\tau + (t/\tau)^2]/(-2t/\tau)\}} = \frac{\lambda_0}{\Delta\lambda_{3\,\mathrm{dB}}}, \qquad (1)$$

where n_{eff} is the effective index of refraction of the propagating mode in the microring, λ_0 is the resonance wavelength, L is the length of the microring, t is the field transmission coefficient at the waveguide–resonator coupling, and $\tau = \exp(-\alpha L/2)$ is the attenuation of the field per round trip for a microring resonator with attenuation constant α.[14] A reasonably noticeable shift of the resonance wavelength should be of the order of $\Delta\lambda_{\mathrm{detect}} \approx {}^1\!/\!_2\,\Delta\lambda_{3\,\mathrm{dB}}$. Thus it is evident that high Q factors are necessary for sensitive switching or sensing devices. The Q factor of an actual device depends on the chosen geometry, which determines parameters t, L, and n_{eff} in Eq. (1), and on the propagation losses in the ring, which determine τ.

For $t\tau$ close to 1, Eq. (1) can be approximated by

$$Q = \frac{2\pi n_{\mathrm{eff}}}{\lambda_0} \frac{L}{-2 \ln t\tau}; \qquad (2)$$

i.e., Eq. (1) is dependent on the product $t\tau$, which sums up propagation and coupling losses. Coupling losses are a free design parameter. Hence it is useful to estimate the maximum achievable Q factor that can be achieved with a given technology from the propagation loss $\alpha = -2(\ln \tau/L)$ inside the cavity. Neglecting the coupling loss to external waveguides, the maximum achievable Q factor can easily be determined from Eq. (2) as

$$Q_{\mathrm{limit}} = \frac{2\pi n_{\mathrm{eff}}}{\lambda_0} \frac{L}{-2 \ln \tau} = \frac{2\pi n_{\mathrm{eff}}}{\lambda_0} \frac{1}{\alpha}. \qquad (3)$$

Minimizing losses is therefore of prime importance for the development of ultrahigh-Q microcavities. In the case of SOI-based waveguide technology, low propagation losses can only be achieved with ultrasmooth waveguide surfaces, requiring specific optimized processing steps.

For reliable detection of a resonance shift or switching event, a large throughput attenuation of the signal of the coupled waveguide as a result of the resonance in the microring is necessary. This can be achieved by critical coupling, where complete throughput attenuation at resonance is achieved. The condition for critical coupling is given by $t = \tau$ in Eq. (1).[14] In that case the Q factor of the microcavity is given by $Q_{\mathrm{critical}} = Q_{\mathrm{limit}}/2$. Thus, for practical sensor applications only half the maximum Q factor that is possible as a result of the propagation loss can be used effectively.

A further technical parameter of importance is the cavity field enhancement. For applications based on a nonlinear material response, such as photonic switching, stronger fields inside the resonator induce larger shifts of the resonance wavelength, lowering, e.g., switching thresholds. The field enhancement factor at critical coupling conditions is given by

$$\mathrm{FE}_{\mathrm{critical}} = \frac{1}{\sqrt{1 - \tau^2}}. \qquad (4)$$

Here again, the maximum field enhancement coincides with a low propagation loss per round trip in the cavity. Therefore low propagation losses are the key issue in addressing most of the general requirements of microring resonators.

Several wire waveguide microrings based on SOI technology have been reported.[6,14] However, because of technological restrictions, the Q factor has been limited to values of the order of 2.500. Two aspects are optimized here, in comparison to former approaches[14]: an optimization of the pattern generation during electron-beam lithography (EBL) is performed, and the surface roughness during pattern transfer to the silicon waveguides is optimized. The waveguides are fabricated on SOI substrates consisting of a 1-μm-thick buried oxide layer and a 0.45-μm-thick device layer. For the waveguides a width of 0.5 μm has been chosen. The devices are defined by EBL using hydrogen silsesquioxane as an EBL resist.[15] Corrections are performed on the EBL pattern generation by preprocessing the microring into minimal feature size polygons. This minimizes the rectangular discontinuities that are characteristic of standard pattern generation of curved structures and that can reach several tens of nanometers. Pattern transfer is achieved by HBr inductive coupled reactive-ion etching, which selectively stops at the Si/SiO$_2$ interface, optimizing the etching parameters to minimize surface roughness. The input and output facets of the waveguides are prepared by cleaving the sample. A scanning electron microscope image of a typical device is depicted in Fig. 1.

For device characterization a commerical measurement setup consisting of a tunable external cavity diode laser and a photodiode is used. TM-polarized light (electric field perpendicular to the device plane) is butt coupled to the input by a polarization-maintaining optical fiber. The light at the throughput waveguide is

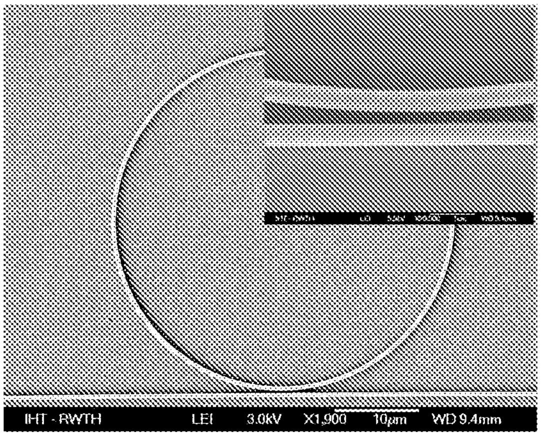

Fig. 1. Scanning electron micrographs of a SOI microring resonator with a radius of 20 μm, including an overview and a coupling region closeup (inset).

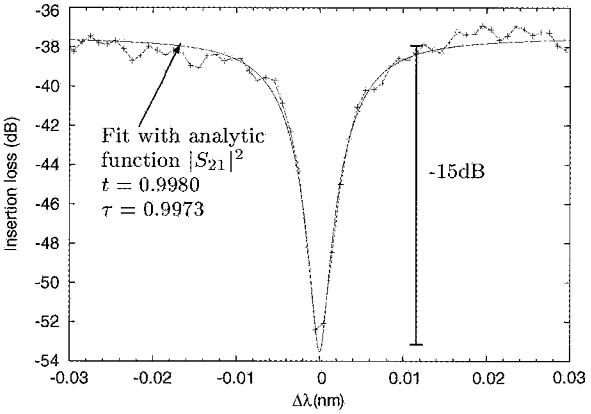

Fig. 2. Measured insertion loss and fit of analytical transfer function of a SOI microring resonator of radius $r = 20\ \mu\text{m}$, with $\Delta\lambda = \lambda - 1547.680$ nm.

butt coupled to a multimode fiber connected to a photodetector. The analytical transfer function of the device is given by[14]

$$|S_{21}|^2 = \frac{t^2 - 2t\tau \cos \phi + \tau^2}{1 - 2t\tau \cos \phi + (t\tau)^2}, \tag{5}$$

where $\phi = 2\pi(L_{\text{eff}}/\lambda) = (4\pi^2 r_{\text{eff}} n_{\text{eff}})/\lambda$ is the phase shift per round trip around the resonator. Figure 2 shows the measured insertion loss spectrum of a SOI microring resonator with a radius of $r = 20\ \mu\text{m}$ and a gap of $0.25\ \mu\text{m}$ between the microring resonator and the adjacent waveguide. The analytical transfer function $|S_{21}|^2$ is fitted to the resonance at the wavelength $\lambda = 1547.68$ nm, and $n_{\text{eff}} = 2.5864$ is derived from the resonance wavelengths. The fit yields values of $t = 0.9980 \pm 0.0002$ and $\tau = 0.9973 \pm 0.0001$, demonstrating that favorable critical coupling has nearly been achieved. Therefore a significant throughput attenuation of -15 dB at resonance is observed. The superposed oscillation is due to Fabry–Perot effects in the periphery of the device. As $|S_{21}|^2$ is invariant to commutation of t and τ, we chose the conservative values where $t > \tau$; i.e., attenuation of the wave propagating through the ring is higher than coupling from the ring to the waveguide. This choice does not influence the Q factor, but it means that the propagation loss may actually be even lower than calculated below.

Applying Eq. (1) to the fitted parameters yields a Q factor of $Q \approx 139.000 \pm 6.000$, which agrees with a direct linewidth estimation. As an illustration, this means that using this resonator as a sensor allows the detection of a resonance wavelength shift as low as $\Delta\lambda_{\text{detect}} \approx 0.006$ nm, which can easily be detected as a -3-dB signal change. This wavelength shift corresponds to a shift of the effective refractive index of as low as $\Delta n_{\text{eff,detect}} \approx 1.7 \times 10^{-5}$.

Taking τ obtained from the fit of $|S_{21}|^2$ to the experimental data and the length L of the device, the propagation loss inside the microring resonator can be deduced from

$$\alpha\left[\frac{\text{dB}}{\text{cm}}\right] = \frac{-2 \times 10^5 \log_{10}(\tau)}{L[\mu\text{m}]}. \tag{6}$$

For the resonance shown in Fig. 2, Eq. (6) gives a propagation loss of $\alpha \approx 1.9 \pm 0.1$ dB/cm. To our knowledge this is the lowest propagation loss reported for a SOI ring resonator or any curved SOI wire waveguide fabricated by reactive-ion etching without any further smoothing steps [e.g., melting and (or) thermal oxidation]. This result is similar to the best values reported for straight SOI waveguides.[16]

In summary, we have presented the design, fabrication, and optical characterization of ultrahigh-Q SOI microring resonators. We illustrate that, in addition to a minimization of losses to attain a high Q factor, the condition of critical coupling is of fundamental relevance for achieving high-efficiency devices. We demonstrate the development of microring resonators based on an optimized SOI fabrication technology, yielding what is to our knowledge the highest Q factor of 139.000 ± 6.000 and the lowest propagation loss without additional smoothing steps ever reported for SOI ring resonator technology.

The authors thank P. Kersten for motivating this work. This work was supported by European Commission contract IST-2001-38919 (PHOENIX) and the Ministerium für Wissenschaft und Forschung des Landes Nordrhein Westfalen. J. Niehusmann's e-mail address is niehusmann@iht.rwth-aachen.de.

References

1. B. N. Kurdi and D. G. Hall, Opt. Lett. **13,** 175 (1988).
2. R. A. Soref, Proc. IEEE **81,** 1687 (1993).
3. K. K. Lee, D. R. Lim, H.-C. Luan, A. Agarwal, J. Foresi, and L. C. Kimerling, Appl. Phys. Lett. **77,** 1617 (2000).
4. T. Tsuchizawa, T. Watanabe, E. Tamechika, T. Shoji, K. Yamada, J. Takahashi, S. Uchiyama, S. Itabashi, and H. Morita, in *LEOS Annual Meeting* (Lasers and Electro-Optics Society, Piscataway, N.J., 2002), p. 287.
5. K. J. Vahala, Nature **424,** 839 (2003).
6. B. E. Little, J. S. Foresi, G. Steinmeyer, E. R. Thoen, S. T. Chu, H. A. Haus, E. P. Ippen, L. C. Kimerling, and W. Greene, IEEE Photon. Technol. Lett. **10,** 549 (1998).
7. B. E. Little, S. T. Chu, W. Pan, and Y. Kokubun, IEEE Photon. Technol. Lett. **12,** 323 (2000).
8. L. Eldada, Rev. Sci. Instrum. **75,** 575 (2004).
9. C.-Y. Chao and L. J. Guo, Appl. Phys. Lett. **83,** 1527 (2003).
10. E. Krioukov, D. J. W. Klunder, A. Driessen, J. Greve, and C. Otto, Opt. Lett. **27,** 512 (2002).
11. S. Blair and Y. Chen, Appl. Opt. **40,** 570 (2001).
12. D. W. Vernooy, V. S. Ilchenko, H. Mabuchi, E. W. Streed, and H. J. Kimble, Opt. Lett. **23,** 247 (1998).
13. D. K. Armani, T. J. Kippenberg, S. M. Spillane, and K. J. Vahala, Nature **421,** 925 (2003).
14. A. Vörckel, M. Mönster, W. Henschel, P. Haring Bolivar, and H. Kurz, IEEE Photon. Technol. Lett. **15,** 912 (2003).
15. W. Henschel, Y. M. Georgiev, and H. Kurz, J. Vac. Sci. Technol. B **21,** 2018 (2003).
16. P. Dumon, W. Bogaerts, J. Van Campenhout, V. Wiaux, J. Wouters, S. Beckx, and R. Baets, in *LEOS Annual Meeting* (Lasers and Electro-Optics Society, Piscataway, N.J., 2003), p. 289.

EXHIBIT 2

Silicon Microtoroidal Resonators With Integrated MEMS Tunable Coupler

Jin Yao, David Leuenberger, Ming-Chang M. Lee, *Member, IEEE*, and Ming C. Wu, *Fellow, IEEE*

***Abstract*—A single crystalline silicon microtoroidal resonator with integrated MEMS-actuated tunable optical coupler is demonstrated for the first time. It is fabricated by combining hydrogen annealing and wafer bonding processes. The device operates in all three coupling regimes: under-, critical, and over-coupling. We have also developed a comprehensive model based on time-domain coupling theory. The experimental and theoretical results agree very well. The quality factor (Q) is extracted by fitting the experimental curve with the model. The unloaded Q is as high as 110 000, and the loaded Q is continuously tunable from 110 000 to 5400. The extinction ratio of the transmittance is 22.4 dB. This device can be used as a building block of resonator-based reconfigurable photonic integrated circuits.**

***Index Terms*—Integrated optics, optical resonators, surface roughness, tunable.**

I. INTRODUCTION

OPTICAL microresonators are key enabling elements for compact filters [1], lasers [2], electro-optic modulators [3], add–drop multiplexers [4], optical dispersion compensators [5], delay lines [6], nonlinear optical devices [7], and optical sensors [8], [9]. The performance of microresonators depends on two parameters: the quality factor (Q) of the resonator and the coupling ratio between the waveguides and the resonator (κ). Microfabricated resonators with very high Q has been demonstrated in SiO_2 [10] and Si [11]. The coupling ratio needs to be controlled precisely to achieve optimum performance [12]. This has been achieved by adjusting prism couplers in fused silica microsphere resonators [13] or by moving tapered fiber couplers [14]–[16] with piezo-controlled micropositioners. However, such setups are bulky and cannot be integrated. In microresonators with integrated waveguides, the coupling ratio is determined by the fabrication process [17]. The value of κ or, perhaps more importantly, its relation with the cavity Q, cannot be controlled precisely. Some trimming processes have been proposed to control the resonance frequency, but not κ [18], [19].

Recently, microresonators with tunable coupling ratios have been reported [20]–[23]. A Mach–Zehnder interferometer (MZI) has been integrated with a racetrack resonator [20]. The resonator can operate in all coupling regimes (uncoupled, under-, critical, or over-coupled). An unloaded Q of 1.9 $\times 10^4$ and an On–Off ratio of 18.5 dB have been achieved. However, the circumference of the resonator is rather large (1430 μm) due to the long MZI structure, which limits the free spectral range and the footprint that it can achieve. Recently, microfluidic approach has also been employed to tune both the resonance wavelength and the coupling ratio of low-index microring resonators made in SU8 [23]. The refractive index of the surrounding media was varied by mixing two different liquids. Critical coupling with an extinction ratio of 37 dB have been attained. However, index variation is small (~ 0.04), which limits the tuning range of κ. In addition, the tuning speed is slow (~ 2 s) and the fluidic packaging is cumbersome.

Previously, we have reported the first silicon microdisk resonator with integrated microelectromechanical systems (MEMS) tunable coupler [21], [22]. By physically changing the gap spacing between the waveguide and the resonator, κ can be varied over a wide range (0 to 34%) and a high Q (100 000) have been achieved simultaneously. Tunable dispersion compensators (185 to 1200 ps/nm) have also been demonstrated [22]. One drawback of that device is the lack of radial mode control in microdisk resonators, which could produce additional resonances due to high-order modes. In this paper, we report on the first single crystalline silicon *microtoroidal* resonator with MEMS tunable optical coupler. Microtoroidal resonators offer tighter confinement of the optical mode and eliminate multiple radial modes observed in microdisks. Microtoroidal resonators have been made in SiO_2 by thermal reflow [10], however, such process cannot be applied to single crystalline structures. Instead, we use hydrogen annealing to create three-dimensional toroidal structures while preserving the single crystalline quality [24]. To integrate the microtoroidal resonators with MEMS tunable waveguides, we have combined the hydrogen annealing process with wafer bonding technique. All the three coupling regimes have been demonstrated, with the loaded Q tunable from 110 000 to 5400.

II. DEVICE DESIGN AND FABRICATION

A. Device Structure Design

The schematic of the tunable microtoroidal resonator is shown in Fig. 1. Two suspended waveguides are vertically coupled to a microtoroidal resonator. It is realized on a two-layer silicon-on-insulator (SOI) structure. The microtoroid and the fixed electrodes of the MEMS actuators are fabricated on the lower SOI layer, while the suspended waveguides are integrated on the upper SOI. The initial spacing between the microtoroid and the

---

Manuscript received October 2, 2006; revised February 12, 2007. This work was supported in part by the Defense Advanced Research Project Agency (DARPA) University Photonics Research (UPR) Program HR0011-04-1-0040. The work of D. Leuenberger was supported by a one-year fellowship from the Swiss National Science Foundation, in 2005.

J. Yao and M. C. Wu are with the Department of Electrical Engineering and Computer Sciences, University of California, Berkeley, CA 94720 USA (e-mail: jinyao@eecs.berkeley.edu; wu@eecs.berkeley.edu).

D. Leuenberger is with the Integrated Photonics Laboratory, University of California, Berkeley, CA 94720 USA (e-mail: dleuen@eecs.berkeley.edu).

M.-C. M. Lee is with the Department of Electrical Engineering and the Institute of Photonics Technologies, National Tsing Hua University, Hsinchu 30055, Taiwan, R.O.C. (e-mail: mclee@ee.nthu.edu.tw).

Digital Object Identifier 10.1109/JSTQE.2007.893743

1077-260X/$25.00 © 2007 IEEE

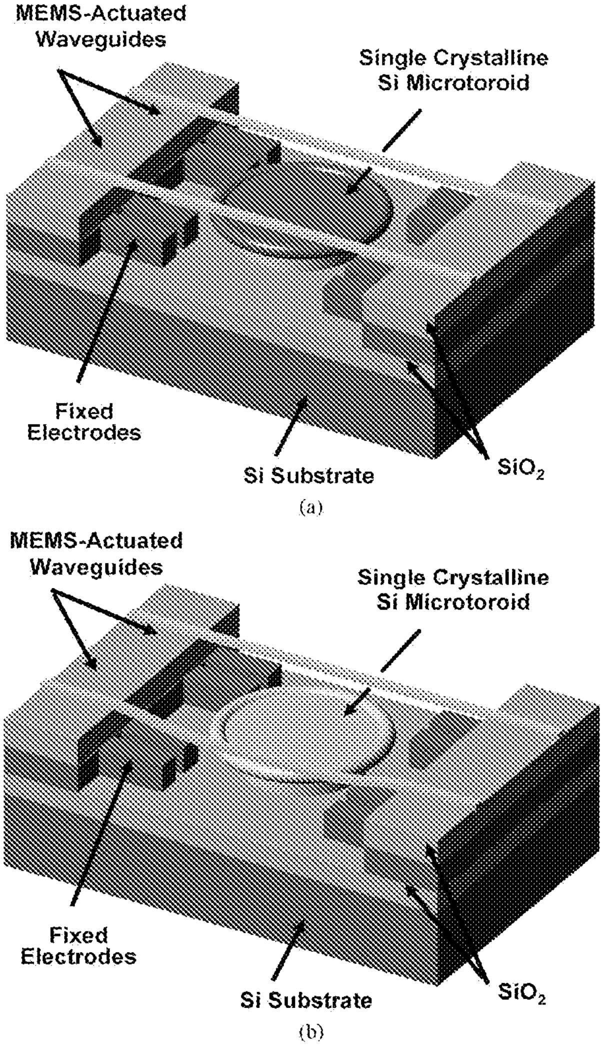

(a)

(b)

Fig. 1. (a) Schematic of the microtoroidal resonator with integrated MEMS tunable couplers. At zero bias, the initial spacing is large enough to ensure negligible coupling between the resonator and the waveguide coupler. (b) Schematic of the microtoroidal resonator with integrated MEMS tunable couplers under biased actuation. Lower waveguide is pulled downward to increase coupling, while the upper waveguide remains straight (uncoupled).

waveguides is 1 μm. It is chosen so that there is negligible coupling at zero bias, as shown in Fig. 1(a). With increasing voltage bias between the waveguide and the fixed electrodes, the suspended waveguide is pulled down toward the microtoroid, increasing the optical coupling exponentially, as illustrated in Fig. 1(b).

This design enables us to bias the microtoroidal resonator in all coupling regimes: under-coupling, critical coupling, and over-coupling, or even decoupled from the waveguide bus. Details of the MEMS actuator design have been reported in [22].

There is a design tradeoff in the doping concentration of the Si device layers. High doping is desired for the MEMS actuation, while low doping is necessary to minimize the optical absorption due to free carriers. Fortunately, electrostatic actuation does not require low resistivity. With a doping concentration of 10^{14} cm^{-3} (n-type dopants), a resistivity of 10 $\Omega\cdot$cm and an optical loss smaller than 0.01 cm^{-1} can be achieved. This absorption coefficient corresponds to a Q of 10^8 for microresonators if it is the dominant loss.

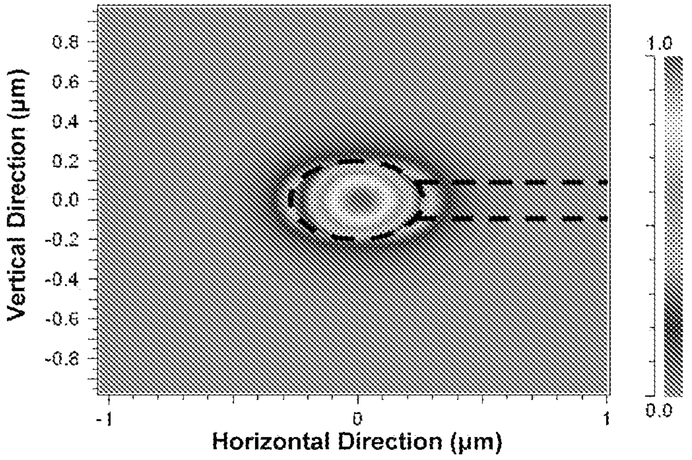

Fig. 2. Optical mode profile of the toroid for TE-like polarized light at 1.55 μm.

B. Waveguide Design for Phase Matching

Phase matching between the waveguide and the resonator is important to achieve an efficient coupling. Phase matching is satisfied when the two wave modes have the same propagation constant β.

We calculated the propagation constants of the microtoroid with the actual shape produced by hydrogen annealing using beam propagation method (BPM).[1] The optical field profile of the toroidal resonator at 1.55-μm wavelength is shown in Fig. 2. We used the following parameters in the calculation: refractive indexes of Si and air are 3.46 and 1.0, respectively; the bend radius of the toroid is 19.5 μm; and the radius of the toroid is 200 nm. It supports only one TE-like optical mode tightly confined to silicon.

Phase matching is achieved by controlling the dimensions of the waveguide. Fig. 3 shows the calculated propagation constants of the waveguide (lines) and the microtoroid (dots) versus wavelength for various waveguide dimensions. Here, we fix the waveguide width at 0.69 μm, the smallest linewidth that can regularly be produced by our lithography tool (10:1 reduction stepper). As shown in Fig. 3, the waveguide with 0.25-μm thickness is best matched to the microtoroid mode over a wide wavelength range around 1550 nm.

C. Fabrication Process

Our vertically coupled tunable microresonator was fabricated on a two-layer SOI using the wafer bonding process. The main challenge, here, was the nonplanar topography of the microtoroids that prevents the tight contact necessary for wafer bonding. We solved this problem by thinning the edges of the microdisks before hydrogen annealing so that the microtoroid surface was lower than the surrounding planar area. The detailed

---

[1] http://www.rsoftdesign.com/products/component_design/BeamPROP/

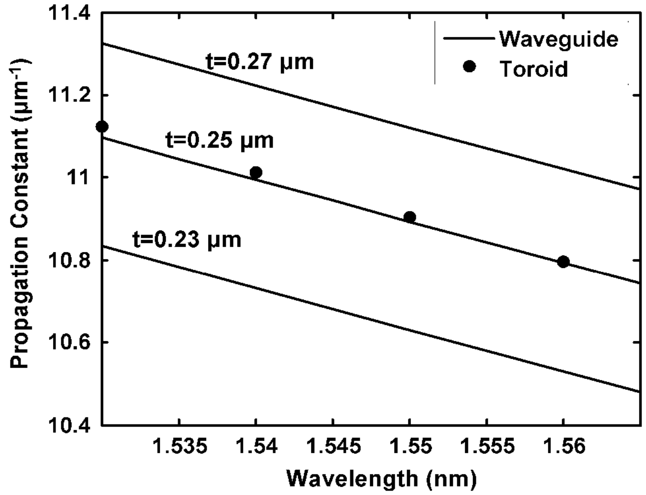

Fig. 3. Calculated propagation constants of the waveguide and the microtoroid versus wavelengths for various waveguide thicknesses, t. The width of the waveguide is fixed at 0.69 μm.

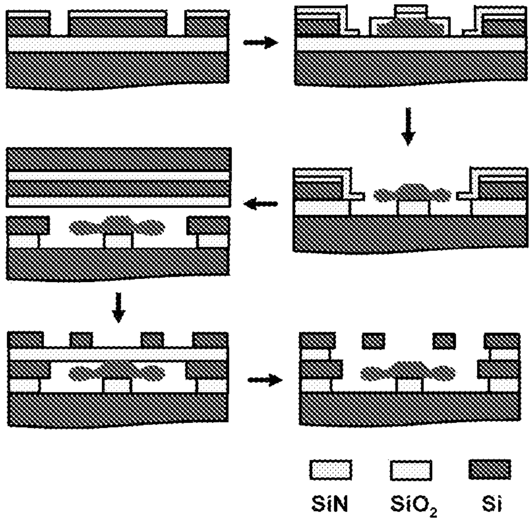

Fig. 4. Fabrication process for the tunable microtoroidal resonator.

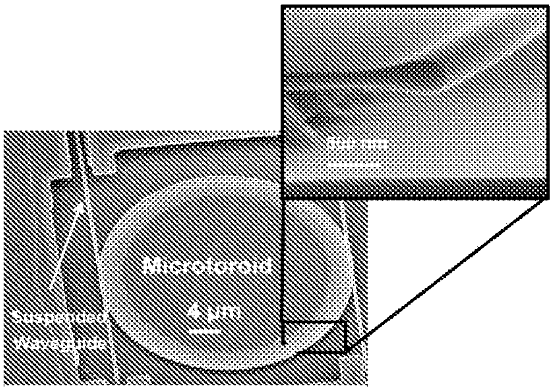

Fig. 5. SEM of the microtoroidal resonator and the suspended waveguides. Inset shows the cross-sectional view of the microtoroid.

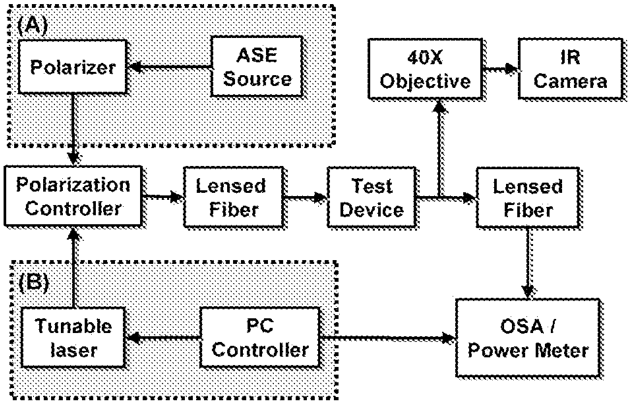

Fig. 6. Experimental setup for optical characterization. Amplified spontaneous emission (ASE) source is used (a) for quick measurement of the spectral response and (b) while the tunable laser provides high-resolution characterization.

fabrication process is shown in Fig. 4. First, microdisks were patterned and etched on an SOI wafer with a 350-nm-thick device layer. The edges of the disks were thinned down to 200 nm by thermal oxidation. This allowed room for the microtoroids to expand in the vertical direction during hydrogen annealing. The sample was then partially released in buffered HF and annealed in 10-Torr hydrogen ambient at 1050 °C for 5 min, creating a toroidal rim around the disks. The hydrogen annealing condition was optimized for the formation of the microtoroids, as reported in [24], [25]. A second SOI wafer with a 700-nm-thick device layer was thermally oxidized to create a SiO_2 spacer of 1-μm thickness. After oxidation, the thickness of the device layer was reduced to 250 nm. The toroid wafer was then fusion-bonded to the SOI wafer, whose substrate was subsequently removed to reveal the second SOI layer. The microtoroids were visible through the thin SOI layer, and the waveguide patterns were aligned to the edges of the underneath microtoroids. Finally, the waveguides around the toroids were released in buffered HF and supercritical dryer. In addition to creating a toroidal shape, the hydrogen annealing also reduced the surface roughness (to < 0.26 nm as reported in [26]), which was critical to attain high Q.

The scanning electron micrograph (SEM) of the fabricated device is shown in Fig. 5. The dimensions of the waveguides are measured to be 0.69-μm wide and 0.25-μm thick, very close to the designed parameters. The resonator exhibits a very smooth sidewall.

III. OPTICAL CHARACTERIZATION

The optical performance of the tunable microtoroidal resonator is tested using either a broadband amplified spontaneous emission (ASE) source (OpticWave Mini BLS-C-13) or a tunable laser (Agilent 81680A), as shown in Fig. 6. Light is coupled to the waveguides by polarization-maintaining lensed fibers. A calibrated optical power meter (HP 8153A) and an optical spectrum analyzer (OSA) (ANDO AQ6317B) are placed at the output to measure the transmitted power. The ASE provides a broadband source for quick measurement over a wide spectral range, while the tunable laser is used for high-resolution characterization. We have used TE-polarized input, which is attained by a linear polarizer and a polarization controller.

To actuate the waveguide, a voltage bias is applied to the fixed electrodes while the waveguide is grounded. At zero bias, almost

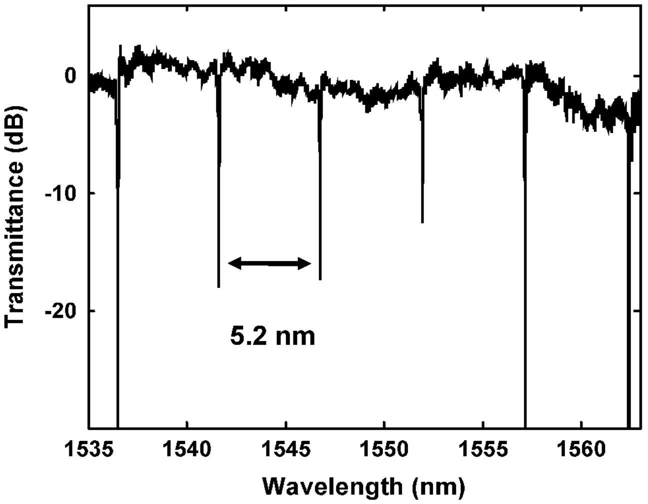

Fig. 7. Measured optical spectrum of a microtoroidal resonator at a bias voltage of 67 V. Measured free spectral range (FSR) of the TE mode is 5.2 nm.

100% of the light is transmitted to the output port. With increasing bias, sharp dips gradually appear in the transmission spectrum (Fig. 7). Each dip corresponds to a resonance wavelength. The free spectral range (FSR) of the TE mode is measured to be 5.2 nm. The small ripples are due to the reflections from the cleaved facets (Fabry–Perot effect). They can be eliminated by antireflection coating of the facets. Only a resonance peak is observed within each FSR, confirming the successful suppression of multiple radial modes observed in microdisk resonators.

The integrated tunable coupler enables the microresonator to operate in all coupling regimes. At low voltage, the microresonator is under-coupled. Fig. 8(a) shows the normalized transmission spectra of the resonator around one of the resonant wavelengths at 1548.2 nm at bias voltages of 51.0, 56.0, and 64.8 V. As the voltage increases, the optical coupling becomes stronger, leading to a larger dip at resonance. The three coupling regimes are clearly visible in Fig. 8(b), which plots the normalized transmittance at the resonant wavelength changes as a function of the applied voltage. In the under-coupling regime ($V_{\text{bias}} < 114$ V), the transmittance decreases continuously with the increasing voltage. The transmittance reaches a minimum at critical coupling ($V_{\text{bias}} = 114$ V). The extinction ratio is measured to be 22.4 dB at critical coupling. Further increase in voltage moves the resonator into the over-coupling regime. The increase in transmittance is accompanied by a broadening of the resonance linewidth since the coupling to waveguide is now stronger than the intrinsic loss of the resonator.

IV. THEORETICAL MODELING AND ANALYSIS

According to the time-domain coupling theory [1], the optical transfer function of the microresonator can be expressed as a function of resonant frequency (ω_0) and amplitude decay time constants τ_0 and τ_e, due to intrinsic loss and external coupling respectively

$$t_{\text{res}} = \frac{j(\omega - \omega_0) + \frac{1}{\tau_0} - \frac{1}{\tau_e}}{j(\omega - \omega_0) + \frac{1}{\tau_0} + \frac{1}{\tau_e}} \qquad (1)$$

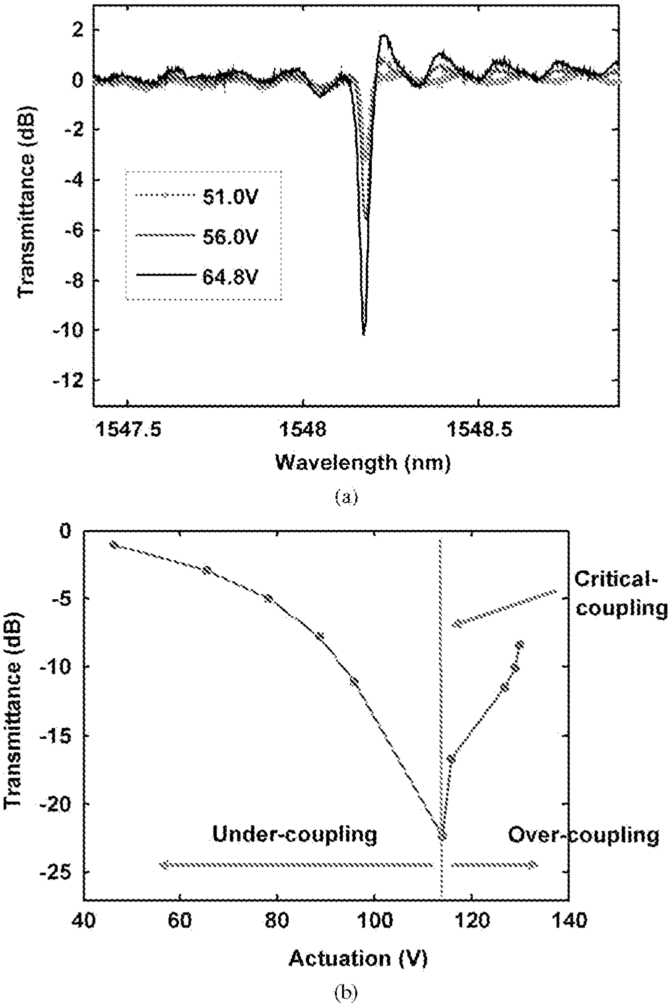

(a)

(b)

Fig. 8. (a) Measured normalized optical spectra of a microtoroidal resonator at bias voltages of 51.0, 56.0, and 64.8 V. (b) Normalized transmittance at resonance versus actuation voltage. Microresonator can be tuned continuously from under-coupling regime to over-coupling regime.

where t_{res} is the amplitude transfer function of the microresonator.

Alternatively, the transfer function can also be expressed in terms of the unloaded quality factor Q_0 and the external quality factor Q_e

$$t_{\text{res}} = \frac{2j\left(\frac{\lambda_0 - \lambda}{\lambda}\right) + \left(\frac{2}{Q_0} - \frac{1}{Q_L}\right)}{2j\left(\frac{\lambda_0 - \lambda}{\lambda}\right) + \left(\frac{1}{Q_L}\right)} \qquad (2)$$

where $Q_0 = \omega_0 \tau_0 / 2$, $Q_e = \omega_0 \tau_e / 2$, and the loaded quality factor Q_L is defined as

$$\frac{1}{Q_L} = \frac{1}{Q_0} + \frac{1}{Q_e} \qquad (3)$$

The measured spectra are usually complicated by the Fabry–Perot resonance between the two cleaved facets, as illustrated in Fig. 9. To model the measured spectrum more precisely, and extract the Q values of the resonator more accurately, particularly when the resonance peak is small, we develop a comprehensive

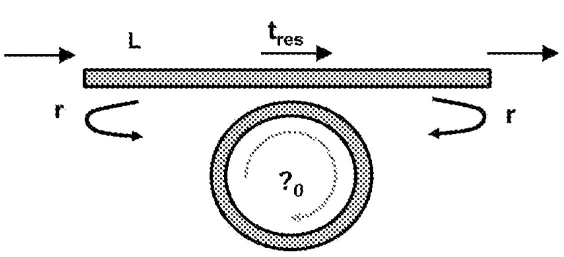

Fig. 9. Schematics illustrating the interaction between the microresonator and the Fabry–Perot resonance of the coupling waveguide.

model that includes both the effect of the microresonator and the Fabry–Perot ripples.

The total transmission t_{tot} is now a summation of multiple transmissions through the waveguide, as shown in

$$\begin{aligned} t_{\mathrm{tot}} &= (1-r)^2 \exp(-\alpha L)\exp(jkLn_{\mathrm{eff}})t_{\mathrm{res}} \\ &\quad + (1-r)^2 r^2 \exp(-3\alpha L)\exp(j(3kLn_{\mathrm{eff}} + 2\phi_{\mathrm{R}}))t_{\mathrm{res}}^3 \\ &\quad + (1-r)^2 r^4 \exp(-5\alpha L)\exp(j(5kLn_{\mathrm{eff}} + 4\phi_{\mathrm{R}}))t_{\mathrm{res}}^5 \\ &\quad + L \end{aligned} \tag{4}$$

where r is the amplitude reflection coefficient at the facet of the silicon waveguide, α is the optical loss per unit length in the waveguide, L is the length of the waveguide, k is the free-space propagation constant, n_{eff} is the effective refractive index of the Si waveguide, and ϕ_{R} is the optical phase change at the reflection per interface. Since there is a π phase shift at the reflection interface, the total transmission t_{tot} can be simplified to

$$\begin{aligned} t_{\mathrm{tot}} &= (1-r)^2 \exp(-\alpha L)\exp(jkLn_{\mathrm{eff}})t_{\mathrm{res}} \\ &\quad \{1 + r^2 \exp(-2\alpha L)\exp(j2kLn_{\mathrm{eff}})t_{\mathrm{res}}^2 \\ &\quad + r^4 \exp(-4\alpha L)\exp(j4kLn_{\mathrm{eff}})t_{\mathrm{res}}^4 + L\} \\ &= a_0(1 + q + q^2 + q^3 + L) \\ &= \frac{a_0}{1-q} \end{aligned} \tag{5}$$

where $a_0 = (1-r)^2 \exp(-\alpha L)\exp(jkLn_{\mathrm{eff}})t_{\mathrm{res}}$, and $q = r^2 \exp(-2\alpha L)\exp(j2kLn_{\mathrm{eff}})t_{\mathrm{res}}^2$.

In this derivation, we have assumed that the backscattering effect is small and can be neglected. The total intensity transmittance is then given by

$$T_{\mathrm{res}} = |t_{\mathrm{tot}}|^2 \tag{6}$$

To include the effect of waveguide dispersion, the phase factor kLn_{eff} is replaced by

$$\begin{aligned} \phi &= kL\left[n_{\mathrm{eff}} + \frac{dn}{d\lambda}(\lambda - \lambda_0)\right] \\ &= kLn_{\mathrm{eff}}\left[1 + \frac{dn}{d\lambda}\frac{1}{n_{\mathrm{eff}}}(\lambda - \lambda_0)\right] \\ &= kLn_{\mathrm{eff}}\left[1 + D_\lambda(\lambda - \lambda_0)\right] \end{aligned} \tag{7}$$

where $D_\lambda = \frac{dn}{d\lambda}\frac{1}{n_{\mathrm{eff}}}$.

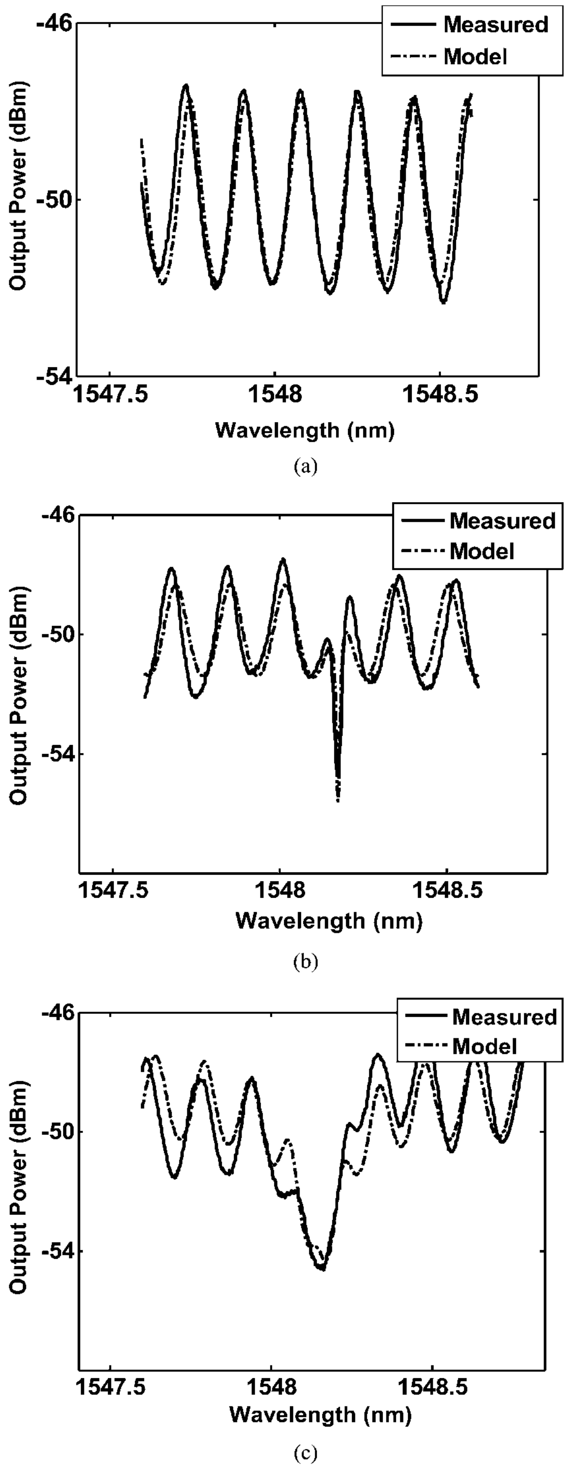

(a)

(b)

(c)

Fig. 10. (a) Measured and modeled spectra at 0 V (microresonator is decoupled). (b) Measured and modeled spectra at 64.8 V (microresonator is undercoupled). (c) Measured and modeled spectra at 130 V (microresonator is overcoupled).

The quality factors Q_0 and Q_L are extracted from the measured optical spectra by least-mean-square-error fitting to the model. Fig. 10 shows the measured and the fitted spectra around the resonance peak at 1548.2 nm when the resonator is:

a) decoupled; b) under-coupled; and c) over-coupled. The experimental data agree very well with the theoretical model. From the fitted spectral response, the unloaded quality factor Q_0 of the microtoroidal resonator is extracted to be 110 000. The loaded Q, i.e., Q_L, is continuously tunable from 110 000 to 5400, exhibiting a tuning ratio of more than 20:1.

The model described in this paper fit not only the resonance peak but also the ripples due to Fabry–Perot resonance. The quality factor extracted by this method is more accurate than by the lumped resonator model alone [27], especially when the resonance peak is small.

V. DISCUSSION

Hydrogen annealing is a simple and powerful technique to fabricate suspended microring resonators with high-quality factor and single radial mode. Comparing the etched ring with tethered anchor [17], the seamless toroidal structure has lower scattering loss and higher Q. The hydrogen annealing process also greatly reduces the surface roughness, as confirmed by the high Q measured in our devices. These tunable microresonators described in this paper can be cascaded to form reconfigurable optical add–drop multiplexers, wavelength-selective switches, and crossconnects. It can also be used for bandwidth-tunable filters in dynamic optical networks. With the successful suppression of multiple radial modes, we expect the microtoroidal resonator to have even larger bandwidth tuning ratio than the microdisk-based filters in [28].

VI. CONCLUSION

We have successfully demonstrated a novel single crystalline silicon microtoroidal resonator with MEMS-actuated tunable optical coupler. It is fabricated by combining the hydrogen annealing and the wafer bonding processes. We have achieved an unloaded Q of 110 000 for a 39-μm-diameter resonator with a toroidal radius of 200 nm. The device is able to operate in all the three coupling regimes: under-, critical, and over-coupling. The resonator can also be decoupled from the waveguide, allowing them to be cascaded without loading the waveguides. We have developed a detailed model combining the time-domain coupling theory with the Fabry–Perot resonance of the waveguide. The experimental and the theoretical results agree very well. The loaded Q is continuously tunable from 110 000 to 5400. This device has potential applications in variable-bandwidth filters, reconfigurable add–drop multiplexers, wavelength-selective switches and crossconnects, and optical sensors.

ACKNOWLEDGMENT

The authors would like to thank the staff of the Microfabrication Laboratory, University of California, Berkeley. Part of the fabrication process was performed at Stanford Nanofabrication Facility, Stanford University. In particular, they would also like to acknowledge the assistance of M. Stevens and M. Mansourpour. They would also like to thank Dr. S. Mathai of the University of California, Berkeley, for helpful discussions and technical assistance.

REFERENCES

[1] B. E. Little, S. T. Chu, H. A. Haus, J. Foresi, and J. P. Laine, "Microring resonator channel dropping filters," *J. Lightw. Technol.*, vol. 15, no. 6, pp. 998–1005, Jun. 1997.

[2] S. J. Choi, K. Djordjev, S. J. Choi, and P. D. Dapkus, "Microdisk lasers vertically coupled to output waveguides," *IEEE Photon. Technol. Lett.*, vol. 15, no. 10, pp. 1330–1332, Oct. 2003.

[3] Q. Xu, B. Schmidt, S. Pradhan, and M. Lipson, "Micrometre-scale silicon electro-optic modulator," *Nature*, vol. 435, no. 7040, pp. 325–327, May 2005.

[4] B. E. Little, S. T. Chu, W. Pan, and Y. Kokubun, "Microring resonator arrays for VLSI photonics," *IEEE Photon. Technol. Lett.*, vol. 12, no. 3, pp. 323–325, Mar. 2000.

[5] C. K. Madsen, G. Lenz, A. J. Bruce, M. A. Cappuzzo, L. T. Gomez, T. N. Nielsen, L. E. Adams, and I. Brenner, "An all-pass filter dispersion compensator using planar waveguide ring resonators," in *Proc. Opt. Fiber Commun. Conf. Int. Conf. Integr. Opt. Opt. Fiber Commun. (OFC/IOOC)*, Piscataway, NJ, Feb. 1999, vol. 4, pp. 99–101.

[6] G. Lenz, B. J. Eggleton, C. K. Madsen, and R. E. Slusher, "Optical delay lines based on optical filters," *IEEE J. Quantum Electron.*, vol. 37, no. 4, pp. 525–532, Apr. 2001.

[7] T. J. Kippenberg, S. M. Spillane, D. K. Armani, and K. J. Vahala, "Ultralow-threshold microcavity Raman laser on a microelectronic chip," *Opt. Lett.*, vol. 29, pp. 1224–1227, Jun. 2004.

[8] F. Vollmer, S. Arnold, D. Braun, I. Teraoka, and A. Libchaber., "Multiplexed DNA quantification by spectroscopic shift of two microsphere cavities," *Biophys. J.*, vol. 85, pp. 1974–1979, Sep. 2003.

[9] A. M. Armani and K. J. Vahala, "Heavy water detection using ultra-high-Q microcavities," *Opt. Lett.*, vol. 31, no. 12, pp. 1896–1898, Jun. 2006.

[10] D. K. Armani, T. J. Kippenberg, S. M. Spillane, and K. J. Vahala, "Ultra-high-Q toroid microcavity on a chip," *Nature*, vol. 421, pp. 925–929, Feb. 2003.

[11] M. Borselli, T. Johnson, and O. Painter, "Beyond the Rayleigh scattering limit in high-Q silicon microdisks: theory and experiment," *Opt. Express*, vol. 13, no. 5, pp. 1515–1530, Mar. 2005.

[12] A. Yariv, "Critical coupling and its control in optical waveguide-ring resonator systems," *IEEE Photon. Technol. Lett.*, vol. 14, no. 4, pp. 483–485, Apr. 2002.

[13] V. B. Braginsky, M. L. Gorodetsky, and V. S. Ilchenko, "Quality-factor and nonlinear properties of optical whispering-gallery modes," *Phys. Lett. A*, vol. 137, pp. 393–397, May 1989.

[14] J. C. Knight, G. Cheung, F. Jacques, and T. A. Birks, "Phase-matched excitation of whispering-gallery-mode resonances by a fiber taper," *Opt. Lett.*, vol. 22, pp. 1129–1131, Aug. 1997.

[15] M. Cai, O. Painter, and K. J. Vahala, "Observation of critical coupling in a fiber taper to a silica-microsphere whispering-gallery mode system," *Phys. Rev. Lett.*, vol. 85, pp. 74–77, Jul. 2000.

[16] M. Borselli, K. Srinivasan, P. E. Barclay, and O. Painter, "Rayleigh scattering, mode coupling, and optical loss in silicon microdisks," *Appl. Phys. Lett.*, vol. 85, pp. 3693–3695, 2004.

[17] L. Martinez and M. Lipson, "High confinement suspended micro-ring resonators in silicon-on-insulator," *Opt. Express*, vol. 14, no. 13, pp. 6259–6263, Jun. 2006.

[18] S. T. Chu, W. Pan, S. Sato, T. Kaneko, Y. Kokubun, and B. E. Little, "Wavelength trimming of a microring resonator filters by means of a UV sensitive polymer overlay," *IEEE Photon. Technol. Lett.*, vol. 11, no. 6, pp. 688–690, Jun. 1999.

[19] D. K. Sparacin, J. P. Lock, C. Hong, K. K. Gleason, L. C. Kimerling, and J. Michel, "Trimming of microring resonators using photo-oxidation of a plasma-polymerized organosilane cladding material," *Opt. Lett.*, vol. 30, no. 17, pp. 2251–2253, 2005.

[20] W. M. J. Green, R. K. Lee, G. DeRose, A. Scherer, and A. Yariv, "Hybrid InGaAsP-InP Mach-Zehnder racetrack resonator for thermooptic switching and coupling control," *Opt. Exp.*, vol. 13, pp. 1651–1659, Mar. 2005.

[21] M.-C. M. Lee and M. C. Wu, "MEMS-actuated microdisk resonators with variable power coupling ratios," *IEEE Photon. Technol. Lett.*, vol. 17, no. 5, pp. 1034–1036, May 2005.

[22] M.-C. M. Lee and M. C. Wu, "Tunable coupling regimes of silicon microdisk resonators using MEMS actuators," *Opt. Exp.*, vol. 14, no. 11, pp. 4703–4712, May 2006.

[23] U. Levy *et al.*, "On-chip microfluidic tuning of an optical microring resonator," *Appl. Phys. Lett.*, vol. 88, pp. 111107–111109, Mar. 2006.

[24] M.-C. M. Lee and M. C. Wu, "Thermal annealing in hydrogen for 3-D profile transformation on silicon-on-insulator and sidewall roughness reduction," *J. Microelectromech. Syst.*, vol. 15, no. 2, pp. 338–343, Apr. 2006.

[25] J. Yao, M.-C. M. Lee, and M. C. Wu, "Hydrogen annealing and bonding processes for integrated MEMS tunable microtoroidal resonators," to be published.

[26] M.-C. M. Lee, J. Yao, and M. C. Wu, "Silicon profile transformation and sidewall roughness reduction using hydrogen annealing," in *Proc. 18th IEEE Int. Conf. Microelectromech. Syst.*, Miami, FL, Jan. 30–Feb. 3, 2005, pp. 596–599.

[27] J. Yao, M.-C. M. Lee, D. Leuenberger, and M. C. Wu, "Silicon microtoroidal resonators with integrated MEMS tunable optical coupler," in *Proc. IEEE Opt. Microelectromech. Syst.*, Big Sky, MT, 2006, pp. 17–18.

[28] J. Yao, M.-C. M. Lee, D. Leuenberger, and M. C. Wu, "Wavelength- and bandwidth-tunable filters based on MEMS-actuated microdisk resonators," in *Proc. Opt. Fiber Commun. Conf. Nat. Fiber Opt. Eng. Long.*, Anaheim, CA, Mar. 5–10, 2006, p. 3.

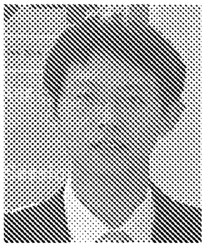

Jin Yao received the B.S. and M.S. degrees in electronic engineering from Tsinghua University, China, in 2000 and 2002, respectively. He is currently working toward the Ph.D. degree from the Department of Electrical Engineering and Computer Sciences, University of California, Berkeley.

His current research is focussed on silicon-based integrated microresonators, including design, simulation, fabrication, characterization, and their applications. His research interests include silicon-based photonic integrated circuits and micro-nano scale MEMS.

Mr. Yao won the California NanoSystems Institute (CNSI) Fellowship Award, in 2002–2003.

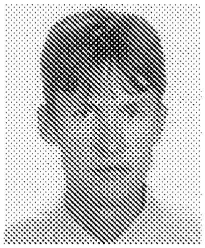

David Leuenberger received the graduate degree from the Institute of Applied Physics, University of Bern, Switzerland, in 2000. He received the Ph.D. degree from the Swiss Federal Institute of Technology, Lausanne, Switzerland, in 2004.

Currently, he is a Postdoctoral Researcher with the Integrated Photonics Laboratory, University of California, Berkeley. His current research interests include integrated microresonators for optical communication and sensing applications and optical antennas for surface enhanced Raman scattering. He is the author or coauthor of five journal papers and five conference papers.

Dr. Leuenberger is a member of the Optical Society of America (OSA).

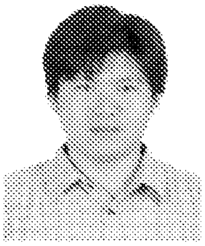

Ming-Chang M. Lee (S'04–M'05) was born in Taiwan, R.O.C. He received the B.S. degree in control engineering from the National Chiao Tung University, Hsinchu, Taiwan and the M.S. degree in electrical engineering from the National Taiwan University, Taipei, Taiwan, in 1994 and 1996, respectively. He received the Ph.D. degree in electrical engineering from the University of California, Los Angeles, in 2005.

Currently, he is with the faculty at the Institute of Photonics Technologies and the Department of Electrical Engineering, National Tsing Hua University, Taiwan. His research interests include optical MEMS, studies of nanophotonics, and the development of integrated photonic devices for optical communication and sensing.

Dr. Lee is a member of the Optical Society of America (OSA).

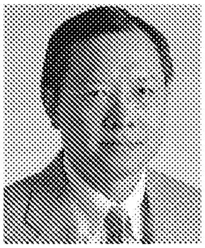

Ming C. Wu (S'82–M'83–SM'00–F'02) received the B.S. degree from National Taiwan University, Taipei, Taiwan, in 1983, and the M.S. and Ph.D. degrees from the University of California, Berkeley, in 1985 and 1988, respectively, all in electrical engineering.

Currently, he is a Professor of electrical engineering and computer sciences at the University of California, Berkeley, and a Co-Director of Berkeley Sensors and Actuators Center (BSAC). From 1988 to 1992, he was a Technical Staff at AT&T Bell Laboratories, Murray Hill, NJ. From 1993 to 2004, he was a Professor of electrical engineering at the University of California, Los Angeles (UCLA). He was also the Director of Nanoelectronics Research Facility and Vice Chair for Industrial Relations during his tenure at UCLA. In 1997, he cofounded OMM in San Diego, CA, to commercialize MEMS optical switches. He has published more than 400 papers, contributed five book chapters, and holds 11 U.S. patents. His research interests include optical MEMS, optoelectronics, and biophotonics. He has also participated in many technical conferences. He was the Guest Editor of two IEEE/OSA JOURNAL OF LIGHTWAVE TECHNOLOGY Special Issues on Optical MEMS.

Dr. Wu was a Fellow of David and Lucile Packard Foundation, from 1992 to 1997. He was the founding Co-Chair of the IEEE/LEOS Summer Topical Meeting on Optical MEMS in 1996.

EXHIBIT D

XP-002300373

in the theory (for one extra dimension). For the ADD theory with two large extra compact dimensions, we do not quite reach the limit on the size of these dimensions already set in refs 11 and 12.

Besides forces from extra dimensions, two other ideas have suggested new weak forces at submillimetre scales. The cosmological energy density needed to close the universe, if converted to a length by taking its inverse fourth root (in natural units where $\hbar = c = 1$), corresponds to about 100 µm. This fact has led to repeated attempts[17–19] to address difficulties connected with the very small observed size of Einstein's cosmological constant by introducing new forces with a range near 100 µm. Our result is the best upper bound on α in this region, but we have not quite reached gravitational sensitivity. Finally, the oldest of these predictions, still out of reach, is the very feeble axion-mediated force[20,21]. The axion is a field intended to explain why the violation of charge-parity symmetry is so small in quantum chromodynamics, the theory of the strong nuclear force.

Experiments of the sort reported here constrain string-inspired scenarios by setting very restrictive limits on predicted submillimetre forces. Of course, the actual observation of any new force would be a major advance. Because several theoretical scenarios point especially to these length scales, it is an important goal for the future to reach gravitational strength at even shorter distances, perhaps down to 10 µm. Experiments attempting to reach such distances will confront rapidly increasing background forces, especially electrostatic forces arising from the spatially non-uniform surface potentials of metals[22]. Electric fields due to surface potentials can be shielded with good conductors, but because of the finite stiffness of any shield they still cause background forces to be transmitted between test masses. Stretched membranes (as used by the Washington group) are more effective than stiff plates at the shortest distances, but it remains to be seen down to what distance the background forces can be effectively suppressed. □

Received 21 October 2002; accepted 13 January 2003; doi:10.1038/nature01432.

1. Greene, B. *The Elegant Universe: Superstrings, Hidden Dimensions, and the Quest for the Ultimate Theory* (Norton, New York, 1999).
2. Kaplan, D. B. & Wise, M. B. Couplings of a light dilaton and violations of the equivalence principle. *J. High Energy Phys.* 8, 37 (2000).
3. Taylor, T. R. & Veneziano, G. Dilaton couplings at large distances. *Phys. Lett. B* 213, 450–454 (1988).
4. Dimopoulos, S. & Giudice, G. Macroscopic forces from supersymmetry. *Phys. Lett. B* 379, 105–114 (1996).
5. Antoniadis, I. A possible new dimension at a few TeV. *Phys. Lett. B* 246, 377–384 (1990).
6. Antoniadis, I., Dimopoulos, S. & Dvali, G. Millimeter-range forces in superstring theories with weak-scale compactification. *Nucl. Phys. B* 516, 70–82 (1998).
7. Chacko, Z. & Perazzi, E. Extra dimensions at the weak scale and deviations from Newtonian gravity. Preprint hep-ph/0210254 available at ⟨arXiv.org⟩ (2002).
8. Fischbach, E. & Talmadge, C. *The Search for Non-Newtonian Gravity* (Springer, New York, 1999).
9. Bordag, M., Mohideen, U. & Mostepanenko, V. M. New Developments in the Casimir effect. *Phys. Rep.* 353, 1–205 (2001).
10. Long, J. C., Chan, H. W. & Price, J. C. Experimental status of gravitational-strength forces in the sub-centimeter regime. *Nucl. Phys. B* 539, 23–34 (1999).
11. Hoyle, C. D. *et al.* Sub-millimeter tests of the gravitational inverse-square law: A search for "large" extra dimensions. *Phys. Rev. Lett.* 86, 1418–1421 (2001).
12. Adelberger, E. G. Sub-mm tests of the gravitational inverse-square law. Preprint hep-ex/0202008 available at ⟨arXiv.org⟩ (2002).
13. Fischbach, E., Krause, D. E., Mostepanenko, V. M. & Novello, M. New constraints on ultrashort-ranged Yukawa interactions from atomic force microscopy. *Phys. Rev. D* 64, 075010 (2001).
14. Arkani-Hamed, N., Dimopoulos, S. & Dvali, G. The hierarchy problem and new dimensions at a millimeter. *Phys. Lett. B* 429, 263–272 (1998).
15. Kleiman, R. N., Kaminsky, G. K., Reppy, J. D., Pindak, R. & Bishop, D. J. Single-crystal silicon high-Q torsional oscillators. *Rev. Sci. Instrum.* 56, 2088–2091 (1985).
16. Long, J. C. *et al.* New experimental limits on macroscopic forces below 100 microns. Preprint hep-ph/0210004 available at ⟨arXiv.org⟩ (2002).
17. Beane, S. R. On the importance of testing gravity at distances less than 1 cm. *Gen. Rel. Grav.* 29, 945–951 (1997).
18. Sundrum, R. Towards an effective particle-string resolution of the cosmological constant problem. *J High Energy Phys.* 7, 1 (1999).
19. Schmidhuber, C. Old puzzles. Preprint hep-th/0207203 available at ⟨arXiv.org⟩ (2002).
20. Moody, J. E. & Wilczek, F. New macroscopic forces? *Phys. Rev. D* 30, 130–138 (1984).
21. Rosenberg, L. J. & van Bibber, K. A. Searches for invisible axions. *Phys. Rep.* 325, 1–39 (2000).
22. Price, J. C. in *Proc. Int. Symp. on Experimental Gravitational Physics* (eds Michelson, P., En-ke, H. & Pizzella, G.) 436–439 (World Scientific, Singapore, 1988).
23. Chan, H. W., Long, J. C. & Price, J. C. Taber vibration isolator for vacuum and cryogenic applications. *Rev. Sci. Instrum.* 70, 2742–2750 (1999).
24. Lamoreaux, S. K. Demonstration of the Casimir force in the 0.6 to 6 µm range. *Phys. Rev. Lett.* 78, 5–8 (1997).
25. Hoskins, J. K., Newman, R. D., Spero, R. & Shultz, J. Experimental tests of the gravitational inverse-square law for mass separations from 2 to 105 cm. *Phys. Rev. D* 32, 3084–3095 (1985).
26. Chiaverini, J., Smullin, S. J., Geraci, A. A., Weld, D. M. & Kapitulnik, A. New experimental constraints on non-Newtonian forces below 100 microns. Preprint hep-ph/0209325 available at ⟨arXiv.org⟩ (2002).
27. Floratos, E. G. & Leontaris, G. K. Low scale unification, Newton's law and extra dimensions. *Phys. Lett. B* 465, 95–100 (1999).
28. Kehagias, A. & Sfetsos, K. Deviations from the $1/r^2$ Newton law due to extra dimensions. *Phys. Lett. B* 472, 39–44 (2000).

Acknowledgements We thank E. Lagae for work in the laboratory, and C. Briggs, T. Buxkemper, L. Czaia, H. Green, S. Gustafson and H. Rohner of the University of Colorado and JILA instrument shops for technical assistance. We also gratefully acknowledge discussions with S. de Alwis, B. Dobrescu and S. Dimopoulos. This work is supported by grants from the US National Science Foundation.

Competing interests statement The authors declare that they have no competing financial interests.

Correspondence and requests for materials should be addressed to J.C.P.
(e-mail: john.price@colorado.edu).

Ultra-high-*Q* toroid microcavity on a chip

D. K. Armani, T. J. Kippenberg, S. M. Spillane & K. J. Vahala

Department of Applied Physics, California Institute of Technology, Pasadena, California 91125, USA

The circulation of light within dielectric volumes enables storage of optical power near specific resonant frequencies and is important in a wide range of fields including cavity quantum electrodynamics[1,2], photonics[3,4], biosensing[5,6] and nonlinear optics[7–9]. Optical trajectories occur near the interface of the volume with its surroundings, making their performance strongly dependent upon interface quality. With a nearly atomic-scale surface finish, surface-tension-induced microcavities such as liquid droplets or spheres[10–13] are superior to all other dielectric microresonant structures when comparing photon lifetime or, equivalently, cavity *Q* factor. Despite these advantageous properties, the physical characteristics of such systems are not easily controlled during fabrication. It is known that wafer-based processing[14] of resonators can achieve parallel processing and control, as well as integration with other functions. However, such resonators-on-a-chip suffer from *Q* factors that are many orders of magnitude lower than for surface-tension-induced microcavities, making them unsuitable for ultra-high-*Q* experiments. Here we demonstrate a process for producing silica toroid-shaped microresonators-on-a-chip with *Q* factors in excess of 100 million using a combination of lithography, dry etching and a selective reflow process. Such a high *Q* value was previously attainable only by droplets or microspheres and represents an improvement of nearly four orders of magnitude over previous chip-based resonators.

Devices were fabricated upon silicon wafers prepared with a 2-µm layer of silicon dioxide (SiO_2). The fabrication process flow is composed of four steps: photolithography; pattern transfer into the silicon dioxide layer; selective, dry etch of the exposed silicon; and selective reflow of the patterned silica. The process details are as follows (Fig. 1). First, photolithography is performed to create disk-shaped photo-resist pads (160 µm in diameter) on a (100) prime grade silicon substrate with 2 µm of oxide grown using wet thermal oxidation in a horizontal tube furnace. An additional bake follows in order to reflow the photo-resist, smoothing the edges in the

© 2003 Nature Publishing Group

BEST AVAILABLE COPY

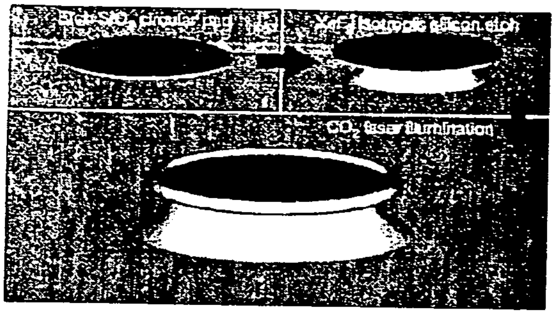
Etch SiO$_2$ circular pad
XeF$_2$ isotropic silicon etch
CO$_2$ laser illumination

Figure 1 Flow diagram illustrating the process used to fabricate ultra-high-*Q* planar microcavities.

process. The circular disks of photo-resist act as an etch mask during immersion in buffered HF solution at room temperature. Acetone is then used to remove residual photo-resist and organic contamination. The remaining SiO$_2$ disks act as etch masks during exposure to XeF$_2$ gas at 3 torr. XeF$_2$ was specifically chosen for the purpose of isotropic selective removal of silicon. As a result, the edges of the SiO$_2$ disks are equally undercut, leaving circular silicon pillars supporting larger SiO$_2$ disks. As the optical trajectories of interest reside at the periphery of the silica disk, the removal of the higher-index silicon below a portion of the periphery is required to inhibit power leakage into the substrate. We observe Q values in excess of 10^5 for these structures using the spectral characterization approach described below. The above process flow leaves lithographic blemishes, visible in an optical microscope, at the all-important disk periphery. Therefore we used additional processing to achieve the surface finish characteristic of surface-tension-induced microcavity structures (root-mean-square (r.m.s) roughness of several nanometres or less[13]).

Next, a processing step is introduced to selectively heat and reflow the undercut SiO$_2$ disks without affecting the underlying silicon support pillar. An undercut SiO$_2$ disk is surface-normal-irradiated using a CO$_2$ laser (10.6-μm wavelength), similar to techniques proposed for integrated circuit planarization[15]. The beam intensity profile follows an approximately gaussian distribution and is focused to a circular spot approximately 200 μm in diameter. The resulting beam intensity can be varied by electronic control of the laser power, but is typically 100 MW m^{-2} during reflow. Owing to the strong temperature dependence of the silica optical extinction coefficient near 10.6 μm (ref. 16) as well as the thermal isolation of the undercut SiO$_2$ disk, melting of the disk occurs along the periphery, and significantly not over the silicon pillar. In addition to having a far weaker optical absorption at 10.6 μm, silicon is 100 times more thermally conductive than silica[16,17]. The silicon pillar therefore remains significantly cooler and physically unaffected throughout the silica reflow process, serving as a heat sink to the selectively absorbed optical power in the silica layer. As the disk diameter shrinks, the effective cross-section available to absorb laser power decreases and shrinkage is observed to terminate when a toroid-like silica structure has formed. Beyond this point, continued laser treatment at the same intensity results in no observable change of the structure. The process is therefore self-quenching with the final diameter of the molten disk rim controlled by lithography and chemical etch steps. It should be noted that it is possible to interrupt the reflow prior to quenching thereby producing a toroid with a diameter intermediate to the initial disk diameter and terminal diameter.

Thus, in this process step, surface tension both smoothes the surface and collapses the silica disk to a toroid shape with limiting dimensions defined by the support pillar and the initial thickness of the silica layer. Micrographs showing disks both before and after the laser-activated selective reflow process are shown in Fig. 2. In these micrographs, the overall disk diameter was reduced to 120 μm as silica was consumed to form a 7-μm-thick toroid-shaped perimeter.

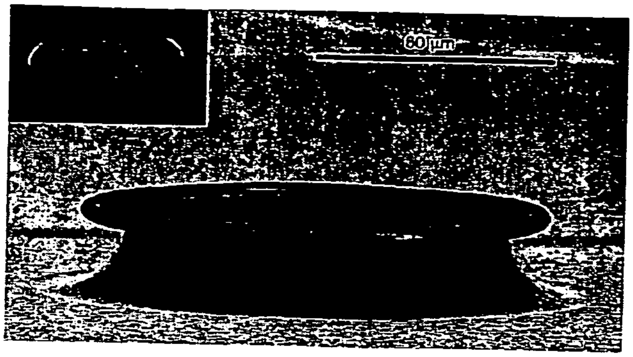

Figure 2 Scanning electron micrograph of a silica microdisk after selective reflow treatment with a CO$_2$ laser. The inset shows the microdisk prior to laser treatment. This toroidal microresonator had an intrinsic cavity *Q* of 1.00×10^8.

The mode structure and quality factor of the toroidal cavities were characterized in the optical telecommunication band (1,500 nm wavelength band). Tapered optical fibres connected to a single-mode, tunable, external-cavity laser were used to efficiently excite 'whispering gallery' modes of the resonators. Tapered waveguides were positioned on a 20-nm-resolution stage and could be moved freely over the silicon sample to couple individually to each of the toroid-shaped microresonators. Dual microscopes were used to simultaneously image disk resonators and fibre tapers from the side and the top. Proper alignment required the taper axis to reside in the equatorial plane of the toroidal cavity with minimal tilt angle. Briefly, taper fabrication[18] proceeds by stretching a standard optical fibre (SMF-28), which has been heated using a hydrogen flame. By observing the adiabatic condition, the tapered fibers exhibit low fibre-to-fibre insertion loss (typically <10%). Taper waist diameters are typically several micrometres, adjusted to properly phase-match to the resonator. Critical coupling[19] (the resonant transfer of all optical waveguide power into the resonator) was achieved by appropriately adjusting the taper–resonator gap. Non-resonant loss was observed to be low (<5%).

Figure 3 shows the transmission spectra through a taper in close proximity (of the order of hundreds of nanometres) to a 94-μm-diameter toroidal microresonator. The observed free spectral range corresponds to the equatorial mode number (*l*-index). Inspection of the data shows that the resonator supports very few radial and azimuthal (*m*-index or transverse) modes. This is in contrast to spheres, which support $(2l + 1)$ azimuthal modes. The quality factor, or *Q*, of the resonators was measured in two ways. First, the full-width at half-maximum (FWHM) of the lorentzian-shaped resonance in the undercoupled regime was directly measured by scanning a single-mode laser (short-term linewidth about 300 kHz) through a resonance. Low input power levels (typically less than 5 μW) were used to avoid thermally induced distortion of the line shape caused by resonant-field build-up within the cavity. Repeated measurements on samples fabricated with various radii (80–120 μm) and tori thickness (5–10 μm) yielded *Q* values in excess of 100 million (10^8). This is a record value for a planar device, and constitutes an improvement of nearly four orders of magnitude over all previous planar microresonators fabricated by wafer-scale processing (the highest values[20,21] reported thus far are less than 2×10^4).

As an independent and more precise measurement of quality factor, the photon lifetime was directly measured by cavity ring-down. This was done by repeatedly scanning the laser into resonance with a mode that was critically coupled to the taper. As the laser

© 2003 Nature Publishing Group

BNSDOCID: <XP_______2300373A__I_>

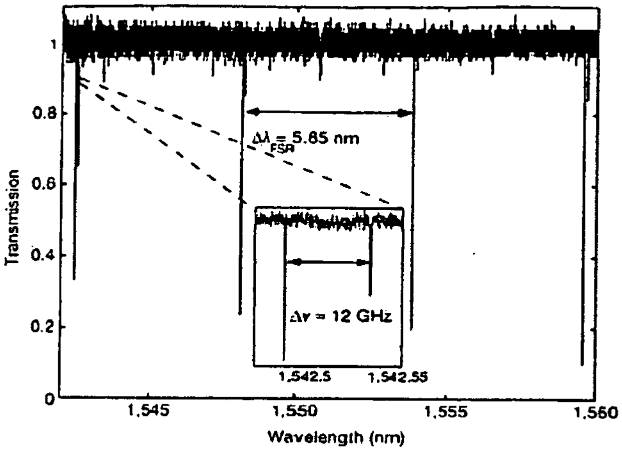

Figure 3 Transmission spectra of a toroidal resonator. The free spectral range (defined as the wavelength spacing between modes with successive angular mode number) is 5.65 nm, which corresponds to a torus approximately 94 μm in diameter. The inset shows what we believe to be the two lowest-order radial modes (based on modelling of a microdisk resonator). Additional subsidiary peaks are attributed to other radial or azimuthal modes.

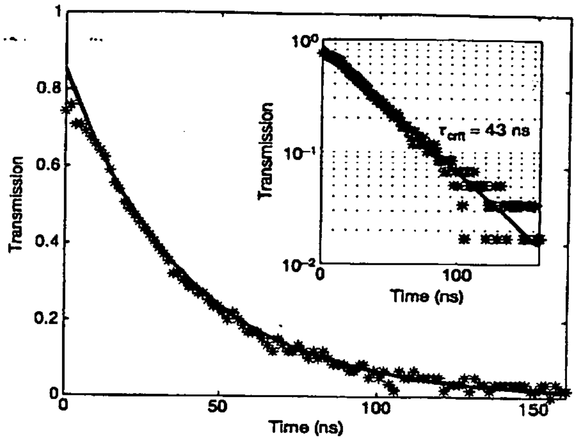

Figure 4 Ringdown measurement of a 90-μm-diameter toroid microcavity at the critical-coupling point. The measured lifetime of $\tau_{crit} = 43$ ns corresponds to an intrinsic quality factor of $Q = 1.25 \times 10^8$.

scanned into resonance, power transfer increased until maximal 'charging' of the resonant mode was attained. At this moment, the laser input was gated 'off' by use of a high-speed, external modulator and cavity ringdown is observed as the resonant power discharges. Because the resonator is by necessity loaded during this measurement, the observed ringdown time yields the cavity lifetime at the critical point, τ_{crit}, and the loaded Q-factor (not the intrinsic quality factor, Q_0). Data from a typical ringdown measurement are shown in Fig. 4. At time $t = 0$ in the figure, a signal is applied to 'gate' the laser off. When the laser input is fully off, the detected power is due entirely to the cavity discharge field. The solid line represents an exponential fit as expected for decay of a single cavity mode. The inset shows a logarithmic plot to infer the cavity lifetime. The loaded lifetime in this structure was 43 ns. As a further check on this time constant, after gating of the pump laser the waveguide power has dropped to 80% of its predicted maximal value based on extrapolation of data to $t = 0$. This value is in agreement with the gating delay of the ringdown setup ($\Delta t \approx 8$ ns). In particular, using the observed mode-lifetime of $\tau_{crit} = 43$ ns yields $\exp(-\Delta t/\tau_{crit}) = 0.83$.

As noted before, to infer the intrinsic cavity Q it is necessary to correct for loading by the taper waveguide. In addition, it is necessary to take into account excitation of the counter-propagating mode due to scattering centres intrinsic to the resonator (described by a dimensionless intermode coupling parameter Γ). The techniques used to measure this parameter in ultra-high-Q taper-coupled resonators are described elsewhere[22]. For the mode of Fig. 4 the intermode coupling was measured to be approximately 1, giving rise to a weak counter-propagating wave excitation (17% of the cavity build-up field is stored in the counter-propagating mode at critical coupling). In the presence of intermode coupling the relationship between the critically coupled lifetime and the intrinsic (unloaded) cavity quality factor, is given by

$$Q_0 \equiv \omega\tau_0 = \omega\tau_{crit}(1 + \sqrt{1 + \Gamma^2})$$

This yields an intrinsic cavity Q of 1.25×10^8 inferred from cavity ringdown. This value agrees with the measurements of the frequency line shape described above.

Thus we have fabricated ultra-high-Q planar cavities on a chip for the first time (to our knowledge). Toroid-shaped microcavities were formed using a combination of lithography, dry etching and a selective reflow process. Self-limited collapse of a molten silica disk enables the dimensional control typical of wafer-scale processing while providing the surface finish (and hence cavity Q) typical of a spherical resonator. Q values obtained by this process are typically four orders of magnitude higher than previous wafer-based resonators. In some applications mode volume is also an important factor, and certain chip-based micro-resonators[20,21] feature smaller mode volumes than the present structures. As a gauge to the lower bound on size, radiation leakage becomes a significant factor in determining Q for diameters less than 20 μm in silica microspheres. It should therefore be possible to reduce toroid diameter (and hence mode volume) substantially from the present 100 μm while maintaining ultra-high-Q values. The planar nature of the toroid microcavity and the large transparency window of silica suggest that these devices will find a wide range of applications in photonics as well as in fundamental studies. As an indication of the possibilities for these structures, in the course of this work nonlinear optical effects have been observed with characteristics comparable to recent studies on spherical ultra-high-Q cavities[9]. As standard processing techniques are used, the addition of optical functionality by techniques such as implantation or coating is possible. Likewise, electrical functionality can be introduced to integrate control functions with the ultra-high-Q microcavities. More generally, this work provides a new functional element that is synergistic with recent demonstrations of basic experimental physics on a chip. For example, by combining the present results with techniques recently demonstrated to integrate atomic traps on a chip[23] it would be possible to achieve chip-scale integration of cavity quantum electrodynamics experiments and related devices. Finally, there is great interest in improving the sensitivity of biological and chemical sensors. Proposals based upon optical resonators will benefit from the ability to attain ultra-high Q on a chip. ☐

Received 10 October; accepted 16 December 2002; doi:10.1038/nature01371.

---

1. Lefevre-Seguin, V. & Haroche, S. Towards cavity-QED experiments with silica microspheres. *Mater. Sci. Eng. B* 48, 53–58 (1997).
2. Vernooy, D. W., Furusawa, A., Georgiades, N. P., Ilchenko, V. S. & Kimble, H. J. Cavity QED with high-Q whispering gallery modes. *Phys. Rev. A* 57, R2293–R2296 (1998).
3. McCall, S. L., Levi, A. F. J., Slusher, R. E., Pearton, S. J. & Logan, R. A. Whispering-gallery mode microdisk lasers. *Appl. Phys. Lett.* 60, 289–291 (1992).
4. Sandoghdar, V. *et al.* Very low threshold whispering-gallery-mode microsphere laser. *Phys. Rev. A* 54, R1777–R1780 (1996).
5. Vollmer, F. *et al.* Protein detection by optical shift of a resonant microcavity. *Appl. Phys. Lett.* 80, 4057–4059 (2002).

© 2003 Nature Publishing Group

BNSDOCID: <XP_________2300373A__I_>

BEST AVAILABLE COPY

6. Serpenguzel, A., Arnold, S. & Griffel, G. Excitation of resonances of microspheres on an optical fiber. *Opt. Lett.* 20, 654–656 (1995).
7. Chang, R. K. & Campillo, A. J. (eds) *Optical Processes in Microcavities* (World Scientific, Singapore, 1996).
8. Treussart, F. *et al.* Evidence for intrinsic Kerr bistability of high-Q microsphere resonators in superfluid helium. *Eur. Phys. J. D* 1, 235–238 (1998).
9. Spillane, S. M., Kippenberg, T. J. & Vahala, K. J. Ultralow-threshold Raman laser using a spherical dielectric microcavity. *Nature* 415, 621–623 (2002).
10. Campillo, A. J., Eversole, J. D. & Lin, H-B. Cavity quantum electrodynamic enhancement of stimulated emission in microdroplets. *Phys. Rev. Lett.* 67, 437–440 (1991).
11. Braginsky, V. B., Gorodetsky, M. L. & Ilchenko, V. S. Quality-factor and nonlinear properties of optical whispering-gallery modes. *Phys. Lett. A* 137, 393–397 (1989).
12. Collot, L., Lefevre-Seguin, V., Brune, M., Raimond, J. M. & Haroche, S. Very high-Q whispering-gallery mode resonances observed on fused-silica microspheres. *Europhys. Lett.* 23, 327–334 (1993).
13. Vernooy, D. W., Ilchenko, V. S., Mabuchi, H., Steed, E. W. & Kimble, H. J. High-Q measurements of fused-silica microspheres in the near infrared. *Opt. Lett.* 23, 247–249 (1998).
14. Himeno, A., Kato, K. & Miya, T. Silica-based planar lightwave circuits. *IEEE J. Sel. Top. Quant.* 4, 913–924 (1998).
15. Delfino, M. & Reifsteck, T. A. Laser activated flow of phosphosilicate glass in integrated circuit devices. *Elect. Device Lett.* 3, 116–118 (1982).
16. McLac[illegible] A. D. & Meyer, F. P. Temperature dependence of the extinction coefficient of fused silica for CO_2 laser wavelengths. *Appl. Opt.* 26, 1728–1731 (1987).
17. Sheik-bahae, M. & Kwok, H. S. Controlled CO_2 laser melting of silicon. *J. Appl. Phys.* 63, 518–524 (1988).
18. Knight, J. C., Cheung, G., Jacques, F. & Birks, T. A. Phase-matched excitation of whispering-gallery-model resonances by a fiber taper. *Opt. Lett.* 22, 1129–1131 (1997).
19. Cai, M., Painter, O. & Vahala, K. J. Observation of critical coupling in a fiber taper to a silica-microsphere whispering-gallery mode system. *Phys. Rev. Lett.* 85, 74–77 (2000).
20. Michler, P. *et al.* Laser emission from quantum dots in microdisk structures. *Appl. Phys. Lett.* 77, 184–186 (2001).
21. Gayral, B. *et al.* High-Q wet-etched GaAs microdisks containing InAs quantum boxes. *Appl. Phys. Lett.* 75, 1908–1910 (1999).
22. Kippenberg, T. J., Spillane, S. M. & Vahala, K. J. Modal coupling in traveling-wave resonators. *Opt. Lett.* 27, 1669–1671 (2002).
23. Hansel, W., Hommelhoff, P., Hansch, T. W. & Reichel, J. Bose–Einstein condensation on a microelectronic chip. *Nature* 413, 498–501 (2001).

Acknowledgements This work was supported by DARPA and the Caltech Lee Center.

Competing interests statement The authors declare that they have no competing financial interests.

Correspondence and requests for materials should be addressed to K.J.V. (e-mail: vahala@caltech.edu).

Logarithmic rate dependence of force networks in sheared granular materials

R. R. Hartley & R. P. Behringer

Department of Physics & Center for Nonlinear and Complex Systems, Duke University, Durham, North Carolina 27708-0305, USA

Many models of slow, dense granular flows[1–5] assume that the internal stresses are independent of the shearing rate. In contrast, logarithmic rate dependence is found in solid-on-solid friction[6–8], geological settings[9–11] and elsewhere[12–15]. Here we investigate the rate dependence of stress in a slowly sheared two-dimensional system of photoelastic disks, in which we are able to determine forces on the granular scale. We find that the mean (time-averaged) stress displays a logarithmic dependence on the shear rate for plastic (irreversible) deformations. However, there is no perceivable dependence on the driving rate for elastic (reversible) deformations, such as those that occur under moderate repetitive compression. Increasing the shearing rate leads to an increase in the strength of the force network and stress fluctuations. Qualitatively, this behaviour resembles the changes associated with an increase in density. Increases in the shearing rate also lead to qualitative changes in the distributions of stress build-up and relaxation events. If shearing is suddenly stopped, stress relaxations occur with a logarithmic functional form over long timescales. This slow collective relaxation of the stress network provides a mechanism for rate-dependent strengthening.

Slow granular flows are typically described in the context of Mohr–Coulomb friction models[2] that resemble those used for describing friction between two solid bodies[16]. In the well-known solid friction scheme[17,18], an object on a frictional surface will resist a force and remain at rest, provided that the magnitude of the tangential force is less than the product of a static friction coefficient and the normal force. This picture was translated into the granular context (for dense granular systems characterized by networks of force chains[19]) by Coulomb[20] and more recent authors[1,2]. In this context the normal and tangential forces are replaced by corresponding normal and shear stresses, and the surface of interaction is replaced by a plane within the material. For large enough tangential force relative to the normal force sliding friction (failure in a granular material) occurs. [illegible] these pictures, sliding friction (deformation following failure) is independent of the speed of sliding (the shear rate).

In reality, experiments in diverse contexts have shown that solid friction exhibits a logarithmic dependence on rate and that static frictional contacts strengthen logarithmically with age. These experiments span a vast range of lengths, and include studies at the atomic[15], laboratory[7,8,12–14] and geological scale[9–11]. Recent experiments[6] using granular materials sliding against the interior wall of a piston showed a clear rate dependence that was associated with ageing effects of individual solid-friction contacts and with the force network. Experiments[7,8] in which a solid rough surface was pushed across a granular bed showed a slow strengthening (or ageing) with time of the (quasi-static) force, and creep before slip events. Other experiments[11] have found strengthening due to ageing for granular samples under large compressions. In the present experiments, which consider the grains and the force network, we show that there is a logarithmic rate-dependence in slowly sheared granular materials that is associated with irreversible rearrangements of the force network within the material itself. This is manifested as a strengthening with rate.

The experiments described here were carried out with a two-dimensional realization of a granular system. The particles were made of a photoelastic material, and were either relatively thin disks or flat particles with a pentagonal cross-section. By using a photoelastic material, we could determine forces at the grain scale. More detailed descriptions of the experimental apparatus and methods[21]

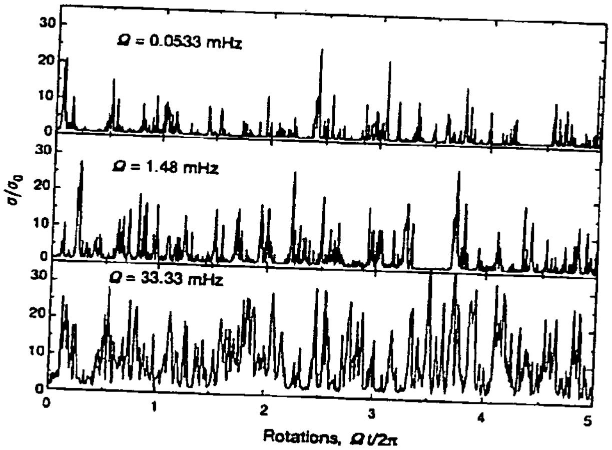

Figure 1 Time series for stress (normalized by $\sigma_0 \approx 4.11\ \mathrm{N\,m^{-1}}$) for a range of shearing rates Ω that span the experimental range. These data are for pentagonal particles, but data for disks are qualitatively similar. Shear wheel radius 13.8 cm, $\gamma = \gamma_c + 0.0152$.

© 2003 Nature Publishing Group

BNSDOCID: <XP_______2300373A__I_>

EXHIBIT E

UNITED STATES PATENT AND TRADEMARK OFFICE

UNITED STATES DEPARTMENT OF COMMERCE
United States Patent and Trademark Office
Address: COMMISSIONER FOR PATENTS
P.O. Box 1450
Alexandria, Virginia 22313-1450
www.uspto.gov

APPLICATION NO.	FILING DATE	FIRST NAMED INVENTOR	ATTORNEY DOCKET NO.	CONFIRMATION NO.
10/678,354	10/02/2003	Deniz K. Armani	70120-00005	1793

58688 7590 10/19/2007
CONNOLLY BOVE LODGE & HUTZ LLP
P.O. BOX 2207
WILMINGTON, DE 19899

EXAMINER	
VAN ROY, TOD THOMAS	

ART UNIT	PAPER NUMBER
2828	

MAIL DATE	DELIVERY MODE
10/19/2007	PAPER

Please find below and/or attached an Office communication concerning this application or proceeding.

The time period for reply, if any, is set in the attached communication.

TH

Office Action Summary	**Application No.** 10/678,354	**Applicant(s)** ARMANI ET AL.
	Examiner Tod T. Van Roy	**Art Unit** 2828

-- The MAILING DATE of this communication appears on the cover sheet with the correspondence address --

Period for Reply

A SHORTENED STATUTORY PERIOD FOR REPLY IS SET TO EXPIRE 3 MONTH(S) OR THIRTY (30) DAYS, WHICHEVER IS LONGER, FROM THE MAILING DATE OF THIS COMMUNICATION.

- Extensions of time may be available under the provisions of 37 CFR 1.136(a). In no event, however, may a reply be timely filed after SIX (6) MONTHS from the mailing date of this communication.
- If NO period for reply is specified above, the maximum statutory period will apply and will expire SIX (6) MONTHS from the mailing date of this communication.
- Failure to reply within the set or extended period for reply will, by statute, cause the application to become ABANDONED (35 U.S.C. § 133). Any reply received by the Office later than three months after the mailing date of this communication, even if timely filed, may reduce any earned patent term adjustment. See 37 CFR 1.704(b).

Status

1)☒ Responsive to communication(s) filed on *30 July 2007*.
2a)☒ This action is **FINAL**. 2b)☐ This action is non-final.
3)☐ Since this application is in condition for allowance except for formal matters, prosecution as to the merits is closed in accordance with the practice under *Ex parte Quayle*, 1935 C.D. 11, 453 O.G. 213.

Disposition of Claims

4)☒ Claim(s) *1-8,10-22,28-41,43-58,60-62 and 67-82* is/are pending in the application.
4a) Of the above claim(s) _____ is/are withdrawn from consideration.
5)☐ Claim(s) _____ is/are allowed.
6)☒ Claim(s) *1-8,10-22,28-41,43-58,60-62 and 67-82* is/are rejected.
7)☐ Claim(s) _____ is/are objected to.
8)☐ Claim(s) _____ are subject to restriction and/or election requirement.

Application Papers

9)☐ The specification is objected to by the Examiner.
10)☐ The drawing(s) filed on _____ is/are: a)☐ accepted or b)☐ objected to by the Examiner.
Applicant may not request that any objection to the drawing(s) be held in abeyance. See 37 CFR 1.85(a).
Replacement drawing sheet(s) including the correction is required if the drawing(s) is objected to. See 37 CFR 1.121(d).
11)☐ The oath or declaration is objected to by the Examiner. Note the attached Office Action or form PTO-152.

Priority under 35 U.S.C. § 119

12)☐ Acknowledgment is made of a claim for foreign priority under 35 U.S.C. § 119(a)-(d) or (f).
a)☐ All b)☐ Some * c)☐ None of:
1.☐ Certified copies of the priority documents have been received.
2.☐ Certified copies of the priority documents have been received in Application No. _____.
3.☐ Copies of the certified copies of the priority documents have been received in this National Stage application from the International Bureau (PCT Rule 17.2(a)).
* See the attached detailed Office action for a list of the certified copies not received.

Attachment(s)

1) ☐ Notice of References Cited (PTO-892)
2) ☐ Notice of Draftsperson's Patent Drawing Review (PTO-948)
3) ☒ Information Disclosure Statement(s) (PTO/SB/08)
Paper No(s)/Mail Date *08/02/2007*.
4) ☐ Interview Summary (PTO-413)
Paper No(s)/Mail Date. _____ .
5) ☐ Notice of Informal Patent Application
6) ☐ Other: _____.

DETAILED ACTION

Response to Amendment

The Examiner acknowledges the amending of claims 78-79.

Response to Arguments

Applicant's arguments filed 07/30/2007 have been fully considered but they are not persuasive.

The Applicant has argued that the combination of McCall in view of Stone is not proper as a reasonable expectation of success is not established. The Examiner does not agree.

McCall was used in the rejections to teach a high Q micro-resonating device. McCall failed to teach the device to have a Q value of at least 1x10^8. Stone was presented to teach that high Q micro-resonator devices similar to McCall's can be created to have Q values exceeding the claimed value. Stone demonstrates this in the plot shown at fig.5. Motivation was then presented to demonstrate a reason to combine the two teachings.

The Applicant further argues that McCall and Stone fall short of teaching how to make the proposed cavity, leading to the lack of expectation of success. Firstly, the Examiner is of the opinion that establishment of a prima facie case of obviousness does not require the need to disclose "how to make" the device in question (MPEP 2142). According to MPEP 2142, all of the claimed limitations must be taught or suggested. McCall teaches all of the structural features outlined in the device claims. Stone suggests creating the similar micro-resonators with a large Q value.

Finally, and building on the previous argument, the Applicant has stated that the plot of Stone outlines only theoretical possibilities. The Examiner agrees that it is not clearly stated that Stone has created a device that corresponds to each and every point on the plot. However, Stone teaches that the resonator structure is of a known type ('typical', see brief description of the drawings), and how to modify the structure by changing the deformation amount to obtain a desired Q value for a given application. In the end, Stone may not have created a device at every plot point, but he did outline the use of a typical structure and how to adjust the physical parameters of that structure to obtain the Q values taught. This, in the Examiner's opinion, is a clear teaching of how such a structure can be made (via adjustment of the deformation amount, Stone, col.4 lines 25-36).

In light of the above arguments the Examiner is of the belief that the rejections made over McCall in view of Stone would be considered both proper and reasonable to one of ordinary skill in the art.

Claim Rejections - 35 USC § 103

The following is a quotation of 35 U.S.C. 103(a) which forms the basis for all obviousness rejections set forth in this Office action:

> (a) A patent may not be obtained though the invention is not identically disclosed or described as set forth in section 102 of this title, if the differences between the subject matter sought to be patented and the prior art are such that the subject matter as a whole would have been obvious at the time the invention was made to a person having ordinary skill in the art to which said subject matter pertains. Patentability shall not be negatived by the manner in which the invention was made.

The factual inquiries set forth in *Graham* **v.** *John Deere Co.*, 383 U.S. 1, 148 USPQ 459 (1966), that are applied for establishing a background for determining obviousness under 35 U.S.C. 103(a) are summarized as follows:

1. Determining the scope and contents of the prior art.
2. Ascertaining the differences between the prior art and the claims at issue.
3. Resolving the level of ordinary skill in the pertinent art.
4. Considering objective evidence present in the application indicating obviousness or nonobviousness.

Claims 1-8, 10-18, 22, 28-41, 43-47, 49-58, 62, 67, and 81-82 are rejected under 35 U.S.C. 103(a) as being unpatentable over McCall (US 5343490) in view of Stone et al. (US 6259717).

With respect to claims 1, 2, 8, and 10, McCall teaches a micro-cavity resonator (70) being substantially parallel to a top surface of the pillar, comprising: a micro-cavity, a substrate portion (73) located below the micro-cavity forming a pillar (73), the pillar supporting the ultra-high Q micro-cavity, whereby optical energy travels along an inner surface of the micro-cavity (col.7 lines 18-50, fig.7). McCall does not teach the Q value to be at least 1x10^8. Stone teaches a micro-cavity optical resonator wherein it is taught that disc shaped micro-resonators (such as that taught by McCall) can have Q factors exceeding 10^10 (fig.5). It would have been obvious to one of ordinary skill in the art at the time of the invention to combine the resonator of McCall with the high Q teaching of Stone in order to allow optical energy to circulate in the resonator with a long photon lifetime and incur low losses.

With respect to claim 3, McCall teaches the micro-resonator of claim 1, including the resonator to be formed of silica (col.6 lines 58-68)

With respect to claim 4, McCall teaches the micro-cavity to be substantially circular and to have a diameter of about 10um (col.7 line 38).

With respect to claims 5-6, McCall teaches a toroid shaped micro-cavity having a thickness of about 5um (4um, col.8 line 39, fig.4).

With respect to claim 7, McCall teaches the use of an elliptical shape (col.9 line 64).

With respect to claim 11, McCall and Maleki teach the resonator as outlined in the rejection to claim 1, and McCall further teaches a 10um diameter (col.7 line 38).

With respect to claims 12, 14, 18, and 28, McCall and Maleki teach the resonator outlined in the rejection to claim 1, but do not teach the use of a silicon substrate. Silicon substrates are materials are known in the art to be used with resonator devices. It would have been obvious to one having ordinary skill in the art at the time the invention was made to make the resonator of these known materials, since it has been held to be within the general skill of a worker in the art to select a known material on the basis of its suitability for the intended use as a matter of obvious design choice. *In re Leshin*, 227 F.2d 197, 125 USPQ 416 (CCPA 1960).

With respect to claim 13, McCall teaches a resonant mode within the resonator comprising a whispering-gallery mode (WGM) (col.6 line 30).

Claims 15-17 are rejected for the same reasons as claim 1. These claims merely detail the methods of forming the device. The method of forming a device is not germane to the patentability of the device itself, therefore these limitations are not given patentable weight. At best these claims could be characterized as product-by-process claims, where the process limitations are not limiting, only the structure implied by the process. See MPEP 2113. Here, the structure implied by the process steps is merely the structure of claim 1.

With respect to claim 22, McCall further teaches an optically active component within the cavity (col.5 lines 1-3).

With respect to claim 81, McCall and Stone teach the resonator outlined in the rejection to claim 1 above, and McCall further teaches reduction of the surface roughness (col.10 lines 10-15), but does not teach the roughness to be less than several nanometers. It would have been obvious to one of ordinary skill in the art at the time of the invention to adjust the surface roughness to less than several nanometers as an optimization through routine experimentation (see MPEP 2144.05 II A).

With respect to claims 29, 34, 37, and 43, McCall teaches a high Q micro-cavity resonator comprising a toroid shape and an optical material (inherently meltable, and inherently adhered to itself), and a substrate that supports the optical material wherein optical energy travels along an inner surface of the resonator (col.7 lines 27-68, fig.7). McCall does not teach the Q value to be at least 1x10^8. Stone teaches a micro-cavity optical resonator wherein it is taught that disc shaped micro-resonators (such as that taught by McCall) can have Q factors exceeding 10^10 (fig.5). It would have been obvious to one of ordinary skill in the art at the time of the invention to combine the resonator of McCall with the high Q teaching of Stone in order to allow optical energy to circulate in the resonator with a long photon lifetime and incur low losses.

Claims 30 and 35 are rejected for the same reasons outlined in the rejection to claim 3 above.

Claims 31, 46, and 58 are rejected for the same reasons outlined in the rejections to claims 12, 14, 18, and 28 above.

Claims 32-33, and 49-57 are rejected for the same reasons as claim 29. These claims merely detail the methods of forming the device. The method of forming a device is not germane to the patentability of the device itself, therefore these limitations are not given patentable weight. At best these claims could be characterized as product-by-process claims, where the process limitations are not limiting, only the structure implied by the process. See MPEP 2113. Here, the structure implied by the process steps is merely the structure of claim 29.

Claim 36 is rejected for the same reasons outlined in the rejection to claim 4 above.

Claim 38 is rejected for the same reasons outlined in the rejection to claim 6 above.

Claim 39 is rejected for the same reasons outlined in the rejection to claim 7 above.

With respect to claim 40, McCall further teaches the cavity to be substantially parallel to a top surface of the pillar (fig.7).

With respect to claim 41, it is inherent that the size of the cavity is limited by the size of the top portion of the pillar, as a small pillar would not physically support too large a resonator.

With respect to claim 44, McCall further teaches the micro-cavity to be substantially circular and to have a diameter of about 10um (col.7 line 38).

Claim 45 is rejected for the same reasons outlined in the rejection to claim 13 above.

With respect to claim 47, McCall further teaches the substrate is in the form of a pillar.

Claim 62 is rejected for the same reason outlined in the rejection to claim 22 above.

Claim 67 is rejected for the same reasons given in the rejections to claims 29 and 58 above. *The examiner notes the forming the pillar via isotropically etching the substrate would be considered a non-limiting product by process limitation.*

Claim 82 is rejected for the same reason outlined in the rejection to claim 81 above.

Claims 19 and 48 are rejected under 35 U.S.C. 103(a) as being unpatentable over McCall and Stone and further in view of Gayral ("High-Q Wet-etched GaAs Microdisks Containing InAs quantum Boxes").

With respect to claims 19 and 48, McCall and Stone teach the resonators outlined in the rejections to claims 1 and 29, but do not teach the substrate to be tapered. Gayral teaches a tapered substrate (pg.1908). It would have been obvious to one of ordinary skill in the art at the time of the invention to combine the resonator of

McCall and Stone with the tapered shape of Gayral in order to realize low threshold light emitting or lasing devices, and aid in the prevention of oxidation.

Claims 20-21 and 60-61 are rejected under 35 U.S.C. 103(a) as being unpatentable over McCall and Stone in view of Chu ("Observation of Enhanced Photoluminescence in Erbium-Doped Semiconductor Microdisk Resonator").

With respect to claims 20-21 and 60-61, McCall and Stone teach the resonators outlined in the rejections to claims 1 and 29 above, but do not teach the use of a rare earth dopant. Chu teaches a micro-cavity resonator which uses a rare earth dopant (pg.2843). It would have been obvious to one of ordinary skill in the art at the time of the invention to combine the resonator of McCall and Stone with the dopants of Chu to insure a strong emission.

Claims 78-79 are rejected under 35 U.S.C. 103(a) as being unpatentable over McCall in view of Stone and Vollmer et al. ("Protein detection by optical shift of a resonant micro-cavity", applicant submitted prior art).

With respect to claims 78-79, McCall and Stone teach the resonators having the structures outlined in the rejections to claims 1 and 29, but do not teach the use of a biotinylated surface. Vollmer teaches micro-cavities using biotinylated surfaces (pg.2 col.2 para.5). It would have been obvious to one of ordinary skill in the art at the time of the invention to combine the resonator of McCall and Stone with the coating of Vollmer in order to detect biological agents.

Conclusion

THIS ACTION IS MADE FINAL. Applicant is reminded of the extension of time policy as set forth in 37 CFR 1.136(a).

A shortened statutory period for reply to this final action is set to expire THREE MONTHS from the mailing date of this action. In the event a first reply is filed within TWO MONTHS of the mailing date of this final action and the advisory action is not mailed until after the end of the THREE-MONTH shortened statutory period, then the shortened statutory period will expire on the date the advisory action is mailed, and any extension fee pursuant to 37 CFR 1.136(a) will be calculated from the mailing date of the advisory action. In no event, however, will the statutory period for reply expire later than SIX MONTHS from the mailing date of this final action.

Any inquiry concerning this communication or earlier communications from the examiner should be directed to Tod T. Van Roy whose telephone number is (571)272-8447. The examiner can normally be reached on M-F.

If attempts to reach the examiner by telephone are unsuccessful, the examiner's supervisor, Minsun Harvey can be reached on (571)272-1835. The fax phone number for the organization where this application or proceeding is assigned is 571-273-8300.

Information regarding the status of an application may be obtained from the Patent Application Information Retrieval (PAIR) system. Status information for published applications may be obtained from either Private PAIR or Public PAIR. Status information for unpublished applications is available through Private PAIR only. For more information about the PAIR system, see http://pair-direct.uspto.gov. Should you have questions on access to the Private PAIR system, contact the Electronic Business Center (EBC) at 866-217-9197 (toll-free). If you would like assistance from a USPTO Customer Service Representative or access to the automated information system, call 800-786-9199 (IN USA OR CANADA) or 571-272-1000.

TVR

MINSUN OH HARVEY
PRIMARY EXAMINER

EXHIBIT F

UNITED STATES PATENT AND TRADEMARK OFFICE

UNITED STATES DEPARTMENT OF COMMERCE
United States Patent and Trademark Office
Address: COMMISSIONER FOR PATENTS
P.O. Box 1450
Alexandria, Virginia 22313-1450
www.uspto.gov

APPLICATION NO.	FILING DATE	FIRST NAMED INVENTOR	ATTORNEY DOCKET NO.	CONFIRMATION NO.
10/678,354	10/02/2003	Deniz K. Armani	70120-00005	1793

58688 7590 03/07/2008
CONNOLLY BOVE LODGE & HUTZ LLP
P.O. BOX 2207
WILMINGTON, DE 19899

EXAMINER	
VAN ROY, TOD THOMAS	

ART UNIT	PAPER NUMBER
2828	

MAIL DATE	DELIVERY MODE
03/07/2008	PAPER

Please find below and/or attached an Office communication concerning this application or proceeding.

The time period for reply, if any, is set in the attached communication.

Interview Summary	**Application No.** 10/678,354	**Applicant(s)** ARMANI ET AL.	
	Examiner TOD T. VAN ROY	**Art Unit** 2828	

All participants (applicant, applicant's representative, PTO personnel):

(1) *TOD T. VAN ROY, Minsun Harvey*.

(2) *David Morse*.

(3)*Deniz Armani*.

(4)*Kerry Vahala*.

Date of Interview: *28 February 2008*.

Type: a)☒ Telephonic b)☐ Video Conference
c)☐ Personal [copy given to: 1)☐ applicant 2)☐ applicant's representative]

Exhibit shown or demonstration conducted: d)☐ Yes e)☒ No.
If Yes, brief description: _____.

Claim(s) discussed: *independent*.

Identification of prior art discussed: *McCall and Stone*.

Agreement with respect to the claims f)☐ was reached. g)☐ was not reached. h)☒ N/A.

Substance of Interview including description of the general nature of what was agreed to if an agreement was reached, or any other comments: *The Examiner and the Applicants discussed the type of Q values being obtained in the Stone reference as they relate to the instant invention. The Examiner suggests more descriptive claim language be used to differentiate between the two* .

(A fuller description, if necessary, and a copy of the amendments which the examiner agreed would render the claims allowable, if available, must be attached. Also, where no copy of the amendments that would render the claims allowable is available, a summary thereof must be attached.)

THE FORMAL WRITTEN REPLY TO THE LAST OFFICE ACTION MUST INCLUDE THE SUBSTANCE OF THE INTERVIEW. (See MPEP Section 713.04). If a reply to the last Office action has already been filed, APPLICANT IS GIVEN A NON-EXTENDABLE PERIOD OF THE LONGER OF ONE MONTH OR THIRTY DAYS FROM THIS INTERVIEW DATE, OR THE MAILING DATE OF THIS INTERVIEW SUMMARY FORM, WHICHEVER IS LATER, TO FILE A STATEMENT OF THE SUBSTANCE OF THE INTERVIEW. See Summary of Record of Interview requirements on reverse side or on attached sheet.

/TVR/
Examiner's signature, if required

Examiner Note: You must sign this form unless it is an Attachment to a signed Office action.

EXHIBIT G

Patent Docket:
70120-00005

IN THE UNITED STATES PATENT AND TRADEMARK OFFICE

In re the Application of:	Group Art Unit: 2828
Deniz K. Armani et al.	Examiner: Tod Thomas Van Roy
Serial No.: 10/678,354	
Filed: October 2, 2003	
For: ULTRA-HIGH Q MICRO-RESONATOR AND METHOD OF FABRICATION	

INTERVIEW SUMMARY

Hon. Commissioner for Patents
P.O. Box 1450
Alexandria, VA 22313-1450

Sir:

The following is a summary of the Examiner Interview which took place telephonically on February 28, 2008.

INTERVIEW SUMMARY

The Interview took place telephonically on February 28, 2008, with the following individuals in telephonic attendance:

David M. Morse
Kerry J. Vahala
Deniz K. Armani
Examiner Tod Thomas Van Roy
Supervising Examiner Minsun Harvey

Prior to the interview, Applicants faxed the attached Interview Agenda, which included proposed claim amendments, the Declaration of Deniz K. Armani in support of Non-Obviousness, and exhibits thereto to the Examiner.

During the interview, the scope of the independent claims were discussed, including Applicants' proposed amendments, along with the teachings of the prior art and Applicants' assertion that the Armani Declaration negated a finding of obviousness. Applicants presented the arguments outlined in the Interview Agenda, but no agreement was reached regarding allowability of the claims. As such, although the attached documents were provided to the Examiner for review, they were not previously entered.

Respectfully submitted,

CONNOLLY BOVE LODGE & HUTZ LLP

DATE: May 9, 2008

By: David M. Morse
Reg. No. 50,505

CONNOLLY BOVE LODGE & HUTZ LLP
1007 North Orange Street
P.O. Box 2207
Wilmington, Delaware 19899
(302) 658-9141
(302) 658-5614 (Fax)

Attachments:

Agenda For Applicant Initiated Interview, including proposed claim amendments and the Declaration of Deniz K. Armani, with attached Exhibits.

Patent Docket:
70120-00005

IN THE UNITED STATES PATENT AND TRADEMARK OFFICE

In re the Application of:	Group Art Unit: 2828
Deniz K. Armani et al.	Examiner: Tod Thomas Van Roy
Serial No.: 10/678,354	
Filed: October 2, 2003	
For: ULTRA-HIGH Q MICRO-RESONATOR AND METHOD OF FABRICATION	

AGENDA FOR APPLICANT INITIATED INTERVIEW

Dear Examiner Van Roy:

I am writing to confirm the telephonic interview scheduled for Thursday, February 28, 2008, at 2 PM EST concerning the above-encaptioned patent application, and to provide an agenda for the meeting.

The following individuals, exclusive of USPTO personnel, are anticipated to participate in the telephone conferece:

David M. Morse, Applicants' Representative
Deniz K. Armani, Applicant
Kerry J. Vahala, Applicant

Submitted for your consideration as part of the interview process is the proposed claim amendments included below, and the Declaration of Deniz K. Armani, submitted in support of a finding of non-obviousness for the amended claims.

PROPOSED CLAIM AMENDMENTS

1. (Currently Amended) An ultra-high Q micro-cavity resonator, comprising:

an ultra-high Q micro-cavity having a Q value of at least 1.00 x 10^8, the micro-cavity being substantially planar; and

a substrate,

portions of the substrate located below the ultra-high Q micro-cavity being removed to form a pillar, the pillar supporting the ultra-high Q micro-cavity, whereby optical energy travels along an inner surface of the ultra-high Q micro-cavity.

2. (Cancelled)

3. (Original) The resonator of claim 1, the micro-cavity comprising an ultra-high Q silica micro-cavity.

4. (Original) The resonator of claim 1, the micro-cavity being substantially circular and having a diameter of about 10 micrometers to about 500 micrometers.

5. (Original) The resonator of claim 1, the micro-cavity having a toroid shape.

6. (Original) The resonator of claim 5, the toroid-shaped micro-cavity having a thickness of about five to about ten micrometers.

7. (Original) The resonator of claim 1, the micro-cavity having an elliptical shape.

8. (Original) The resonator of claim 1, the micro-cavity being substantially parallel to a top surface of the pillar.

9. (Canceled)

10. (Previously Presented) The resonator of claim 1, the micro-cavity having a Q value of about 10^8 to about 5×10^8.

11. (Previously Presented) The resonator of claim 1, the micro-cavity having a diameter of about 10 micrometers to about 30 micrometers and a Q value of about 500 million.

12. (Original) The resonator of claim 1, the micro-cavity comprising a glass material having a melting point that is lower than a melting point of the substrate.

13. (Original) The resonator of claim 1, a resonant mode within the micro-cavity comprising a whispering-gallery mode (WGM).

14. (Original) The resonator of claim 1, the substrate comprising a silicon substrate.

15. (Previously Presented) The resonator of claim 1, the substrate underneath the micro-cavity being removed by an etchant.

16. (Original) The resonator of claim 15, the etchant comprising a xenon difluoride (XeF_2) gas.

17. (Original) The resonator of claim 16, wherein the XeF_2 gas isotropically etches the substrate beneath a periphery of the micro-cavity to form the pillar.

18. (Original) The resonator of claim 17, the substrate comprising a silicon substrate.

19. (Original) The resonator of claim 1, the pillar having a tapered shape.

20. (Previously Presented) The resonator of claim 1, the micro-cavity including a rare earth dopant.

21. (Original) The resonator of claim 20, the rare Earth dopant being erbium, ytterbium, or neodymium.

22. (Previously Presented) The resonator of claim 1, the micro-cavity including an optically active component.

23. (Canceled)

24. (Canceled)

25. (Canceled)

26. (Canceled)

27. (Canceled)

28. (Original) The resonator of claim 1, the micro-cavity comprising a silica ultra-high Q micro-cavity, and the substrate comprising a silicon substrate.

29. (Currently Amended) An ultra-high Q micro-cavity resonator, comprising:

an optical material; and

a substrate that supports the optical material, wherein

the optical material is meltable by heat so that a periphery of the optical material adheres to itself to form an ultra-high Q micro-cavity having a Q value of at least 1.00 x 10^8, ~~and wherein~~

the micro-cavity is substantially planar, and

optical energy travels along an inner surface of the ultra-high Q micro-cavity.

30. (Original) The resonator of claim 29, the optical material comprising silica.

31. (Original) The resonator of claim 29, the optical material comprising a glass material having a melting point that is lower than a melting point of the substrate.

32. (Previously Presented) The resonator of claim 29, the optical material comprising a disk, wherein a diameter of the optical material becomes smaller when heated to form a disk.

33. (Previously Presented) The resonator of claim 32, wherein the diameter decreases until the molten optical material collapses after which the diameter remains substantially constant.

34. (Cancelled)

35. (Original) The resonator of claim 29, the ultra-high Q micro-cavity comprising an ultra-high Q silica micro-cavity.

36. (Original) The resonator of claim 29, the ultra-high Q micro-cavity being substantially circular and having a diameter of about 10 micrometers to about 500 micrometers

37. (Original) The resonator of claim 29, the ultra-high Q micro-cavity having a toroid shape.

38. (Original) The resonator of claim 37, the toroid having a thickness of about five to about ten micrometers.

39. (Original) The resonator of claim 29, the ultra-high Q micro-resonator having an elliptical shape.

40. (Original) The resonator of claim 29, the ultra-high Q micro-cavity being substantially parallel to a top surface of the pillar.

41. (Original) The resonator of claim 29, wherein a size of the ultra-high Q micro-cavity is limited by a size of a top surface of the substrate.

42. (Canceled)

43. (Previously Presented) The resonator of claim 29, the ultra-high Q micro-cavity having a Q value of about 10^8 to about 5×10^8.

44. (Previously Presented) The resonator of claim 29, the ultra-high Q micro-cavity having a diameter of about 10 micrometers to about 30 micrometers and a Q value of about 500 million.

45. (Original) The resonator of claim 29, a resonant mode within the ultra-high Q micro-cavity being a whispering-gallery mode (WGM).

46. (Original) The resonator of claim 29, the substrate comprising a silicon substrate.

47. (Original) The resonator of claim 29, wherein portions of the substrate located below the ultra-high Q micro-cavity are removed to form a pillar, the pillar supporting the ultra-high Q micro-cavity.

48. (Previously Presented) The resonator of claim 47, the pillar having a tapered shape.

49. (Previously Presented) The resonator of claim 29, the substrate underneath the periphery of the ultra-high Q micro-cavity being removed by an etchant.

50. (Original) The resonator of claim 49, the etchant comprising xenon difluoride (XeF_2) gas.

51. (Original) The resonator of claim 50, wherein the XeF_2 gas isotropically etches the substrate beneath the periphery of the micro-cavity.

52. (Original) The resonator of claim 29, the heat source comprising an Excimer laser.

53. (Previously Presented) The resonator of claim 52, wherein the Excimer laser heats and liquefies the optical material.

54. (Original) The resonator of claim 29, the heat source comprising a CO_2 laser.

55. (Original) The resonator of claim 54, wherein the CO_2 laser emits radiation having a wavelength of about 10.6 micrometers.

56. (Original) The resonator of claim 54, wherein the CO_2 laser heats the optical material for about 1 microsecond to about 10 seconds.

57. (Original) The resonator of claim 54, wherein the CO_2 laser heats and liquefies the optical material.

58. (Original) The resonator of claim 29, wherein the optical material comprises silica and the substrate comprises silicon.

59. (Canceled)

60. (Previously Presented) The resonator of claim 29, the ultra-high Q micro-cavity including a dopant.

61. (Original) The resonator of claim 60, the dopant being erbium, ytterbium, or neodymium.

62. (Previously Presented) The resonator of claim 29, the ultra-high Q micro-cavity including an optically active component.

63. (Canceled)

64. (Canceled)

65. (Canceled)

66. (Canceled)

67. (Previously Presented) A planar micro-cavity resonator, comprising:

an ultra-high Q toroid-shaped planar silica micro-cavity having a Q value of at least 1.00 x 10^8; and

a silicon substrate;

wherein portions of the silicon substrate located below a periphery of the ultra high-Q toroid-shaped planar silica micro-cavity are isotropically etched to form a silicon pillar, the silicon pillar supporting the ultra-high Q toroid-shaped planar silica micro-cavity, and wherein light energy traverses along an inner surface of the ultra-high Q toroid-shaped planar micro-cavity.

68. (Withdrawn) A method of forming an ultra-high Q micro-cavity, comprising:

providing a substrate and an optical material;

etching the substrate to form a pillar, the pillar supporting the optical material; and

heating a periphery of the optical material so that the periphery melts and adheres to itself to form the ultra-high Q micro-cavity having a Q value of at least 1.00 x 10^8, whereby optical energy travels along an inner surface of the ultra-high Q micro-cavity.

69. (Withdrawn) The method of claim 68, providing the substrate further comprising providing a silicon substrate.

70. (Withdrawn) The method of claim 69, wherein etching the silicon substrate to form a silicon pillar further comprises isotropically etching the silicon substrate with a xenon difluoride gas.

71. (Withdrawn) The method of claim 69, providing the optical material further comprising providing silica (SiO2).

72. (Withdrawn) The method of claim 69, wherein heating the periphery of the optical material further comprises heating the periphery with an Excimer laser.

73. (Withdrawn) The method of claim 72, wherein heating the periphery with the Excimer laser further comprises liquefying the optical material.

74. (Withdrawn) The method of claim 69, wherein heating the periphery of the optical material further comprises heating the periphery with a CO_2 laser.

75. (Withdrawn) The method of claim 74, wherein heating the periphery with the CO_2 laser further comprises heating the periphery with the CO_2 laser at a wavelength of about 10.6 micrometers.

76. (Withdrawn) The method of claim 74, wherein heating the periphery with the CO_2 laser further comprises heating the periphery for about 1 microsecond to about 10 seconds.

77. (Withdrawn) The method of claim 74, wherein heating the periphery with the CO_2 laser further comprises liquefying the optical material.

78. (Currently Amended) A micro-cavity resonator, comprising:

an ultra-high Q micro-cavity having a Q value of at least 1.00 x 10^8 and having a biotinylated surface, the micro-cavity being substantially planar; and

a substrate, portions of the substrate located below the ultra-high micro-cavity being removed to form a pillar that supports the ultra-high Q micro-cavity, whereby optical energy travels along an inner surface of the micro-cavity.

79. (Previously Presented) An ultra-high Q micro-cavity resonator, comprising:

an optical material; and

a substrate that supports the optical material, wherein

the optical material is meltable by a heat source so that a periphery of the optical material adheres to itself to form an ultra-high Q micro-cavity, the ultra-high Q micro-cavity having a Q value of at least 1.00 x 10^8 and having a biotinylated surface, ~~and wherein~~

the micro-cavity is substantially planar, and

optical energy travels along an inner surface of the ultra-high Q micro-cavity.

80. (Withdrawn) The method of claim 68, further comprising etching the optical material.

81. (Previously Presented) The ultra-high Q micro-cavity resonator of claim 1 having a root mean square (rms) roughness of several nanometers.

82. (Previously Presented) The ultra-high Q micro-cavity resonator of claim 29 having a root mean square (rms) roughness of several nanometers.

INTERVIEW AGENDA

At the scheduled interview, Applicants intent to discuss the following:

1. The proposed claim amendments in view of the prior art of record. Each of the independent claims, namely claims 1, 29, 67, 78, and 79, in the application now include limitations indicating that the micro-cavity is substantially planar or planar.

2. The Declaration of Deniz K. Armani in Support of Non-Obviousness. This Declaration and the accompanying exhibits have been submitted as evidence to support Applicants' assertion that the proposed amended claims are not obvious on the basis that the prior art of record could not be modified with a reasonable expectation of success to create the subject matter of the claims. A reasonable expectation of success is a requirement of establishing a prima facie case of obviousness. *See* MPEP § 2143.02; *See also*, *In re Dow Chemical Co.*, 837 F.2d 469, 473, 5 U.S.P.Q.2d (BNA) 1529, 1531 (Fed. Cir. 1988) ("Both the suggestion and the expectation of success must be founded in the prior art, not in applicant's disclosure."); *In re O'Farrell*, 853 F.2d 894, 903, 7 USPQ2d 1673, 1681 (Fed. Cir. 1988) (evidence suggesting the modification to prior art would be successful was a key factor in a finding of obviousness.).

Here, Applicants present evidence showing that, at the time the present application was filed and for at least 5 years afterward, other independent studies confirm that attempts have been made to fabricate planar microresonators, and that those attempts have resulted in planar microresonators having Q factors of no more than 3 magnitudes less than what is described and claimed in the present application.

In view of this evidence, Applicants submit that when the respective teachings of the prior art of record are considered, a person of skill in the art would have no reasonable expectation of successfully fabricating a substantially planar or planar microresonator having a Q factor of at least 1.00×10^8 on a substrate.

Applicants and the undersigned thank the Examiner for taking the time to review these materials in advance of the Interview.

Respectfully submitted,

CONNOLLY BOVE LODGE & HUTZ LLP

DATE: February 25, 2008

By: ____________________
David M. Morse
Reg. No. 50,505

CONNOLLY BOVE LODGE & HUTZ LLP
The Nemours Building
1007 North Orange Street
P.O. Box 2207
Wilmington, Delaware 19899
(302) 658-9141
(302) 658-5614 (Fax)

Patent Docket:
70120-00005

IN THE UNITED STATES PATENT AND TRADEMARK OFFICE

In re the Application of:	Group Art Unit: 2828
Deniz K. Armani et al.	Examiner: Tod Thomas Van Roy
Serial No.: 10/678,354	
Filed: October 2, 2003	
For: ULTRA-HIGH Q MICRO-RESONATOR AND METHOD OF FABRICATION	

DECLARATION OF DENIZ K. ARMANI SUBMITTED IN SUPPORT OF NON-OBVIOUSNESS

I, Deniz K Armani, one of the named inventors in the above-encaptioned patent application, hereby declare as follows:

1. I am familiar with the timeline associated with the development of the technology disclosed in the present application and the subsequent publication reporting on the technological developments. The present application claims priority to U.S. Provisional Application Serial No. 60/415,412, filed October 2, 2002 (hereinafter the "Priority Application"). The technological developments disclosed in the present application were publicly reported in an article published as D. K. Armani et al., "Ultra high-Q toroid microcavity on a chip," *Nature*, Vol. 421, pp. 925–929, Feb. 2003 (hereinafter the "*Nature* Article").

2. I have reviewed the article entitled "Ultrahigh-quality-factor silicon-on-insulator microring resonator", as published by Jan Niehusmann et al. in *Optics Letters*, Vol. 29, No. 24, December 15, 2004, a true and correct copy of which is attached as Exhibit 1.

Niehusmann et al. describe the development of Silicon-on-insulator (SOI) microring resonators.

3. Niehusmann et al. state that SOI integrated technology is anticipated to be highly beneficial for the convergence of microelectronics and photonics because due to cost savings that can be realized by integrating photonic and electronic functions on the same substrate. These same benefits were understood, but not fully realized, in October 2002 when the Priority Application was filed. This article also describes possible applications for microring resonators having a "high Q factor" or a "very high Q factor", such as for telecommunication applications in providing wavelength selective filtering, add-drop multiplexing, compact dispersion compensation, and frequency-selective coupling, or for chemical or biomolecule sensor applications, or even to enhance evanescent-field fluorescence sensing.

4. The Q factor reported for the SOI microring resonators developed by Niehusmann et al. were 139.000 ± 6.000. These SOI microring resonators were fabricated directly on a substrate, and Niehusmann et al. reported that the Q factor was "much higher than [any Q factor values that] have been reported up to now" for integrated microring resonators. Niehusmann et al. recognized a single exception to their statement based upon SOI microring resonators fabricated by utilizing surface tension in the materials generated by a melting process. In recognizing this exception, Niehusmann et al. cited to the *Nature* Article. Moreover, Niehusmann et al. stated in the abstract of the paper that:

> "These [(the Q factor reported)] are *believed to be the highest values reported* for a curved SOI waveguide device and for any directly structured semiconductor microring fabricated without additional melting-induced surface smoothing."

(Emphasis added.)

5. I have reviewed the article entitled "Silicon Microtoroidal Resonators With Integrated MEMS Tunable Coupler", as published by Jin Yao et al. in *IEEE Journal Of Selected Topics In Quantum Electronics*, Vol. 13, No. 2, March/April 2007, a true and correct copy of which is attached as Exhibit 2. Yao et al. describe an silicon microtoroidal resonator integrated on a substrate with a tunable optical coupler.

6. In this 2007 paper, Yao et al. report a process for fabricating a microtoroidal resonator integral to a substrate that also includes a MEMS-actuated tunable optical coupler. The process used to fabricate the microtoroidal resonator is a hydrogen annealing process, which enables creation of the microtoroidal structure and preserves the desired optical qualities of the microtoroidal resonator. The unloaded Q factor achieved by this fabrication process is reported to be as high as 1.0×10^5. Yao et al. indicate that very high Q factors have been demonstrated in SiO^2, but that because of the thermal reflow process used to create such microtoroidal resonators, such processes cannot be applied to integrated SOI photonics devices. The thermal reflow process referred to by Yao et al. is the one described in the *Nature* Article authored by the named inventors of the present application, which produces microtoroidal resonators having Q factors as high as 5×10^8.

7. Through my work in developing the technology disclosed in the present application, I am now and was, at the time the Priority Application was filed, familiar with the state of the art for microring and microdisk resonators. When the Priority Application was filed, I was aware of microdisk resonators having Q factors as high as 17,000. Those microdisk resonators were constructed from GaAs formed into disks upon a pedestal formed from a substrate AlGaAs. The article reporting and describing these microdisk resonators was included as part of the Information Disclosure Statement filed on March 1, 2004 as cite No. 7 in the Non-Patent Literature Documents section of form PTO/SB/08B. I was also aware of microring resonators having Q factors as high as 13,000. Those microring resonators were constructed from polymers forming a

microring on a silicon substrate (but not on a pedestal). The article reporting and describing these microdisk resonators was included as part of the Information Disclosure Statement filed on March 1, 2004 as cite No. 12 in the Non-Patent Literature Documents section of form PTO/SB/08B. At the time the Priority Application was filed, I was not aware, nor am I currently aware, of any other microring or microdisk resonators achieving Q factors approaching within three orders of magnitude of 10^7, other than those fabricated using the techniques developed by myself and my co-inventors.

8. I have reviewed U.S. Patent No. 6,259,717 to Stone et al., which is part of the prosecution record for the present patent application. Stone et al. do not disclose any of microring resonators, microtoroidal resonators, or any other type of substantially planar microresonator. Rather, Stone et al. disclose deformed cylindrical resonators and prolate spheroidal resonators as shown in Figs. 3a & 3b, respectively. Moreover, Fig. 5, which is a plot obtained by numerical solutions to the wave equation, illustrates *anticipated* Q factors for a cylindrical asymmetric resonant cavity only. As such, the stated theoretical values for such a cylindrical resonator are inapplicable to Q factors achievable for microring resonators.

9. I further declare under penalty of perjury that all statements made herein of my own knowledge are true and that all statements made on information and belief are believed to be true; and further that these statements are made with the knowledge that willful false statements and the like so made are punishable by fine or imprisonment, or both, under Title 18, United States Code § 1001, and that such willful false statements may jeopardize the validity of the application or any patent issuing thereon.

DATE: 2/12/2008

By: ______________________
Deniz K. Armani

EXHIBIT 1

Ultrahigh-quality-factor silicon-on-insulator microring resonator

Jan Niehusmann, Andreas Vörckel, and Peter Haring Bolivar

Institut für Halbleitertechnik, Rheinisch-Westfälische Technische Hochschule Aachen, Sommerfeldstrasse 24, 52056 Aachen, Germany

Thorsten Wahlbrink and Wolfgang Henschel

Advanced Micro-electronic Center Aachen (AMICA), AMO GmbH, Huyskensweg 25, 52074 Aachen, Germany

Heinrich Kurz

Institut für Halbleitertechnik, Rheinisch-Westfälische Technische
Hochschule Aachen, Sommerfeldstrasse 24, 52056 Aachen, Germany, and
Advanced Micro-electronic Center Aachen (AMICA), AMO GmbH, Huyskensweg 25, 52074 Aachen, Germany

Received May 27, 2004

The development of ultrahigh-quality-factor (Q) silicon-on-insulator (SOI) microring resonators based on silicon wire waveguides is presented. An analytical description is derived, illustrating that in addition to low propagation losses the critical coupling condition is essential for optimizing device characteristics. Propagation losses as low as 1.9 ± 0.1 dB/cm in a curved waveguide with a bending radius of 20 μm and a Q factor as high as 139.000 ± 6.000 are demonstrated. These are believed to be the highest values reported for a curved SOI waveguide device and for any directly structured semiconductor microring fabricated without additional melting-induced surface smoothing. © 2004 Optical Society of America

OCIS codes: 130.3120, 230.5750.

Silicon-on-insulator (SOI) technology is a promising platform for the convergence of microelectronics and photonics. It has a large potential given the high photonic integration capabilities that are made possible by the high refractive-index contrast between silicon and typical cladding materials, the natural vertical confinement of optical waves given by the buried oxide layer, and the potential cost-efficient integration of photonic and electronic functions on the same substrate given by silicon technology.[1,2] However, at the same time, these beneficial characteristics lead to stringent manufacturing tolerances and a high sensitivity to surface roughness, as the higher refractive index of silicon in comparison with silica implies smaller silicon wire waveguide dimensions.[3] It is therefore critical to optimize manufacturing tolerance and to minimize surface roughness to facilitate useful low-loss SOI photonic solutions.[4]

In this Letter we present the development of high-quality SOI microring resonators based on silicon wire waveguides. These microrings can find direct application in the areas of telecommunication, sensors, quantum electrodynamics, and nonlinear optics.[5] For telecommunication, microrings have a multitude of applications, allowing wavelength-selective filtering, add–drop multiplexing, compact dispersion compensation, and frequency-selective coupling in optical networks.[6–8] Additionally, microrings are excellent model systems for deriving fundamental properties of curved waveguides as a crucial building block of photonic integrated circuits. Here we demonstrate a microring resonator with maximized quality factor Q to illustrate and quantify the low loss that can be achieved by use of an improved SOI process technology. Although the high Q factor demonstrated here surpasses typical needs of actual telecommunication data channels, the associated low loss is an indicator of the large degree of freedom in the future design of more complex and very large scale integrated telecommunication components that can be achieved with advanced SOI waveguide technology.

Microrings with a very high Q factor can also be used directly for sensor applications, where the dielectric loading and concomitant frequency shift of a resonator are used to monitor chemicals or biomolecules[9,10] or the higher field in the resonator is used to enhance evanescent-field fluorescence sensing.[11] In this type of application higher Q factors allow smaller resonance shifts to be detected. The internal field enhancement also increases sensitivity. Ultrahigh-Q optical microcavities with Q factors of up to 8×10^9 were recently demonstrated by use of microspheres.[12] However, these and similarly attractive microtoroids demonstrated in silicon[13] make use of the formation of ultraflat surfaces on the spheres and (or) microtoroids by using the surface tension during a melting process. This makes integration into photonic circuits and the dimensional control of the device during manufacture problematic. Here we present directly structured SOI-based microring resonators with Q factors that are much higher than have been reported up to now.

For proper design and optimization of a high-quality resonator, several aspects have to be considered. Most obviously, a sharp resonance, i.e., a high Q, is desired to observe small resonance wavelength shifts, which is necessary for sensing or switching applications. The

0146-9592/04/242861-03$15.00/0 © 2004 Optical Society of America

Q factor of a microring resonator coupled to a single waveguide is given by

$$Q = \frac{2\pi n_{\mathrm{eff}}}{\lambda_0}\,\frac{L}{2\arccos\{[1 - 4t/\tau + (t/\tau)^2]/(-2t/\tau)\}} = \frac{\lambda_0}{\Delta\lambda_{3\,\mathrm{dB}}}, \tag{1}$$

where n_{eff} is the effective index of refraction of the propagating mode in the microring, λ_0 is the resonance wavelength, L is the length of the microring, t is the field transmission coefficient at the waveguide–resonator coupling, and $\tau = \exp(-\alpha L/2)$ is the attenuation of the field per round trip for a microring resonator with attenuation constant α.[14] A reasonably noticeable shift of the resonance wavelength should be of the order of $\Delta\lambda_{\mathrm{detect}} \approx {}^{1}\!/_{2}\,\Delta\lambda_{3\,\mathrm{dB}}$. Thus it is evident that high Q factors are necessary for sensitive switching or sensing devices. The Q factor of an actual device depends on the chosen geometry, which determines parameters t, L, and n_{eff} in Eq. (1), and on the propagation losses in the ring, which determine τ.

For $t\tau$ close to 1, Eq. (1) can be approximated by

$$Q = \frac{2\pi n_{\mathrm{eff}}}{\lambda_0}\,\frac{L}{-2\ln t\tau}; \tag{2}$$

i.e., Eq. (1) is dependent on the product $t\tau$, which sums up propagation and coupling losses. Coupling losses are a free design parameter. Hence it is useful to estimate the maximum achievable Q factor that can be achieved with a given technology from the propagation loss $\alpha = -2(\ln \tau/L)$ inside the cavity. Neglecting the coupling loss to external waveguides, the maximum achievable Q factor can easily be determined from Eq. (2) as

$$Q_{\mathrm{limit}} = \frac{2\pi n_{\mathrm{eff}}}{\lambda_0}\,\frac{L}{-2\ln\tau} = \frac{2\pi n_{\mathrm{eff}}}{\lambda_0}\,\frac{1}{\alpha}. \tag{3}$$

Minimizing losses is therefore of prime importance for the development of ultrahigh-Q microcavities. In the case of SOI-based waveguide technology, low propagation losses can only be achieved with ultrasmooth waveguide surfaces, requiring specific optimized processing steps.

For reliable detection of a resonance shift or switching event, a large throughput attenuation of the signal of the coupled waveguide as a result of the resonance in the microring is necessary. This can be achieved by critical coupling, where complete throughput attenuation at resonance is achieved. The condition for critical coupling is given by $t = \tau$ in Eq. (1).[14] In that case the Q factor of the microcavity is given by $Q_{\mathrm{critical}} = Q_{\mathrm{limit}}/2$. Thus, for practical sensor applications only half the maximum Q factor that is possible as a result of the propagation loss can be used effectively.

A further technical parameter of importance is the cavity field enhancement. For applications based on a nonlinear material response, such as photonic switching, stronger fields inside the resonator induce larger shifts of the resonance wavelength, lowering, e.g., switching thresholds. The field enhancement factor at critical coupling conditions is given by

$$\mathrm{FE}_{\mathrm{critical}} = \frac{1}{\sqrt{1-\tau^2}}. \tag{4}$$

Here again, the maximum field enhancement coincides with a low propagation loss per round trip in the cavity. Therefore low propagation losses are the key issue in addressing most of the general requirements of microring resonators.

Several wire waveguide microrings based on SOI technology have been reported.[6,14] However, because of technological restrictions, the Q factor has been limited to values of the order of 2.500. Two aspects are optimized here, in comparison to former approaches[14]: an optimization of the pattern generation during electron-beam lithography (EBL) is performed, and the surface roughness during pattern transfer to the silicon waveguides is optimized. The waveguides are fabricated on SOI substrates consisting of a 1-μm-thick buried oxide layer and a 0.45-μm-thick device layer. For the waveguides a width of 0.5 μm has been chosen. The devices are defined by EBL using hydrogen silsesquioxane as an EBL resist.[15] Corrections are performed on the EBL pattern generation by preprocessing the microring into minimal feature size polygons. This minimizes the rectangular discontinuities that are characteristic of standard pattern generation of curved structures and that can reach several tens of nanometers. Pattern transfer is achieved by HBr inductive coupled reactive-ion etching, which selectively stops at the Si/SiO$_2$ interface, optimizing the etching parameters to minimize surface roughness. The input and output facets of the waveguides are prepared by cleaving the sample. A scanning electron microscope image of a typical device is depicted in Fig. 1.

For device characterization a commerical measurement setup consisting of a tunable external cavity diode laser and a photodiode is used. TM-polarized light (electric field perpendicular to the device plane) is butt coupled to the input by a polarization-maintaining optical fiber. The light at the throughput waveguide is

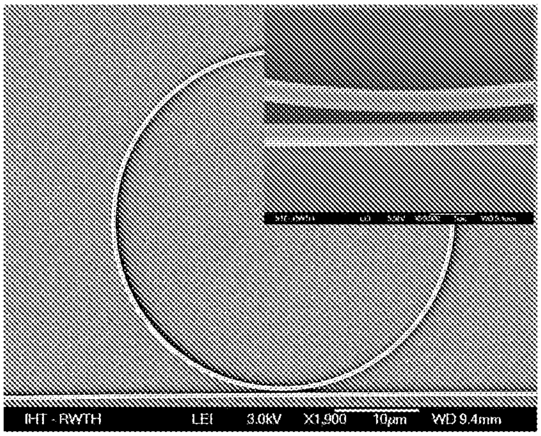

Fig. 1. Scanning electron micrographs of a SOI microring resonator with a radius of 20 μm, including an overview and a coupling region closeup (inset).

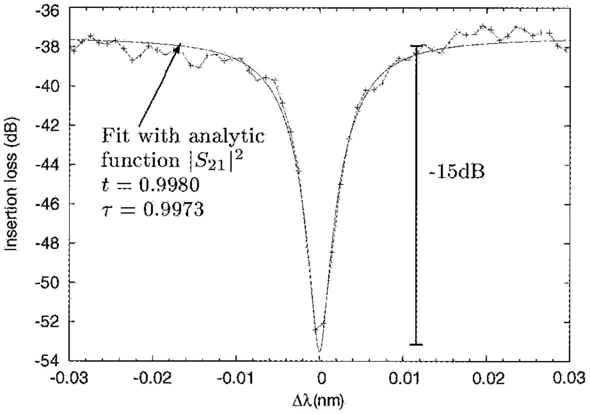

Fig. 2. Measured insertion loss and fit of analytical transfer function of a SOI microring resonator of radius $r = 20\ \mu\text{m}$, with $\Delta\lambda = \lambda - 1547.680$ nm.

butt coupled to a multimode fiber connected to a photodetector. The analytical transfer function of the device is given by[14]

$$|S_{21}|^2 = \frac{t^2 - 2t\tau \cos \phi + \tau^2}{1 - 2t\tau \cos \phi + (t\tau)^2}, \tag{5}$$

where $\phi = 2\pi(L_{\text{eff}}/\lambda) = (4\pi^2 r_{\text{eff}} n_{\text{eff}})/\lambda$ is the phase shift per round trip around the resonator. Figure 2 shows the measured insertion loss spectrum of a SOI microring resonator with a radius of $r = 20\ \mu\text{m}$ and a gap of $0.25\ \mu\text{m}$ between the microring resonator and the adjacent waveguide. The analytical transfer function $|S_{21}|^2$ is fitted to the resonance at the wavelength $\lambda = 1547.68$ nm, and $n_{\text{eff}} = 2.5864$ is derived from the resonance wavelengths. The fit yields values of $t = 0.9980 \pm 0.0002$ and $\tau = 0.9973 \pm 0.0001$, demonstrating that favorable critical coupling has nearly been achieved. Therefore a significant throughput attenuation of -15 dB at resonance is observed. The superposed oscillation is due to Fabry–Perot effects in the periphery of the device. As $|S_{21}|^2$ is invariant to commutation of t and τ, we chose the conservative values where $t > \tau$; i.e., attenuation of the wave propagating through the ring is higher than coupling from the ring to the waveguide. This choice does not influence the Q factor, but it means that the propagation loss may actually be even lower than calculated below.

Applying Eq. (1) to the fitted parameters yields a Q factor of $Q \approx 139.000 \pm 6.000$, which agrees with a direct linewidth estimation. As an illustration, this means that using this resonator as a sensor allows the detection of a resonance wavelength shift as low as $\Delta\lambda_{\text{detect}} \approx 0.006$ nm, which can easily be detected as a -3-dB signal change. This wavelength shift corresponds to a shift of the effective refractive index of as low as $\Delta n_{\text{eff, detect}} \approx 1.7 \times 10^{-5}$.

Taking τ obtained from the fit of $|S_{21}|^2$ to the experimental data and the length L of the device, the propagation loss inside the microring resonator can be deduced from

$$\alpha\left[\frac{\text{dB}}{\text{cm}}\right] = \frac{-2 \times 10^5 \log_{10}(\tau)}{L[\mu\text{m}]}. \tag{6}$$

For the resonance shown in Fig. 2, Eq. (6) gives a propagation loss of $\alpha \approx 1.9 \pm 0.1$ dB/cm. To our knowledge this is the lowest propagation loss reported for a SOI ring resonator or any curved SOI wire waveguide fabricated by reactive-ion etching without any further smoothing steps [e.g., melting and (or) thermal oxidation]. This result is similar to the best values reported for straight SOI waveguides.[16]

In summary, we have presented the design, fabrication, and optical characterization of ultrahigh-Q SOI microring resonators. We illustrate that, in addition to a minimization of losses to attain a high Q factor, the condition of critical coupling is of fundamental relevance for achieving high-efficiency devices. We demonstrate the development of microring resonators based on an optimized SOI fabrication technology, yielding what is to our knowledge the highest Q factor of 139.000 ± 6.000 and the lowest propagation loss without additional smoothing steps ever reported for SOI ring resonator technology.

The authors thank P. Kersten for motivating this work. This work was supported by European Commission contract IST-2001-38919 (PHOENIX) and the Ministerium für Wissenschaft und Forschung des Landes Nordrhein Westfalen. J. Niehusmann's e-mail address is niehusmann@iht.rwth-aachen.de.

References

1. B. N. Kurdi and D. G. Hall, Opt. Lett. **13,** 175 (1988).
2. R. A. Soref, Proc. IEEE **81,** 1687 (1993).
3. K. K. Lee, D. R. Lim, H.-C. Luan, A. Agarwal, J. Foresi, and L. C. Kimerling, Appl. Phys. Lett. **77,** 1617 (2000).
4. T. Tsuchizawa, T. Watanabe, E. Tamechika, T. Shoji, K. Yamada, J. Takahashi, S. Uchiyama, S. Itabashi, and H. Morita, in *LEOS Annual Meeting* (Lasers and Electro-Optics Society, Piscataway, N.J., 2002), p. 287.
5. K. J. Vahala, Nature **424,** 839 (2003).
6. B. E. Little, J. S. Foresi, G. Steinmeyer, E. R. Thoen, S. T. Chu, H. A. Haus, E. P. Ippen, L. C. Kimerling, and W. Greene, IEEE Photon. Technol. Lett. **10,** 549 (1998).
7. B. E. Little, S. T. Chu, W. Pan, and Y. Kokubun, IEEE Photon. Technol. Lett. **12,** 323 (2000).
8. L. Eldada, Rev. Sci. Instrum. **75,** 575 (2004).
9. C.-Y. Chao and L. J. Guo, Appl. Phys. Lett. **83,** 1527 (2003).
10. E. Krioukov, D. J. W. Klunder, A. Driessen, J. Greve, and C. Otto, Opt. Lett. **27,** 512 (2002).
11. S. Blair and Y. Chen, Appl. Opt. **40,** 570 (2001).
12. D. W. Vernooy, V. S. Ilchenko, H. Mabuchi, E. W. Streed, and H. J. Kimble, Opt. Lett. **23,** 247 (1998).
13. D. K. Armani, T. J. Kippenberg, S. M. Spillane, and K. J. Vahala, Nature **421,** 925 (2003).
14. A. Vörckel, M. Mönster, W. Henschel, P. Haring Bolivar, and H. Kurz, IEEE Photon. Technol. Lett. **15,** 912 (2003).
15. W. Henschel, Y. M. Georgiev, and H. Kurz, J. Vac. Sci. Technol. B **21,** 2018 (2003).
16. P. Dumon, W. Bogaerts, J. Van Campenhout, V. Wiaux, J. Wouters, S. Beckx, and R. Baets, in *LEOS Annual Meeting* (Lasers and Electro-Optics Society, Piscataway, N.J., 2003), p. 289.

EXHIBIT 2

Silicon Microtoroidal Resonators With Integrated MEMS Tunable Coupler

Jin Yao, David Leuenberger, Ming-Chang M. Lee, *Member, IEEE*, and Ming C. Wu, *Fellow, IEEE*

***Abstract*—A single crystalline silicon microtoroidal resonator with integrated MEMS-actuated tunable optical coupler is demonstrated for the first time. It is fabricated by combining hydrogen annealing and wafer bonding processes. The device operates in all three coupling regimes: under-, critical, and over-coupling. We have also developed a comprehensive model based on time-domain coupling theory. The experimental and theoretical results agree very well. The quality factor (Q) is extracted by fitting the experimental curve with the model. The unloaded Q is as high as 110 000, and the loaded Q is continuously tunable from 110 000 to 5400. The extinction ratio of the transmittance is 22.4 dB. This device can be used as a building block of resonator-based reconfigurable photonic integrated circuits.**

***Index Terms*—Integrated optics, optical resonators, surface roughness, tunable.**

I. INTRODUCTION

OPTICAL microresonators are key enabling elements for compact filters [1], lasers [2], electro-optic modulators [3], add–drop multiplexers [4], optical dispersion compensators [5], delay lines [6], nonlinear optical devices [7], and optical sensors [8], [9]. The performance of microresonators depends on two parameters: the quality factor (Q) of the resonator and the coupling ratio between the waveguides and the resonator (κ). Microfabricated resonators with very high Q has been demonstrated in SiO_2 [10] and Si [11]. The coupling ratio needs to be controlled precisely to achieve optimum performance [12]. This has been achieved by adjusting prism couplers in fused silica microsphere resonators [13] or by moving tapered fiber couplers [14]–[16] with piezo-controlled micropositioners. However, such setups are bulky and cannot be integrated. In microresonators with integrated waveguides, the coupling ratio is determined by the fabrication process [17]. The value of κ or, perhaps more importantly, its relation with the cavity Q, cannot be controlled precisely. Some trimming processes have been proposed to control the resonance frequency, but not κ [18], [19].

Recently, microresonators with tunable coupling ratios have been reported [20]–[23]. A Mach–Zehnder interferometer (MZI) has been integrated with a racetrack resonator [20]. The resonator can operate in all coupling regimes (uncoupled, under-, critical, or over-coupled). An unloaded Q of 1.9×10^4 and an On–Off ratio of 18.5 dB have been achieved. However, the circumference of the resonator is rather large (1430 μm) due to the long MZI structure, which limits the free spectral range and the footprint that it can achieve. Recently, microfluidic approach has also been employed to tune both the resonance wavelength and the coupling ratio of low-index microring resonators made in SU8 [23]. The refractive index of the surrounding media was varied by mixing two different liquids. Critical coupling with an extinction ratio of 37 dB have been attained. However, index variation is small (~ 0.04), which limits the tuning range of κ. In addition, the tuning speed is slow (~ 2 s) and the fluidic packaging is cumbersome.

Previously, we have reported the first silicon microdisk resonator with integrated microelectromechanical systems (MEMS) tunable coupler [21], [22]. By physically changing the gap spacing between the waveguide and the resonator, κ can be varied over a wide range (0 to 34%) and a high Q (100 000) have been achieved simultaneously. Tunable dispersion compensators (185 to 1200 ps/nm) have also been demonstrated [22]. One drawback of that device is the lack of radial mode control in microdisk resonators, which could produce additional resonances due to high-order modes. In this paper, we report on the first single crystalline silicon *microtoroidal* resonator with MEMS tunable optical coupler. Microtoroidal resonators offer tighter confinement of the optical mode and eliminate multiple radial modes observed in microdisks. Microtoroidal resonators have been made in SiO_2 by thermal reflow [10], however, such process cannot be applied to single crystalline structures. Instead, we use hydrogen annealing to create three-dimensional toroidal structures while preserving the single crystalline quality [24]. To integrate the microtoroidal resonators with MEMS tunable waveguides, we have combined the hydrogen annealing process with wafer bonding technique. All the three coupling regimes have been demonstrated, with the loaded Q tunable from 110 000 to 5400.

II. DEVICE DESIGN AND FABRICATION

A. Device Structure Design

The schematic of the tunable microtoroidal resonator is shown in Fig. 1. Two suspended waveguides are vertically coupled to a microtoroidal resonator. It is realized on a two-layer silicon-on-insulator (SOI) structure. The microtoroid and the fixed electrodes of the MEMS actuators are fabricated on the lower SOI layer, while the suspended waveguides are integrated on the upper SOI. The initial spacing between the microtoroid and the

---

Manuscript received October 2, 2006; revised February 12, 2007. This work was supported in part by the Defense Advanced Research Project Agency (DARPA) University Photonics Research (UPR) Program HR0011-04-1-0040. The work of D. Leuenberger was supported by a one-year fellowship from the Swiss National Science Foundation, in 2005.

J. Yao and M. C. Wu are with the Department of Electrical Engineering and Computer Sciences, University of California, Berkeley, CA 94720 USA (e-mail: jinyao@eecs.berkeley.edu; wu@eecs.berkeley.edu).

D. Leuenberger is with the Integrated Photonics Laboratory, University of California, Berkeley, CA 94720 USA (e-mail: dleuen@eecs.berkeley.edu).

M.-C. M. Lee is with the Department of Electrical Engineering and the Institute of Photonics Technologies, National Tsing Hua University, Hsinchu 30055, Taiwan, R.O.C. (e-mail: mclee@ee.nthu.edu.tw).

Digital Object Identifier 10.1109/JSTQE.2007.893743

1077-260X/$25.00 © 2007 IEEE

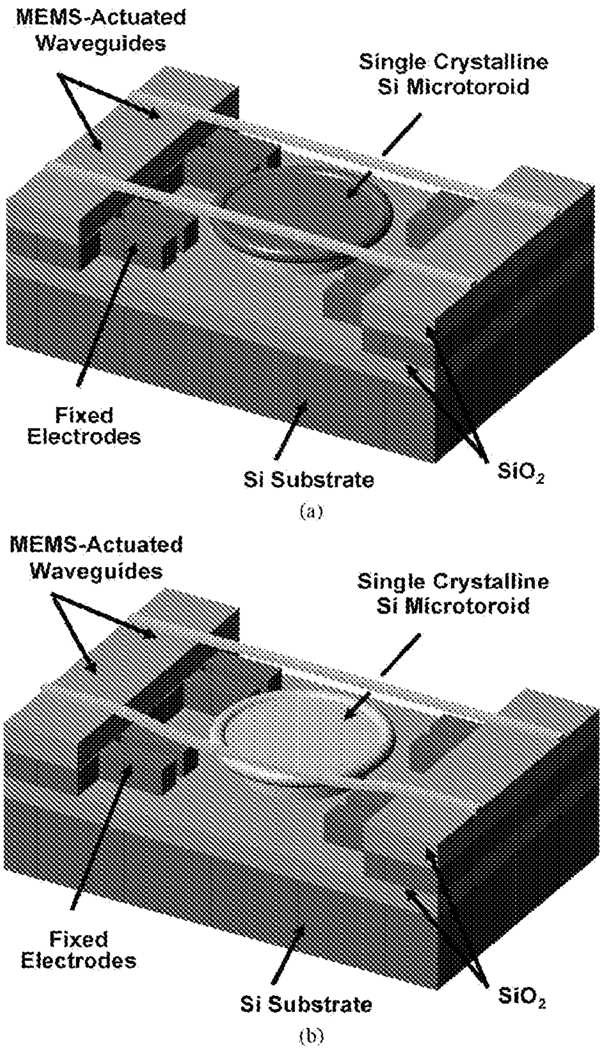

(a)

(b)

Fig. 1. (a) Schematic of the microtoroidal resonator with integrated MEMS tunable couplers. At zero bias, the initial spacing is large enough to ensure negligible coupling between the resonator and the waveguide coupler. (b) Schematic of the microtoroidal resonator with integrated MEMS tunable couplers under biased actuation. Lower waveguide is pulled downward to increase coupling, while the upper waveguide remains straight (uncoupled).

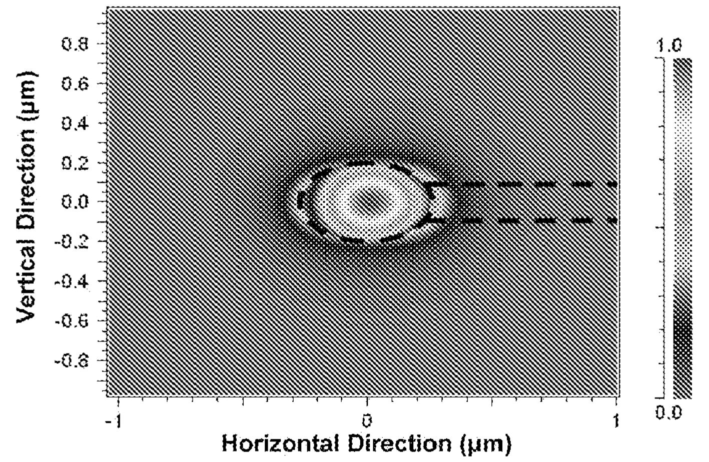

Fig. 2. Optical mode profile of the toroid for TE-like polarized light at 1.55 μm.

waveguides is 1 μm. It is chosen so that there is negligible coupling at zero bias, as shown in Fig. 1(a). With increasing voltage bias between the waveguide and the fixed electrodes, the suspended waveguide is pulled down toward the microtoroid, increasing the optical coupling exponentially, as illustrated in Fig. 1(b).

This design enables us to bias the microtoroidal resonator in all coupling regimes: under-coupling, critical coupling, and over-coupling, or even decoupled from the waveguide bus. Details of the MEMS actuator design have been reported in [22].

There is a design tradeoff in the doping concentration of the Si device layers. High doping is desired for the MEMS actuation, while low doping is necessary to minimize the optical absorption due to free carriers. Fortunately, electrostatic actuation does not require low resistivity. With a doping concentration of 10^{14} cm^{-3} (n-type dopants), a resistivity of 10 $\Omega\cdot$cm and an optical loss smaller than 0.01 cm^{-1} can be achieved. This absorption coefficient corresponds to a Q of 10^8 for microresonators if it is the dominant loss.

B. Waveguide Design for Phase Matching

Phase matching between the waveguide and the resonator is important to achieve an efficient coupling. Phase matching is satisfied when the two wave modes have the same propagation constant β.

We calculated the propagation constants of the microtoroid with the actual shape produced by hydrogen annealing using beam propagation method (BPM).[1] The optical field profile of the toroidal resonator at 1.55-μm wavelength is shown in Fig. 2. We used the following parameters in the calculation: refractive indexes of Si and air are 3.46 and 1.0, respectively; the bend radius of the toroid is 19.5 μm; and the radius of the toroid is 200 nm. It supports only one TE-like optical mode tightly confined to silicon.

Phase matching is achieved by controlling the dimensions of the waveguide. Fig. 3 shows the calculated propagation constants of the waveguide (lines) and the microtoroid (dots) versus wavelength for various waveguide dimensions. Here, we fix the waveguide width at 0.69 μm, the smallest linewidth that can regularly be produced by our lithography tool (10:1 reduction stepper). As shown in Fig. 3, the waveguide with 0.25-μm thickness is best matched to the microtoroid mode over a wide wavelength range around 1550 nm.

C. Fabrication Process

Our vertically coupled tunable microresonator was fabricated on a two-layer SOI using the wafer bonding process. The main challenge, here, was the nonplanar topography of the microtoroids that prevents the tight contact necessary for wafer bonding. We solved this problem by thinning the edges of the microdisks before hydrogen annealing so that the microtoroid surface was lower than the surrounding planar area. The detailed

[1] http://www.rsoftdesign.com/products/component_design/BeamPROP/

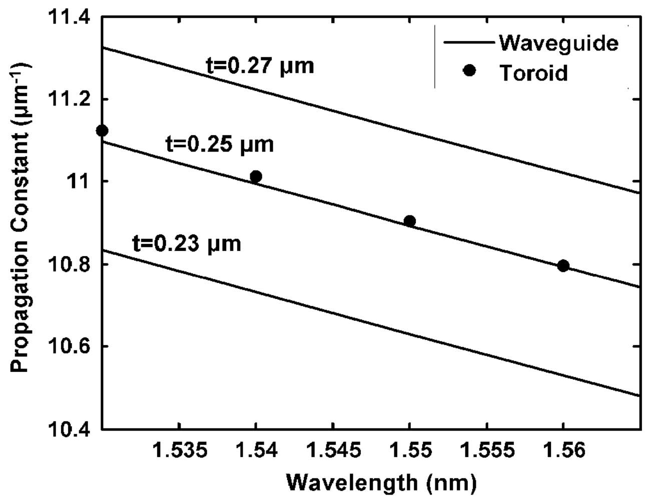

Fig. 3. Calculated propagation constants of the waveguide and the microtoroid versus wavelengths for various waveguide thicknesses, t. The width of the waveguide is fixed at 0.69 μm.

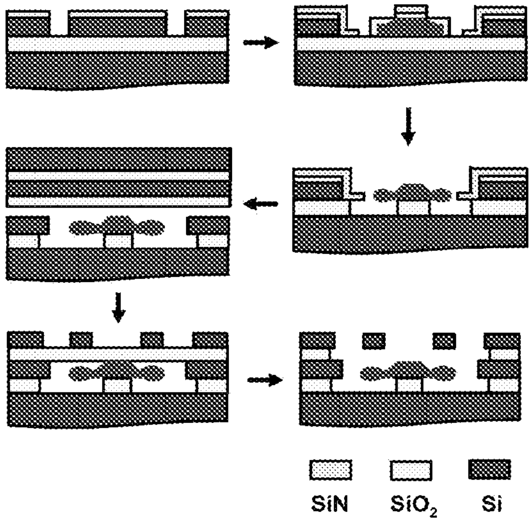

Fig. 4. Fabrication process for the tunable microtoroidal resonator.

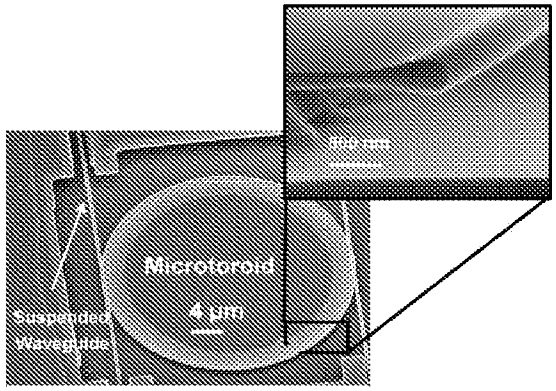

Fig. 5. SEM of the microtoroidal resonator and the suspended waveguides. Inset shows the cross-sectional view of the microtoroid.

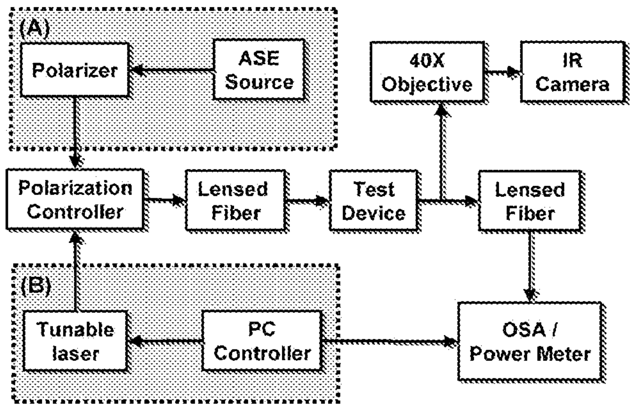

Fig. 6. Experimental setup for optical characterization. Amplified spontaneous emission (ASE) source is used (a) for quick measurement of the spectral response and (b) while the tunable laser provides high-resolution characterization.

fabrication process is shown in Fig. 4. First, microdisks were patterned and etched on an SOI wafer with a 350-nm-thick device layer. The edges of the disks were thinned down to 200 nm by thermal oxidation. This allowed room for the microtoroids to expand in the vertical direction during hydrogen annealing. The sample was then partially released in buffered HF and annealed in 10-Torr hydrogen ambient at 1050 °C for 5 min, creating a toroidal rim around the disks. The hydrogen annealing condition was optimized for the formation of the microtoroids, as reported in [24], [25]. A second SOI wafer with a 700-nm-thick device layer was thermally oxidized to create a SiO_2 spacer of 1-μm thickness. After oxidation, the thickness of the device layer was reduced to 250 nm. The toroid wafer was then fusion-bonded to the SOI wafer, whose substrate was subsequently removed to reveal the second SOI layer. The microtoroids were visible through the thin SOI layer, and the waveguide patterns were aligned to the edges of the underneath microtoroids. Finally, the waveguides around the toroids were released in buffered HF and supercritical dryer. In addition to creating a toroidal shape, the hydrogen annealing also reduced the surface roughness (to < 0.26 nm as reported in [26]), which was critical to attain high Q.

The scanning electron micrograph (SEM) of the fabricated device is shown in Fig. 5. The dimensions of the waveguides are measured to be 0.69-μm wide and 0.25-μm thick, very close to the designed parameters. The resonator exhibits a very smooth sidewall.

III. OPTICAL CHARACTERIZATION

The optical performance of the tunable microtoroidal resonator is tested using either a broadband amplified spontaneous emission (ASE) source (OpticWave Mini BLS-C-13) or a tunable laser (Agilent 81680A), as shown in Fig. 6. Light is coupled to the waveguides by polarization-maintaining lensed fibers. A calibrated optical power meter (HP 8153A) and an optical spectrum analyzer (OSA) (ANDO AQ6317B) are placed at the output to measure the transmitted power. The ASE provides a broadband source for quick measurement over a wide spectral range, while the tunable laser is used for high-resolution characterization. We have used TE-polarized input, which is attained by a linear polarizer and a polarization controller.

To actuate the waveguide, a voltage bias is applied to the fixed electrodes while the waveguide is grounded. At zero bias, almost

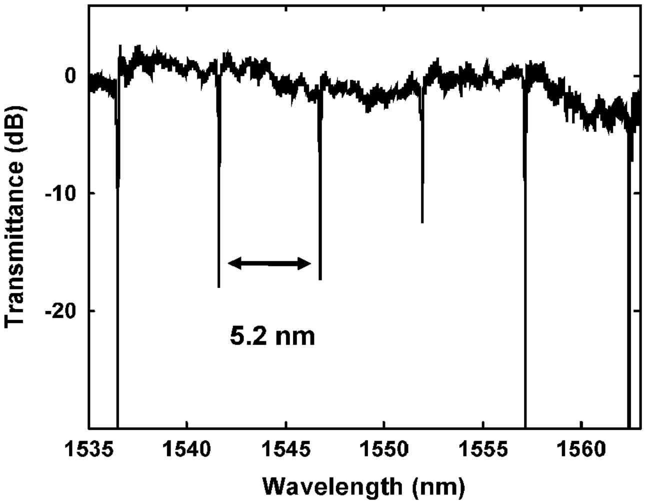

Fig. 7. Measured optical spectrum of a microtoroidal resonator at a bias voltage of 67 V. Measured free spectral range (FSR) of the TE mode is 5.2 nm.

100% of the light is transmitted to the output port. With increasing bias, sharp dips gradually appear in the transmission spectrum (Fig. 7). Each dip corresponds to a resonance wavelength. The free spectral range (FSR) of the TE mode is measured to be 5.2 nm. The small ripples are due to the reflections from the cleaved facets (Fabry–Perot effect). They can be eliminated by antireflection coating of the facets. Only a resonance peak is observed within each FSR, confirming the successful suppression of multiple radial modes observed in microdisk resonators.

The integrated tunable coupler enables the microresonator to operate in all coupling regimes. At low voltage, the microresonator is under-coupled. Fig. 8(a) shows the normalized transmission spectra of the resonator around one of the resonant wavelengths at 1548.2 nm at bias voltages of 51.0, 56.0, and 64.8 V. As the voltage increases, the optical coupling becomes stronger, leading to a larger dip at resonance. The three coupling regimes are clearly visible in Fig. 8(b), which plots the normalized transmittance at the resonant wavelength changes as a function of the applied voltage. In the under-coupling regime ($V_{\text{bias}} < 114$ V), the transmittance decreases continuously with the increasing voltage. The transmittance reaches a minimum at critical coupling ($V_{\text{bias}} = 114$ V). The extinction ratio is measured to be 22.4 dB at critical coupling. Further increase in voltage moves the resonator into the over-coupling regime. The increase in transmittance is accompanied by a broadening of the resonance linewidth since the coupling to waveguide is now stronger than the intrinsic loss of the resonator.

IV. THEORETICAL MODELING AND ANALYSIS

According to the time-domain coupling theory [1], the optical transfer function of the microresonator can be expressed as a function of resonant frequency (ω_0) and amplitude decay time constants τ_0 and τ_e, due to intrinsic loss and external coupling respectively

$$t_{\text{res}} = \frac{j(\omega - \omega_0) + \frac{1}{\tau_0} - \frac{1}{\tau_e}}{j(\omega - \omega_0) + \frac{1}{\tau_0} + \frac{1}{\tau_e}} \tag{1}$$

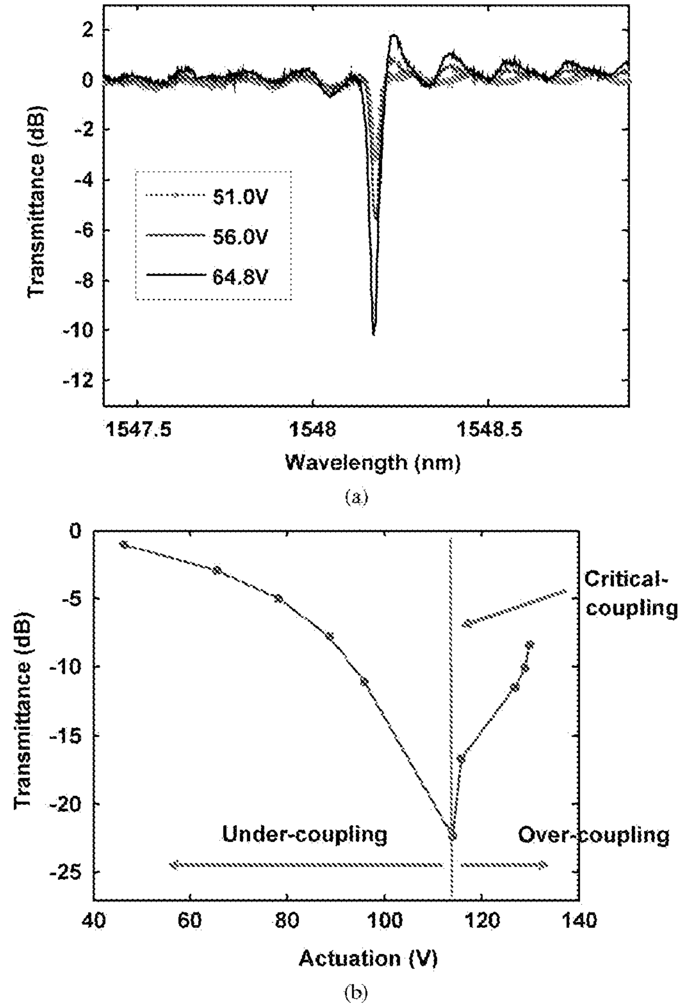

Fig. 8. (a) Measured normalized optical spectra of a microtoroidal resonator at bias voltages of 51.0, 56.0, and 64.8 V. (b) Normalized transmittance at resonance versus actuation voltage. Microresonator can be tuned continuously from under-coupling regime to over-coupling regime.

where t_{res} is the amplitude transfer function of the microresonator.

Alternatively, the transfer function can also be expressed in terms of the unloaded quality factor Q_0 and the external quality factor Q_e

$$t_{\text{res}} = \frac{2j\left(\frac{\lambda_0 - \lambda}{\lambda}\right) + \left(\frac{2}{Q_0} - \frac{1}{Q_L}\right)}{2j\left(\frac{\lambda_0 - \lambda}{\lambda}\right) + \left(\frac{1}{Q_L}\right)} \tag{2}$$

where $Q_0 = \omega_0\tau_0/2$, $Q_e = \omega_0\tau_e/2$, and the loaded quality factor Q_L is defined as

$$\frac{1}{Q_L} = \frac{1}{Q_0} + \frac{1}{Q_e} \tag{3}$$

The measured spectra are usually complicated by the Fabry–Perot resonance between the two cleaved facets, as illustrated in Fig. 9. To model the measured spectrum more precisely, and extract the Q values of the resonator more accurately, particularly when the resonance peak is small, we develop a comprehensive

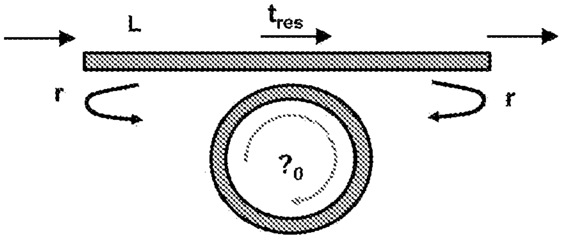

Fig. 9. Schematics illustrating the interaction between the microresonator and the Fabry–Perot resonance of the coupling waveguide.

model that includes both the effect of the microresonator and the Fabry–Perot ripples.

The total transmission t_{tot} is now a summation of multiple transmissions through the waveguide, as shown in

$$\begin{aligned} t_{\mathrm{tot}} &= (1-r)^2 \exp(-\alpha L)\exp(jkLn_{\mathrm{eff}})t_{\mathrm{res}} \\ &\quad + (1-r)^2 r^2 \exp(-3\alpha L)\exp(j(3kLn_{\mathrm{eff}} + 2\phi_{\mathrm{R}}))t_{\mathrm{res}}^3 \\ &\quad + (1-r)^2 r^4 \exp(-5\alpha L)\exp(j(5kLn_{\mathrm{eff}} + 4\phi_{\mathrm{R}}))t_{\mathrm{res}}^5 \\ &\quad + L \end{aligned} \tag{4}$$

where r is the amplitude reflection coefficient at the facet of the silicon waveguide, α is the optical loss per unit length in the waveguide, L is the length of the waveguide, k is the free-space propagation constant, n_{eff} is the effective refractive index of the Si waveguide, and ϕ_{R} is the optical phase change at the reflection per interface. Since there is a π phase shift at the reflection interface, the total transmission t_{tot} can be simplified to

$$\begin{aligned} t_{\mathrm{tot}} &= (1-r)^2 \exp(-\alpha L)\exp(jkLn_{\mathrm{eff}})t_{\mathrm{res}} \\ &\quad \{1 + r^2 \exp(-2\alpha L)\exp(j2kLn_{\mathrm{eff}})t_{\mathrm{res}}^2 \\ &\quad + r^4 \exp(-4\alpha L)\exp(j4kLn_{\mathrm{eff}})t_{\mathrm{res}}^4 + L\} \\ &= a_0(1 + q + q^2 + q^3 + L) \\ &= \frac{a_0}{1-q} \end{aligned} \tag{5}$$

where $a_0 = (1-r)^2 \exp(-\alpha L)\exp(jkLn_{\mathrm{eff}})t_{\mathrm{res}}$, and $q = r^2 \exp(-2\alpha L)\exp(j2kLn_{\mathrm{eff}})t_{\mathrm{res}}^2$.

In this derivation, we have assumed that the backscattering effect is small and can be neglected. The total intensity transmittance is then given by

$$T_{\mathrm{res}} = |t_{\mathrm{tot}}|^2 \tag{6}$$

To include the effect of waveguide dispersion, the phase factor kLn_{eff} is replaced by

$$\begin{aligned} \phi &= kL\left[n_{\mathrm{eff}} + \frac{dn}{d\lambda}(\lambda - \lambda_0)\right] \\ &= kLn_{\mathrm{eff}}\left[1 + \frac{dn}{d\lambda}\frac{1}{n_{\mathrm{eff}}}(\lambda - \lambda_0)\right] \\ &= kLn_{\mathrm{eff}}\left[1 + D_\lambda(\lambda - \lambda_0)\right] \end{aligned} \tag{7}$$

where $D_\lambda = \frac{dn}{d\lambda}\frac{1}{n_{\mathrm{eff}}}$.

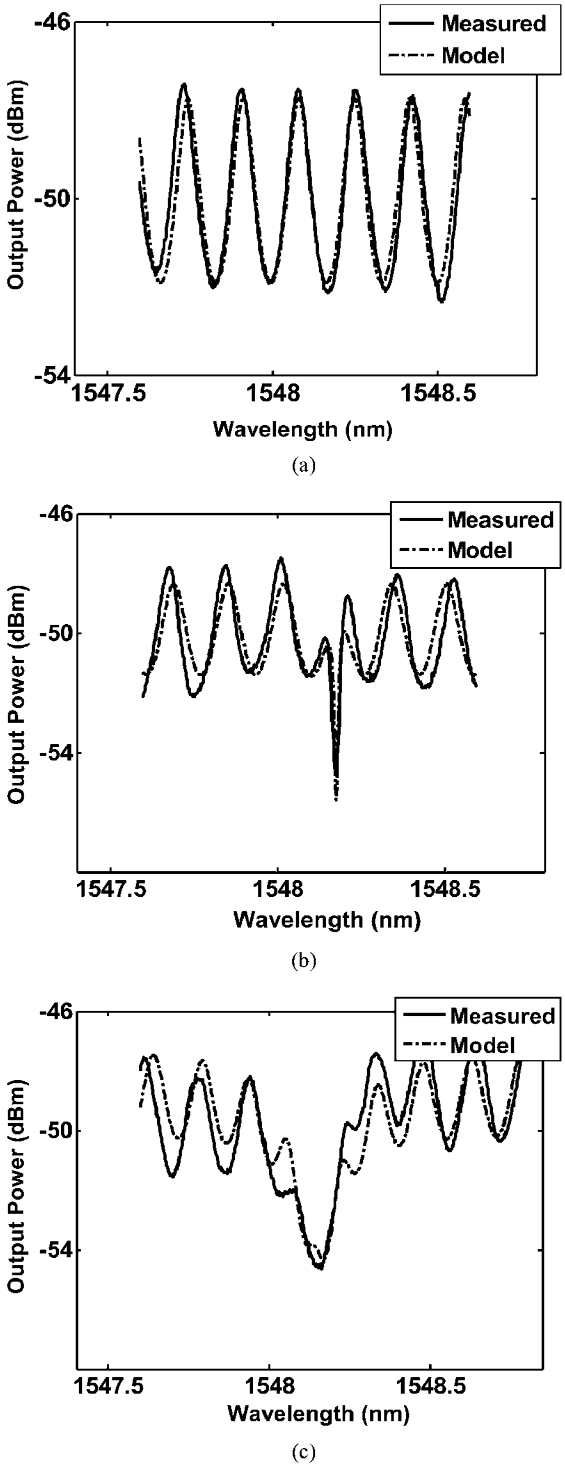

(a)

(b)

(c)

Fig. 10. (a) Measured and modeled spectra at 0 V (microresonator is decoupled). (b) Measured and modeled spectra at 64.8 V (microresonator is undercoupled). (c) Measured and modeled spectra at 130 V (microresonator is overcoupled).

The quality factors Q_0 and Q_L are extracted from the measured optical spectra by least-mean-square-error fitting to the model. Fig. 10 shows the measured and the fitted spectra around the resonance peak at 1548.2 nm when the resonator is:

a) decoupled; b) under-coupled; and c) over-coupled. The experimental data agree very well with the theoretical model. From the fitted spectral response, the unloaded quality factor Q_0 of the microtoroidal resonator is extracted to be 110 000. The loaded Q, i.e., Q_L, is continuously tunable from 110 000 to 5400, exhibiting a tuning ratio of more than 20:1.

The model described in this paper fit not only the resonance peak but also the ripples due to Fabry–Perot resonance. The quality factor extracted by this method is more accurate than by the lumped resonator model alone [27], especially when the resonance peak is small.

V. DISCUSSION

Hydrogen annealing is a simple and powerful technique to fabricate suspended microring resonators with high-quality factor and single radial mode. Comparing the etched ring with tethered anchor [17], the seamless toroidal structure has lower scattering loss and higher Q. The hydrogen annealing process also greatly reduces the surface roughness, as confirmed by the high Q measured in our devices. These tunable microresonators described in this paper can be cascaded to form reconfigurable optical add–drop multiplexers, wavelength-selective switches, and crossconnects. It can also be used for bandwidth-tunable filters in dynamic optical networks. With the successful suppression of multiple radial modes, we expect the microtoroidal resonator to have even larger bandwidth tuning ratio than the microdisk-based filters in [28].

VI. CONCLUSION

We have successfully demonstrated a novel single crystalline silicon microtoroidal resonator with MEMS-actuated tunable optical coupler. It is fabricated by combining the hydrogen annealing and the wafer bonding processes. We have achieved an unloaded Q of 110 000 for a 39-μm-diameter resonator with a toroidal radius of 200 nm. The device is able to operate in all the three coupling regimes: under-, critical, and over-coupling. The resonator can also be decoupled from the waveguide, allowing them to be cascaded without loading the waveguides. We have developed a detailed model combining the time-domain coupling theory with the Fabry–Perot resonance of the waveguide. The experimental and the theoretical results agree very well. The loaded Q is continuously tunable from 110 000 to 5400. This device has potential applications in variable-bandwidth filters, reconfigurable add–drop multiplexers, wavelength-selective switches and crossconnects, and optical sensors.

ACKNOWLEDGMENT

The authors would like to thank the staff of the Microfabrication Laboratory, University of California, Berkeley. Part of the fabrication process was performed at Stanford Nanofabrication Facility, Stanford University. In particular, they would also like to acknowledge the assistance of M. Stevens and M. Mansourpour. They would also like to thank Dr. S. Mathai of the University of California, Berkeley, for helpful discussions and technical assistance.

REFERENCES

[1] B. E. Little, S. T. Chu, H. A. Haus, J. Foresi, and J. P. Laine, “Microring resonator channel dropping filters,” *J. Lightw. Technol.*, vol. 15, no. 6, pp. 998–1005, Jun. 1997.

[2] S. J. Choi, K. Djordjev, S. J. Choi, and P. D. Dapkus, “Microdisk lasers vertically coupled to output waveguides,” *IEEE Photon. Technol. Lett.*, vol. 15, no. 10, pp. 1330–1332, Oct. 2003.

[3] Q. Xu, B. Schmidt, S. Pradhan, and M. Lipson, “Micrometre-scale silicon electro-optic modulator,” *Nature*, vol. 435, no. 7040, pp. 325–327, May 2005.

[4] B. E. Little, S. T. Chu, W. Pan, and Y. Kokubun, “Microring resonator arrays for VLSI photonics,” *IEEE Photon. Technol. Lett.*, vol. 12, no. 3, pp. 323–325, Mar. 2000.

[5] C. K. Madsen, G. Lenz, A. J. Bruce, M. A. Cappuzzo, L. T. Gomez, T. N. Nielsen, L. E. Adams, and I. Brenner, “An all-pass filter dispersion compensator using planar waveguide ring resonators,” in *Proc. Opt. Fiber Commun. Conf. Int. Conf. Integr. Opt. Opt. Fiber Commun. (OFC/IOOC)*, Piscataway, NJ, Feb. 1999, vol. 4, pp. 99–101.

[6] G. Lenz, B. J. Eggleton, C. K. Madsen, and R. E. Slusher, “Optical delay lines based on optical filters,” *IEEE J. Quantum Electron.*, vol. 37, no. 4, pp. 525–532, Apr. 2001.

[7] T. J. Kippenberg, S. M. Spillane, D. K. Armani, and K. J. Vahala, “Ultralow-threshold microcavity Raman laser on a microelectronic chip,” *Opt. Lett.*, vol. 29, pp. 1224–1227, Jun. 2004.

[8] F. Vollmer, S. Arnold, D. Braun, I. Teraoka, and A. Libchaber., “Multiplexed DNA quantification by spectroscopic shift of two microsphere cavities,” *Biophys. J.*, vol. 85, pp. 1974–1979, Sep. 2003.

[9] A. M. Armani and K. J. Vahala, “Heavy water detection using ultra-high-Q microcavities,” *Opt. Lett.*, vol. 31, no. 12, pp. 1896–1898, Jun. 2006.

[10] D. K. Armani, T. J. Kippenberg, S. M. Spillane, and K. J. Vahala, “Ultra-high-Q toroid microcavity on a chip,” *Nature*, vol. 421, pp. 925–929, Feb. 2003.

[11] M. Borselli, T. Johnson, and O. Painter, “Beyond the Rayleigh scattering limit in high-Q silicon microdisks: theory and experiment,” *Opt. Express*, vol. 13, no. 5, pp. 1515–1530, Mar. 2005.

[12] A. Yariv, “Critical coupling and its control in optical waveguide-ring resonator systems,” *IEEE Photon. Technol. Lett.*, vol. 14, no. 4, pp. 483–485, Apr. 2002.

[13] V. B. Braginsky, M. L. Gorodetsky, and V. S. Ilchenko, “Quality-factor and nonlinear properties of optical whispering-gallery modes,” *Phys. Lett. A*, vol. 137, pp. 393–397, May 1989.

[14] J. C. Knight, G. Cheung, F. Jacques, and T. A. Birks, “Phase-matched excitation of whispering-gallery-mode resonances by a fiber taper,” *Opt. Lett.*, vol. 22, pp. 1129–1131, Aug. 1997.

[15] M. Cai, O. Painter, and K. J. Vahala, “Observation of critical coupling in a fiber taper to a silica-microsphere whispering-gallery mode system,” *Phys. Rev. Lett.*, vol. 85, pp. 74–77, Jul. 2000.

[16] M. Borselli, K. Srinivasan, P. E. Barclay, and O. Painter, “Rayleigh scattering, mode coupling, and optical loss in silicon microdisks,” *Appl. Phys. Lett.*, vol. 85, pp. 3693–3695, 2004.

[17] L. Martinez and M. Lipson, “High confinement suspended micro-ring resonators in silicon-on-insulator,” *Opt. Express*, vol. 14, no. 13, pp. 6259–6263, Jun. 2006.

[18] S. T. Chu, W. Pan, S. Sato, T. Kaneko, Y. Kokubun, and B. E. Little, “Wavelength trimming of a microring resonator filters by means of a UV sensitive polymer overlay,” *IEEE Photon. Technol. Lett.*, vol. 11, no. 6, pp. 688–690, Jun. 1999.

[19] D. K. Sparacin, J. P. Lock, C. Hong, K. K. Gleason, L. C. Kimerling, and J. Michel, “Trimming of microring resonators using photo-oxidation of a plasma-polymerized organosilane cladding material,” *Opt. Lett.*, vol. 30, no. 17, pp. 2251–2253, 2005.

[20] W. M. J. Green, R. K. Lee, G. DeRose, A. Scherer, and A. Yariv, “Hybrid InGaAsP-InP Mach-Zehnder racetrack resonator for thermooptic switching and coupling control,” *Opt. Exp.*, vol. 13, pp. 1651–1659, Mar. 2005.

[21] M.-C. M. Lee and M. C. Wu, “MEMS-actuated microdisk resonators with variable power coupling ratios,” *IEEE Photon. Technol. Lett.*, vol. 17, no. 5, pp. 1034–1036, May 2005.

[22] M.-C. M. Lee and M. C. Wu, “Tunable coupling regimes of silicon microdisk resonators using MEMS actuators,” *Opt. Exp.*, vol. 14, no. 11, pp. 4703–4712, May 2006.

[23] U. Levy *et al.*, “On-chip microfluidic tuning of an optical microring resonator,” *Appl. Phys. Lett.*, vol. 88, pp. 111107–111109, Mar. 2006.

[24] M.-C. M. Lee and M. C. Wu, "Thermal annealing in hydrogen for 3-D profile transformation on silicon-on-insulator and sidewall roughness reduction," *J. Microelectromech. Syst.*, vol. 15, no. 2, pp. 338–343, Apr. 2006.

[25] J. Yao, M.-C. M. Lee, and M. C. Wu, "Hydrogen annealing and bonding processes for integrated MEMS tunable microtoroidal resonators," to be published.

[26] M.-C. M. Lee, J. Yao, and M. C. Wu, "Silicon profile transformation and sidewall roughness reduction using hydrogen annealing," in *Proc. 18th IEEE Int. Conf. Microelectromech. Syst.*, Miami, FL, Jan. 30–Feb. 3, 2005, pp. 596–599.

[27] J. Yao, M.-C. M. Lee, D. Leuenberger, and M. C. Wu, "Silicon microtoroidal resonators with integrated MEMS tunable optical coupler," in *Proc. IEEE Opt. Microelectromech. Syst.*, Big Sky, MT, 2006, pp. 17–18.

[28] J. Yao, M.-C. M. Lee, D. Leuenberger, and M. C. Wu, "Wavelength- and bandwidth-tunable filters based on MEMS-actuated microdisk resonators," in *Proc. Opt. Fiber Commun. Conf. Nat. Fiber Opt. Eng. Long.*, Anaheim, CA, Mar. 5–10, 2006, p. 3.

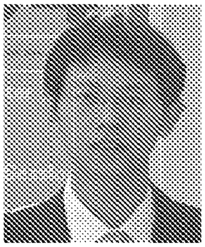

Jin Yao received the B.S. and M.S. degrees in electronic engineering from Tsinghua University, China, in 2000 and 2002, respectively. He is currently working toward the Ph.D. degree from the Department of Electrical Engineering and Computer Sciences, University of California, Berkeley.

His current research is focussed on silicon-based integrated microresonators, including design, simulation, fabrication, characterization, and their applications. His research interests include silicon-based photonic integrated circuits and micro-nano scale MEMS.

Mr. Yao won the California NanoSystems Institute (CNSI) Fellowship Award, in 2002–2003.

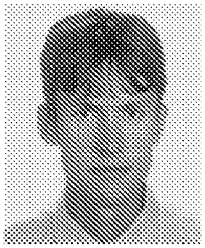

David Leuenberger received the graduate degree from the Institute of Applied Physics, University of Bern, Switzerland, in 2000. He received the Ph.D. degree from the Swiss Federal Institute of Technology, Lausanne, Switzerland, in 2004.

Currently, he is a Postdoctoral Researcher with the Integrated Photonics Laboratory, University of California, Berkeley. His current research interests include integrated microresonators for optical communication and sensing applications and optical antennas for surface enhanced Raman scattering. He is the author or coauthor of five journal papers and five conference papers.

Dr. Leuenberger is a member of the Optical Society of America (OSA).

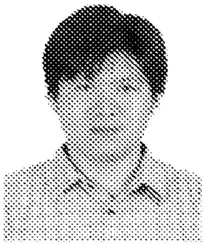

Ming-Chang M. Lee (S'04–M'05) was born in Taiwan, R.O.C. He received the B.S. degree in control engineering from the National Chiao Tung University, Hsinchu, Taiwan and the M.S. degree in electrical engineering from the National Taiwan University, Taipei, Taiwan, in 1994 and 1996, respectively. He received the Ph.D. degree in electrical engineering from the University of California, Los Angeles, in 2005.

Currently, he is with the faculty at the Institute of Photonics Technologies and the Department of Electrical Engineering, National Tsing Hua University, Taiwan. His research interests include optical MEMS, studies of nanophotonics, and the development of integrated photonic devices for optical communication and sensing.

Dr. Lee is a member of the Optical Society of America (OSA).

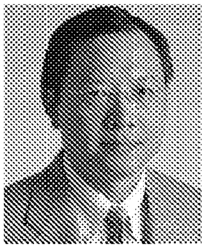

Ming C. Wu (S'82–M'83–SM'00–F'02) received the B.S. degree from National Taiwan University, Taipei, Taiwan, in 1983, and the M.S. and Ph.D. degrees from the University of California, Berkeley, in 1985 and 1988, respectively, all in electrical engineering.

Currently, he is a Professor of electrical engineering and computer sciences at the University of California, Berkeley, and a Co-Director of Berkeley Sensors and Actuators Center (BSAC). From 1988 to 1992, he was a Technical Staff at AT&T Bell Laboratories, Murray Hill, NJ. From 1993 to 2004, he was a Professor of electrical engineering at the University of California, Los Angeles (UCLA). He was also the Director of Nanoelectronics Research Facility and Vice Chair for Industrial Relations during his tenure at UCLA. In 1997, he cofounded OMM in San Diego, CA, to commercialize MEMS optical switches. He has published more than 400 papers, contributed five book chapters, and holds 11 U.S. patents. His research interests include optical MEMS, optoelectronics, and biophotonics. He has also participated in many technical conferences. He was the Guest Editor of two IEEE/OSA JOURNAL OF LIGHTWAVE TECHNOLOGY Special Issues on Optical MEMS.

Dr. Wu was a Fellow of David and Lucile Packard Foundation, from 1992 to 1997. He was the founding Co-Chair of the IEEE/LEOS Summer Topical Meeting on Optical MEMS in 1996.

EXHIBIT H

UNITED STATES PATENT AND TRADEMARK OFFICE

UNITED STATES DEPARTMENT OF COMMERCE
United States Patent and Trademark Office
Address: COMMISSIONER FOR PATENTS
P.O. Box 1450
Alexandria, Virginia 22313-1450
www.uspto.gov

APPLICATION NO.	FILING DATE	FIRST NAMED INVENTOR	ATTORNEY DOCKET NO.	CONFIRMATION NO.
10/678,354	10/02/2003	Deniz K. Armani	70120-00005	1793

58688 7590 11/05/2008
CONNOLLY BOVE LODGE & HUTZ LLP
P.O. BOX 2207
WILMINGTON, DE 19899

EXAMINER	
VAN ROY, TOD THOMAS	

ART UNIT	PAPER NUMBER
2828	

MAIL DATE	DELIVERY MODE
11/05/2008	PAPER

Please find below and/or attached an Office communication concerning this application or proceeding.

The time period for reply, if any, is set in the attached communication.

DETAILED ACTION

Response to Amendment

The Examiner acknowledges, and enters, the amending of claims 1, 29, 28, and 79, as well as the cancellation of claims 2 and 34.

Response to Arguments

Applicant's arguments filed 08/19/2008 have been fully considered but they are not persuasive.

The addition of the limitation that the micro-cavity is planar is not believed to place the claims in condition for allowance. Firstly, the primary reference, McCall was used to teach this feature in the previous Final office action. Stone was not relied upon to teach the shape of the claimed device, only that the Q value is desirable in devices of a similar structure. Therefor this limitation has previously been shown to be found in McCall.

Stone is believed to be relevant prior art as the shape of the device taught is nearly identical to that of McCall. Firstly, both are taught to be micro-cavity whispering gallery mode devices (McCall-title, Stone-col.1 lines 27-29, col.2 line 57). Both teach the device can be asymmetrical or oval (McCall-col.3 lines 40-44, Stone-col.2 lines 47-52). Each teaches the device to have a flattened (planar) disc-like shape (McCall-col.7 example 1, Stone-col.2 lines 42-44 “spheroid with an oblate deformation” meaning flattened at the poles). Additionally, as was cited previously, US 2002/0018611 teaches discs and spheres function essentially interchangeably in whispering gallery mode resonators ([0005]). Therefor, the shape of Stone is believed to be near enough to that of McCall to be a reasonable combination to one of ordinary skill in the art.

As to Stone teaching how to make such a device, the Examiner refers to the arguments posed in the Final office action included below:

The Applicant has argued that the combination of McCall in view of Stone is not proper as a reasonable expectation of success is not established. The Examiner does not agree.

McCall was used in the rejections to teach a high Q micro-resonating device. McCall failed to teach the device to have a Q value of at least 1x10^8. Stone was presented to teach that high Q micro-resonator devices similar to McCall's can be created to have Q values exceeding the claimed value. Stone demonstrates this in the plot shown at fig.5. Motivation was then presented to demonstrate a reason to combine the two teachings.

The Applicant further argues that McCall and Stone fall short of teaching how to make the proposed cavity, leading to the lack of expectation of success. Firstly, the Examiner is of the opinion that establishment of a prima facie case of obviousness does not require the need to disclose "how to make" the device in question (MPEP 2142). According to MPEP 2142, all of the claimed limitations must be taught or suggested. McCall teaches all of the structural features outlined in the device claims. Stone suggests creating the similar micro-resonators with a large Q value.

Finally, and building on the previous argument, the Applicant has stated that the plot of Stone outlines only theoretical possibilities. The Examiner agrees that it is not *clearly stated that Stone has created a device that corresponds to each and every point on the plot. However, Stone teaches that the resonator structure is of a known type ('typical', see brief description of the drawings), and how to modify the structure by changing the deformation amount to obtain a desired Q value for a given application. In the end, Stone may not have created a device at every plot point, but he did outline the use of a typical structure and how to adjust the physical parameters of that structure to obtain the Q values taught. This, in the Examiner's opinion, is a clear teaching of how such a structure can be made (via adjustment of the deformation amount, Stone, col.4 lines 25-36).*

In light of the above arguments the Examiner is of the belief that the rejections made over McCall in view of Stone would be considered both proper and reasonable to one of ordinary skill in the art.

The Examiner notes that the status of the claims remains the same as that in the Final office action. Claims 1-8, 10-22, 28-41, 43-58, 60-62, and 67-82 are pending, and all are rejected.

Conclusion

Any inquiry concerning this communication or earlier communications from the examiner should be directed to TOD T. VAN ROY whose telephone number is (571)272-8447. The examiner can normally be reached on M-F.

If attempts to reach the examiner by telephone are unsuccessful, the examiner's supervisor, Minsun Harvey can be reached on (571)272-1835. The fax phone number for the organization where this application or proceeding is assigned is 571-273-8300.

Information regarding the status of an application may be obtained from the Patent Application Information Retrieval (PAIR) system. Status information for published applications may be obtained from either Private PAIR or Public PAIR. Status information for unpublished applications is available through Private PAIR only. For more information about the PAIR system, see http://pair-direct.uspto.gov. Should you have questions on access to the Private PAIR system, contact the Electronic Business Center (EBC) at 866-217-9197 (toll-free). If you would like assistance from a USPTO Customer Service Representative or access to the automated information system, call 800-786-9199 (IN USA OR CANADA) or 571-272-1000.

/TVR/

/Minsun Harvey/
Supervisory Patent Examiner, Art Unit 2828

Advisory Action ***After the Filing of an Appeal Brief***	**Application No.** 10/678,354	**Applicant(s)** ARMANI ET AL.
	Examiner TOD T. VAN ROY	**Art Unit** 2828

--The MAILING DATE of this communication appears on the cover sheet with the correspondence address --

The reply filed 19 August 2008 is acknowledged.

1. ☐ The reply filed on or after the date of filing of an appeal brief, but prior to a final decision by the Board of Patent Appeals and Interferences, will not be entered because:

   a. ☐ The amendment is not limited to canceling claims (where the cancellation does not affect the scope of any other pending claims) or rewriting dependent claims into independent form (no limitation of a dependent claim can be excluded in rewriting that claim). See 37 CFR 41.33(b) and (c).

   b. ☐ The affidavit or other evidence is not timely filed before the filing of an appeal brief. See 37 CFR 41.33(d)(2).

2. ☐ The reply is not entered because it was not filed within the two month time period set forth in 37 CFR 41.39(b), 41.50(a)(2), or 41.50(b) (whichever is appropriate). Extensions of time under 37 CFR 1.136(a) are not available.

   Note: This paragraph is for a reply filed in response to one of the following: (a) an examiner's answer that includes a new ground of rejection (37 CFR 41.39(a)(2)); (b) a supplemental examiner's answer written in response to a remand by the Board of Patent Appeals and Interferences for further consideration of rejection (37 CFR 41.50(a)(2)); or (c) a Board of Patent Appeals and Interferences decision that includes a new ground of rejection (37 CFR 41.50(b)).

3. ☒ The reply is entered. An explanation of the status of the claims after entry is below or attached.

4. ☒ Other: *Please see attached. The IDS submitted 09/03/2008 has been considered*

IN THE UNITED STATES PATENT AND TRADEMARK OFFICE

In re the Application of: Deniz K. Armani et al. Serial No.: 10/678,354 Filed: October 2, 2003 For: ULTRA-HIGH Q MICRO-RESONATOR AND METHOD OF FABRICATION	Group Art Unit: 2828 Examiner: Tod Thomas Van Roy

AMENDMENTS SUBMITTED UNDER 37 CFR 41.33(a) FILED CONCURRRENTLY WITH APPEAL BRIEF

Hon. Commissioner for Patents
P.O. Box 1450
Alexandria, VA 22313-1450

Sir:

The following claim amendments are submitted pursuant to 37 CFR 41.33(a) concurrently with the filing of Applicants' Appeal Brief.

A listing of the claims, including amendments thereto, begins on page 2 of this paper.

Remarks begin on page 9 of this paper.

Entered
10/30/2008
TVR